

**DYNAMIC CONTROL OF INTERGRATED WIND FARM BATTERY
ENERGY STORAGE SYSTEMS FOR GRID CONNECTION**

By

Mr. Mandisi Gwabavu

Thesis submitted in fulfilment of the requirements for the degree

Master of Engineering: Electrical Engineering

In the Faculty of Engineering

At the Cape Peninsula University of Technology

Supervisor: Dr AK. Raji

Bellville Campus


2020

CPUT copyright information

The thesis may not be published either in part (in scholarly, scientific, or technical journals), or (as a monograph), unless permission has been obtained from the University.

DECLARATION

I, Mandisi Gwabavu declare that the contents of this thesis represent my own unaided work, and that the dissertation/thesis has not previously been submitted for academic examination towards any qualification. Furthermore, it represents my own opinions and not necessarily those of the Cape Peninsula University of Technology.



09/10/2020

Signed

Date

ABSTRACT

The intermittent nature of wind power is a major challenge for wind as an energy source. Wind power generation is therefore difficult to plan, manage, sustain, and track during the year due to different weather conditions. The uncertainty of energy loads and power generation from wind energy sources heavily affects the system stability. The battery energy storage system (BESS) plays a fundamental role in controlling and improving the efficiency of renewable energy sources. Stochasticity of wind speed and reliability of the main system components are considered.

This paper presents a dynamical control system based on model predictive control (MPC) in real time, to make full use of the flexibility and controllability of energy storage to mitigate problems of wind farm variability and intermittency. The control scheme first plans the expected output, then stochastic optimization is used to optimize grid integrated wind farm BESS output power, develop an optimal operation strategy for BESS, and prevent some unpredictable conditions that may have impacts on the stability of the system. The results show that the proposed method can reduce grid-connected wind power fluctuations, limit system faults, control command for the BESS in the dispatching period, and ensure system stability for grid connection..

ACKNOWLEDGEMENTS

This author acknowledges:

1. Mighty God for giving me the strength.
2. Dr AK Raji for being fantastic Supervisor.
3. Mr Ntanjana for technical and moral support.

ACADEMIC PAPERS EMINATING FROM THE STUDY

MDPI (Basel, Switzerland) issued a certificate of acceptance for the manuscript (sustainability-1094182) titled: “*Dynamic Control of Integrated Wind Farm Battery Energy Storage Systems for Grid Connection*” , Authored by: Atanda Raji; Mandisi Gwabavu in Sustainability (ISSN 2071-1050) on 12 February 2021.

DEDICATION

The research is devoted to:

1. My Mother TP Gwabavu, Siblings, Nieces and Nephews.
2. My Girlfriend N Mayila
3. Sivuyise Organization
4. All the Students

GLOSSARY

PV	Photovoltaics
IPP	Independent Power Producers
RESs	Renewable Energy Sources
DFIG:	Double Fed Induction Generator
BESSs	Battery Energy Storage Systems
HAWT:	Horizontal Axis Wind Turbine
VAWT:	Vertical Axis Wind Turbine
kW:	kilo Watt
WECS	Wind Energy Conversion System
EESS	Electrical Energy Storage Systems
AW	Action Windpower
WES	Wind Energy System
WTs	Wind Turbines
DigSILENT	Digital Simulator for Electrical Network
DoE	Department of Energy

TABLE OF CONTENTS

DECLARATION.....	i
ABSTRACT	ii
ACKNOWLEDGEMENTS.....	iii
ACADEMIC PAPERS EMINATING FROM THE STUDY	iv
DEDICATION	v
GLOSSARY.....	vi
TABLE OF CONTENTS	vii
LIST OF FIGURES.....	xii
LIST OF TABLES	xix
CHAPTER 1. GENERAL INTRODUCTION.....	1
1.1 Introduction.....	1
1.2 Background of the research problem.....	3
1.3 Statement of the research problem.....	4
1.4 Research aim and objective	4
1.5 Delimitation of the research	5
1.6 Research Methodology.....	5
1.7 Thesis Organisation.....	6
1.8 Conclusion.....	7
CHAPTER 2. LITRATURE REVIEW	8
2.1 Introduction.....	8

2.2	Wind Energy Systems	8
2.2.1	Background	8
2.2.2	Wind Turbines.....	11
2.2.3	Classification of Wind turbines.....	11
2.2.4	Wind power parameters.....	16
2.2.5	Wind turbine generators and power electronics converters topologies..	20
2.2.6	Wind Turbines Control	24
2.2.7	Wind Farm	29
2.3	Electrical Energy Storage Systems (EESSs).....	30
2.3.1	Background	30
2.3.2	Pumped Hydro.....	32
2.3.3	Compressed Air Energy Storage (CAES).....	34
2.3.4	Flywheel Energy storage (FES).....	36
2.3.5	Battery Energy Storage System (BESS).....	38
2.3.6	Hydrogen Storage.....	50
2.3.7	Super-Capacitor (SC)	52
2.3.8	Superconducting Magnetic Energy Storage (SMES)	54
2.4	Grid Integration of Wind Farm and BESS	56
2.4.1	Background	56
2.4.2	Wind farm Integration with BESS.....	56
2.4.3	Grid Integration with Wind Farm	58

2.4.4	Grid Integration with Wind Farm BESS.....	59
2.4.5	Grid Code Power Quality Parameters.....	68
2.5	Control of integrated Systems	74
2.5.1	Background	74
2.5.2	Effect of Integrated Wind Generation on Steady-State	76
2.5.3	Effect of Integrated Wind Generation on Dynamic.....	77
2.5.4	Control operation of Grid integrated ESS Wind Farm	81
2.6	Conclusion.....	91
CHAPTER 3. CASE STUDY OF WIND FARM IN SOUTH AFRICA.....		92
3.1	Introduction.....	92
3.2	Wind Turbine Description	93
3.2.1	Rotor.....	94
3.2.2	Pitch System.....	94
3.2.3	Yaw System.....	95
3.2.4	Gearbox Cooling and Lubrication Gearbox System.....	98
3.2.5	Generator	99
3.2.6	Hydraulic Power Unit	101
3.2.7	Rotor Locking and Braking System.....	102
3.2.8	Safety System.....	103
3.2.9	Sensors	105
3.2.10	Control System.....	106

3.2.11	Frequency Converter.....	107
3.3	Grid connection.....	108
3.4	Conclusion.....	108
CHAPTER 4. SYSTEM MODELLING AND SIMULATION		109
4.1	Introduction.....	109
4.2	BESS for Wind Farm Grid Connected	109
4.3	Battery Model	110
4.3.1	Analysis of the battery Charging and discharging.....	110
4.3.2	Modelling battery energy storage for wind power plant application	113
4.3.3	BESS model for Sodium Sulfur (NAS) battery	115
4.4	Nonlinear Control of Wind Farm BESS for Grid Connection.....	118
4.4.1	Control System Design Description	119
4.4.2	Proposed Prediction Model.....	121
4.4.3	Controller Design	122
4.5	Dynamic Control of Wind Farm BESS for Grid Connection	122
4.5.1	Dynamic model of the system.....	123
4.5.2	Reference Generator	125
4.5.3	Wind Power Prediction Model.....	126
4.5.4	Dynamic Controller design.....	128
4.6	Simulation.....	130
4.6.1	Scope	131

4.6.2	Data Collection	131
4.6.3	Battery Selection Type.....	137
4.6.4	Detailed DIgSILENT Simulation Model	138
4.6.5	Simulation Results and Discussion.....	162
4.7	Conclusion.....	189
CHAPTER 5. CONCLUSION, FINDINGS, RESEARCH CONTRIBUTION AND FURTHER REASEARCH.....		190
5.1	Salient findings of the study.....	190
5.2	Achievement of the aims and objectives of the study	191
5.3	Research Contribution	192
5.4	Further Research.....	193
REFERENCES.....		194
APPENDIX 1: CIRCUIT DIAGRAM.....		205
APPENDIX 2: AVERAGE POWER CURVE.....		206

LIST OF FIGURES

Figure 2-1: HAWT and VAWT (Gururaja Murthy.D, 2014)	13
Figure 2-2: HAWT Housing Construction layout (Onwunta, 2014)	13
Figure 2-3 Power Coefficient as function of Tip Speed ratio (Lackner, 2009)	18
Figure 2-4: Power curve (Onwunta, 2014)	18
Figure 2-5: Squirrel Cage Induction Generator (SCIG) (Onwunta, 2014)	21
Figure 2-6: Wound Rotor Induction Generator (WRIM) (Onwunta, 2014)	22
Figure 2-7: Doubly Fed Induction Generator (DFIG) (Onwunta, 2014).....	23
Figure 2-8 Hydraulic Pitch (Tong, 2010).....	25
Figure 2-9: Electrical Pitch (Tong, 2010)	26
Figure 2-10: On-shore and Off-shore (Ali Lorden, Drew Anderson, Luke Donahue, 2010)	29
Figure 2-11:Energy Storage Systems Classification (Zhao et al., 2015)	31
Figure 2-12:Technical maturity of EESS (Zhao et al., 2015)	32
Figure 2-13:Pumped-hydroelectric energy storage layout (Tong, 2010)	33
Figure 2-14: Compressed air energy storage facility (Mahlia et al., 2014)	35
Figure 2-15: Flywheel energy storage device (Tong, 2010)	37
Figure 2-16: Lead acid battery (Tong, 2010).....	40
Figure 2-17: Nickel-cadmium battery (Tong, 2010)	42
Figure 2-18: Sodium-sulphur battery (Tong, 2010).....	43

Figure 2-19: 6 MW, 8 h Sodium-sulphur energy storage facility in Tokyo, Japan (Tong, 2010)	44
Figure 2-20: Vanadium redox flow battery (Tong, 2010)	45
Figure 2-21: Polysulphide Sodium Bromide (Tong, 2010)	47
Figure 2-22: Zinc-bromine battery (Tong, 2010).....	49
Figure 2-23: Basic elements of a hydrogen energy storage system (HESS) (Ali, 2016)	51
Figure 2-24: Supercapacitor energy storage device (Tong, 2010)	53
Figure 2-25: Superconducting magnetic energy storage device(Tong, 2010)	54
Figure 2-26: minimum and maximum operating voltages (Eskom, 2019).....	70
Figure 2-27: Frequency operating range (Eskom, 2019)	72
Figure 2-28: Wind turbine with STATCOM (Farhad et al., 2015).....	73
Figure 2-29: SVC connected to wind farm (Shuchuang, 2015)	74
Figure 2-30: The electrical power system incorporating a wind energy farm(Shepherd & Zhang, 2011).....	76
Figure 2-31: The fixed-speed wind generator connected to a fixed voltage point (Shepherd & Zhang, 2011).....	77
Figure 2-32: Equivalent circuit of a disconnected induction generator(Shepherd & Zhang, 2011).....	81
Figure 2-33: Structure of wind farm with internal DC connection and energy storage (Tran & Khambadkone, 2012)	82

Figure 2-34: Equivalent diagram of wind farm with internal DC connection and energy storage(Tran & Khambadkone, 2012)	82
Figure 2-35: Structure of power control strategy (a) Constant power control (b) Variable power control (Tran & Khambadkone, 2012).....	85
Figure 2-36: Structure of constant current control strategy	87
Figure 2-37: The configuration of constant voltage control strategy	88
Figure 3-1: Cape Town wind farm and Acciona wind turbine (Acciona Windpower, 2011)	92
Figure 3-2: AW 3000 wind turbine (Acciona Windpower, 2011)	93
Figure 4-1: Effect of temperature on battery capacity (Zareifard, 2017)	112
Figure 4-2: Comparison between system size and battery discharge time (Zareifard, 2017)	116
Figure 4-3: A sample of 51MW and 34MW capability built-in NAS with a capability of 245 MWh (Zareifard, 2017).	117
Figure 4-4: Wind farm battery ESS connected to the Grid	119
Figure 4-5: Representation of wind vector (Zareifard, 2017)	121
Figure 4-6: Proposed control system block diagram (Taghi & Fard, 2017)	125
Figure 4-7: NWP Model scheme schematic (Khalid & Savkin, 2012)	127
Figure 4-8: Hourly Energy Production (Acciona Windpower, 2019)	132
Figure 4-9: Monthly Energy Production (Acciona Windpower, 2019)	132
Figure 4-10: 2019 Wind speed in respect to turbine Power January (Acciona Windpower, 2019)	134

Figure 4-11: 2019 Wind speed in respect to turbine Power February (Acciona Windpower, 2019)	134
Figure 4-12: 2019 Wind speed in respect to turbine Power March (Acciona Windpower, 2019)	135
Figure 4-13: 2019 Wind speed in respect to turbine Power April (Acciona Windpower, 2019)	135
Figure 4-14: 2019 Wind speed in respect to turbine Power May (Acciona Windpower, 2019)	136
Figure 4-15: 2019 Wind speed in respect to turbine Power June (Acciona Windpower, 2019)	136
Figure 4-16: Sodium-Sulfur (NAS) Package type unit (NGK Insulators, 2020).....	137
Figure 4-17: Blocks of the DFIG induction generator (A.D. Hansen et al., 2003)	140
Figure 4-18: Double-fed induction machine with rotor side converter induction unit (DIgSILENT GmbH, 2010)	141
Figure 4-19: Generic PWM converter model (DIgSILENT GmbH, 2010)	142
Figure 4-20: PWM converter model (DIgSILENT GmbH, 2010)	142
Figure 4-21: Capacitor bank in DIgSILENT (A.D. Hansen et al., 2003).....	144
Figure 4-22: Positive sequence : three windings transformer equivalent model (A.D. Hansen et al., 2003)	145
Figure 4-23: Zero sequence - grounded star/delta/delta connection (A.D. Hansen et al., 2003)	145
Figure 4-24: Zero sequence - grounded star/grounded star/delta connection (A.D. Hansen et al., 2003)	146

Figure 4-25: Zero sequence - grounded star/grounded star/ grounded star connection (A.D. Hansen et al., 2003)	146
Figure 4-26: Example of grid-connected wind turbine model (A.D. Hansen et al., 2003)	147
Figure 4-27: Simplified Battery Model in DSL (DIgSILENT GmbH, 2010)	149
Figure 4-28: Frame for the Battery Model in DSL.....	149
Figure 4-29: Equivalent Circuit of a PWM Converter (DIgSILENT GmbH, 2010)	150
Figure 4-30: Saturation of a VSC with Sinusoidal PWM (DIgSILENT GmbH, 2010)	151
Figure 4-31: Structure of the BESS	153
Figure 4-32: Frame for the BESS-Controller (*.BlkDef) (DIgSILENT GmbH, 2010)	153
Figure 4-33: Model of the Frequency Controller (*.BlkDef)	154
Figure 4-34: Model of the PQ-Controller (._BlkDef) (DIgSILENT GmbH, 2010)	155
Figure 4-35: Model of the Charge Controller (*.BlkDef) (DIgSILENT GmbH, 2010)	156
Figure 4-36: Composite Model of the Battery (*.ElmComp) (DIgSILENT GmbH, 2010)	157
Figure 4-37: Composite Model of the BESS Controller (*.ElmComp) (DIgSILENT GmbH, 2010).....	158
Figure 4-38: The BESS in the Single Line Diagram (DIgSILENT GmbH, 2010)	158
Figure 4-39: Grid side converter control (A.D. Hansen et al., 2003)	160
Figure 4-40: Grid side converter control in DIgSILENT (A.D. Hansen et al., 2003) .	161
Figure 4-41: Network Modelling on DIgSILENT.....	164

Figure 4-42: Edited Governor Controller for Dispatch Command (DlgSILENT GmbH, 2010)	168
Figure 4-43: Simulation results of Voltage Magnitude at POC	169
Figure 4-44: Simulation Results of frequency magnitude at POC	169
Figure 4-45: Voltage Magnitude of voltage at Grid bus	170
Figure 4-46: Simulation Results of frequency magnitude at Grid bus.....	170
Figure 4-47: Simulation results of Voltage Magnitude at POC bus results	171
Figure 4-48: Simulation results of Voltage Magnitude at POC bus results	171
Figure 4-49: Simulation results of Voltage Magnitude at Grid bus results	172
Figure 4-50: Simulation results of Voltage Magnitude at Grid busbar results	172
Figure 4-51: State of Charge (SOC).....	173
Figure 4-52: Battery Voltage.....	174
Figure 4-53: Battery Total active Power in MW	175
Figure 4-54: Voltage magnitude at POC busbar (bus)	176
Figure 4-55: Frequency at POC bus.....	176
Figure 4-56: Voltage Magnitude at Grid bus.....	177
Figure 4-57: Frequency at Grid bus.....	177
Figure 4-58: Wind Farm Active Power with and without BESS.....	178
Figure 4-59: Wind Farm Operating 50% Active Power with and without	179
Figure 4-60: Wind Farm Speed in pu with and without BESS	179
Figure 4-61: Grid: Active Power with and without BESS	180

Figure 4-62: Wind Farm: Active Power with and without BESS.....	180
Figure 4-63: Wind Farm: Active Power with and without BESS.....	180
Figure 4-64: Wind Farm: Speed in pu with and without BESS	181
Figure 4-65: Grid Active Power with and without BESS	181
Figure 4-66: Wind farm Active Power with and without BESS.....	183
Figure 4-67 Wind Farm Speed in pu with and without BESS	183
Figure 4-68: Grid Active Power with and without BESS	184
Figure 4-69: Wind farm : Active Power with and without BESS.....	184
Figure 4-70: Wind Farm Speed in pu with and without BESS	185
Figure 4-71: Grid Active Power with and without BESS	185

LIST OF TABLES

Table 2-1: Application of BESS (Abhinav & Pindoriya, 2016).....	61
Table 2-2: Minimum and maximum operating voltages (Eskom, 2019).....	69
Table 2-3: Maximum disconnection times (Eskom, 2019)	70
Table 4-1: Parameters of Battery Model (Zareifard, 2017)	114
Table 4-2: NAS Model Battery Parameters (Zareifard, 2017).....	117
Table 4-3: 2016 to 2019 January to June production average and Capacity factor (Acciona Windpower, 2019)	133
Table 4-4: 2019 January to June production average and Capacity factor (Acciona Windpower, 2019)	133
Table 4-5: Simulated Constraints Parameters (NGK Insulators, 2020)	138
Table 4-6: Battery Model in DSL parameter (DIgSILENT GmbH, 2010)	150

CHAPTER 1. GENERAL INTRODUCTION

1.1 Introduction

Electrical energy is a valuable basic human being need and, at the same time, a significant source of operation in corporate industries, agriculture, organizations, activities, machinery, residences, etc. There has been a rise in demand for electrical energy, which has forced the world to explore other alternative energy sources to meet demand, in addition to conventional energy sources such as coal and gas (SFGATE, 2011). Renewable Energy Sources (RES) such as Wind and Solar PV have been considered with substantial growth in large-scale production underway globally (International Energy Agency, 2016).

According to the Statistic Analysis of the World Energy Survey, the RES generation (not including hydro) increased by 14.1% in 2016, slightly below the 10-year average, but the largest increase reported (6 152 270 GWh). Wind energy contributed more than half of the growth and solar energy accounted for 18% of the total. Currently, China is the biggest renewable energy producer in the world (BP, 2017).

Wind Energy is South Africa's most accessible energy source and is located along the coast of the country. The projected average energy is lower than the United States of America and most European countries. The country's current average energy estimate is between 500MW and 1000MW. The country utility company (Eskom) carried out its first case study on wind energy at the Klipheuwel wind farm, located approximately 50 km north of Cape Town. The output of energy in the farm consists of a combined turbine capacity of 3.16MW, a single French Jeumont J48 750KW and a Danish Vestas V47 660KW. The plant was officially opened on 21 February 2003 (Onwunta, 2014).

The initial estimation of the farm capacity factor was 22 % and was favourable compared to California and Germany, which were 23 % and 22 % respectively. The country (South Africa) has exceptional capacity in terms of wind power generation, and wind power has moved from growth to deployment, making it one of the vibrant wind energy markets on the global stage. The first installation of 10MW of wind power took almost a decade and current output ranges from 3000MW to 500MW. The Sere wind farm of Eskom, located near Vredendal on the western coast of Cape Town, has thus far built 46 planned turbines. Wind power generation would add another 100MW to the national grid, saving almost 6Mt of GHG over a 20-year period. The wind farm will have a total of 46 Siemens 2.3VS-108 turbines, each capable of generating 2.3MW and covering a total area of 16km² (Onwunta, 2014).

The Department of Energy (DOE) launched an Integrated Resource Plan (IRP) for South Africa in collaboration with Government, Industry, Labour, Civil Society and Eskom to plan the implementation of a 17,800 MW renewable energy growth plan to be implemented by 2030 (Department of Energy, 2011). Forecast studies were performed in line with the IRP and, in 2017, Eskom released a study outlining the need for up to 2 GW of additional, regular balanced energy storage within the current grid. The incorporation of RESs into the grid does not provide a constant supply of electricity, because the output and input of RESs are variable and thus present some technical challenges to the power system.

Energy storage systems have been considered as a solution for storing and alleviating energy system challenges, subject to the comparison of various energy storage technologies and supplier products under South African environmental conditions, and to the identification of which products are appropriate for potential energy storage needs of IPPs and Eskom's (Admire Moyo, 2017).

1.2 Background of the research problem

Eskom has installed a BESS of 200 kW, 1.0 MWh of AfriDevo (a lithium ion battery developed by BYD of China) and a General Electric test unit to evaluate the best energy storage options for South Africa, although all major wind farms in South Africa have yet to be integrated with energy storage facilities (Admire Moyo, 2017). In South Africa, wind farm owners known as Independent Power Producers (IPP) have signed contracts with Eskom to sell them some of their wind farm electrical capacity. Most farms are not contracted to supply wind farm energy with their maximum potential (Eskom, 2013).

During high wind energy, the energy produced by the wind farm exceeds the Eskom agreement and the excess energy is wasted. Contrarily to the fact that during low wind energy below 5 m/s (10 mph) there will be no generation and the grid-connected device will result in energy instability and hence the farm will be disconnected from the grid (Burton et al., 2001).

Integrating a wind farm battery storage system may play a pivotal role in alleviating the problems described above during high wind generation in the storage of some energy and in a low wind power grid connected system for the supply of electrical energy. However, this can be easily managed during steady state or scheduled outages or maintenance.

The two main control systems of the wind turbine are the pitch control and the generator torque control, which play a key role in ensuring the optimization of the wind capture and stability of the connected grid system, as both systems (wind farm and grid) shift over time (steady state). Nevertheless, because the wind farm input and output are not constant, the integration of the storage system may pose technical challenges to the control system. When the rate of change is large, the systems are said to be dynamic systems (Shearer, 2013).

Dynamic management of interconnected grid-connected wind farm storage systems would therefore be necessary to ensure the mitigation of variable wind farm output variability and to maintain grid power stability.

1.3 Statement of the research problem

Whether dynamic control of integrated wind farm battery energy storage systems, mitigate fluctuations of wind farm variable output and maintain power stability for grid connection?

1.4 Research aim and objective

This research aims to investigate dynamic control model of an integrated wind farm battery energy storage for grid connection in South Africa. Subsequently to achieve this aim, the following objectives would be considered:

- i. Informative and Descriptive Literature Review;
- ii. Identify a suitable dynamic control system model and choose battery type for a South African Grid connected Wind Farm BESS;
- iii. Modelling of an integrated wind farm battery energy storage model for grid connection, and

- iv. Conduct a simulation as to investigate the effects and impacts of integrated wind farm battery energy storage for grid connection.

1.5 Delimitation of the research

The research will focus on large scale integrated wind farm battery energy storage system for grid connection. The study will review all the stationary, large scale EESSs that are capable to be integrated with a Wind Farm and support grid connection excluding thermal storage system, indirect storage systems, demand side management and smart electric vehicles.

The analysis will go up to point of grid connection but excluding the grid network. Large scale integrated power systems refer to a power 660kW and more.

The system considered is an integrated wind farm storage system with Double Fed Induction Generator, battery energy storage system and power electronics back to back converter topology used in Wind Energy Conversion System (WECS). The wind farm wind energy data that will be used is from South African wind farm location.

1.6 Research Methodology

The key concepts of electrical power generation, power system theory, power electronics, control theory and system modelling and simulation is necessary and must be properly incorporated into a research project of this type. The research will be a quantitative research which will presented in a numerical form.

A dynamic modelling for an integrated wind farm battery energy storage for grid connection will be investigated and the Bets law Betz limit which states that a turbine can never extract more than 59.3% power from an air stream will be considered.

Simulation of the systems would be conducted on DIgSILENT Power factory analysis, when analysing dynamic control of integrated wind farm battery energy storage system of a grid connected system. Analysis of the result will be conducted using characteristic curves. Thereafter a suitable dynamic control for an integrated wind farm battery energy storage for grid connection will be identified and recommended for South African wind farms.

1.7 Thesis Organisation

The thesis organisation structure is divided into five chapters and their brief description is provided below:

- **Chapter 1:** This chapter give a detail on introduction under study research topic, background of the research problem with statement research statement, research aim and objective, delimitation of the research and research methodology.
- **Chapter 2:** This chapter contains the literature reviewed for wind energy systems, electrical energy store systems, wind farm energy storage grid integration, automated system management and on-going research and experts and scholars' writings.
- **Chapter 3:** Provide an introduction of case study and operation of the ACCIONA WINDPOWER (AW) 3000 series wind turbine.
- **Chapter 4:** Presents the system modelling and simulation of the dynamic control of integrated wind farm storage systems for grid connection in South Africa, data collection, analysis, and interpretation of the results.

- **Chapter 5:** The conclusion of the research study, research contribution to the body of knowledge and provide recommendation of further areas of study to be considered for further research attention.

1.8 Conclusion

Chapter 1 offers a brief description of the Renewable Energy Sources (RES) in South Africa. The research problem and the statement of the research problem were identified from the background; the aim and objectives of the study were then carefully presented. This chapter also addresses the concept of study and ends with a thesis outline. The next chapter offers a study of literature.

CHAPTER 2. LITRATURE REVIEW

2.1 Introduction

This section summarizes the literature on the subject under discussion and covers the following topics:

- Wind Energy Systems
- Electrical Energy Storage Systems
- Grid integration of wind farms
- Control of Integrated Systems

The literature will cover an overview on these topics with an aim to assist what; current work being done, ongoing research being conducted, has been written by experts and scholars. Below is Wind farm literature review conducted on Wind Energy Systems, Electrical Energy Storage Systems (EESSs), Grid Integration of Wind Farm and BESS, Control of integrated Systems and Summary of the chapter.

2.2 Wind Energy Systems

2.2.1 Background

Wind energy is the cleanest and free renewable energy source that is abundant in windy areas (Union of concerned Scientist, 2014). The Wind energy depends, not directly from the sun's lighting rays. The sun's radiation is changed or converted into kinetic energy due to the imbalances of the latitudes along the atmospheric sphere (Edenhofer et al., 2011).The availability of the wind energy is immensely affected by the places earth's rotation, temperature gradients and the geographical features (Burton et al., 2001).

The wind energy production method requires that the kinetic energy must be changed to the useful energy for the process to reach its end stage. Consequently, the fundamental economics of producing electricity from the wind source has far reaching effects when compared to other production (conventional) methods currently employed. The wind energy is different from the wind speed. The wind turbines must be carefully chosen, as there is no useful power to derive from the wind at less than 5m/s (10 mph) wind speed. The strong winds (gusts) produce a huge power level, which leads to an exceed power capacity of the wind farm and sometimes to a loss of wind power (Burton et al., 2001).

Human beings since back then used the idea of wind energy to perform variety of useful tasks by means of converting the wind energy into useful mechanical energy and that makes the whole concept not new in the scientific world. The usage of mechanised useful energy does not date back more than a thousand years ago and concrete previous evidence explicitly supports the above mentioned fact (Onwunta, 2014).

The theory of Windmills dating back to over 2000 years supports (Stiebler, 2008). The wind energy was used by humans 4000 years ago (Gustavo & Gimenez, 2011). In comparison (Patel, 2005), wind power was first used 5000 years ago. Wind power comes from Asian human civilizations in China, India, Tibet, Persia and Afghanistan (Redlinger et al., 2016). Their belief is that the Hero of Alexandria, who demonstrated wind driven turbine horizontal axis, is the first evidence of the use of wind power.

The also state that profound evidence shows that Persians were using the vertical-axis equipment during the 17th century AD and that subsequently spread to Europeans countries. Grains were grinded by Europeans using the power of the wind energy and to pump the water during the 1700s and the 1800s.

The wind power energy was also used to make the electricity in the USA poor communities during the 1890 (Patel, 2005). King Hammurabi of the Babylon used wind energy to grow Mesopotamia in 1700 BC. Wind energy power was used to make flour by the Persians and others utilized it for transportation over the oceans. Seafaring was revolutionized by means of no longer applying having to apply strong power and currently human beings have utilized the wind energy power to produce electricity and pump water (Gustavo & Gimenez, 2011)

Europe erected several Dutch Windmills in different variants during the 17th -18th century. The Western Mill is another remarkable establishment in the 19th century which is found in the rural areas of the United States of America (Stiebler, 2008). The modern wind energy power converters were developed in the 1920s and they have found important application in the renewable energy sector (Patel, 2005).

Summary of the most crucial advantages of the wind power energy is as follows (Luta, 2014):

- The utility bills are saved substantially and not having to deal with plenty of power failures compared to the people who depends on conventional electricity.
- Producing an environmentally friendly and cost-efficient power at cost effective rates.
- Implementation of the system does not place the homes or building at any risk and when being undone leaves no adverse environmental effects at all.
- Turbines do not need personnel to operate them on a continuous time bases or frequent maintenance.
- The system provides a crucial alternative to the conventional way of production.

Disadvantages of the wind power energy are as follows (Luta, 2014):

- Changing wind energy with time,
- Killings of the birds,
- Too much noise from the wind,
- Worry of the remoteness of wind power sources,
- Turbines being struck by the ice falling on them and the interference of electrical or electronic signals, and
- The installation of wind energy turbine depends on the site location and height of it.

2.2.2 Wind Turbines

Wind Turbine is a machine that converts kinetic energy from wind to mechanical and electrical energy in succession. For the past 30 years, there have been a couple of advances in the design of wind turbine which has been a consequence of evolving modern technological developments. These advances are micrometeorology, aerodynamics and structural dynamics which contributed to annual increase estimate of 5 % of wind turbines energy yield.

The various developments of wind turbine design and manufacturing are to maximize the wind energy capture, minimize costs, and improve the wind turbine efficiency and reliability (Tong, 2010).

2.2.3 Classification of Wind turbines

Turbine generator configuration is used to classify wind turbines, turbine capacity, Power supply mode, and location of the turbine installation.

An understanding of wind energy extraction from Wind is fundamental to wind turbines design. The wind turbines comprise of mechanical and electrical components.

2.2.3.1 Vertical and horizontal axis wind turbines

The wind turbines can be divided into vertical and horizontal axis turbines, with a rotating axis of rotor blades. The horizontal axis wind turbines (HAWT) largely used for commercial purposes. HAWT are considered as the preferred type due to their low cost per unit power output. Other advantages include low cut-in speeds (making it easier to use in low wind areas), higher power densities and high turbine efficiency (Tong, 2010).

Vertical-axis wind turbines (VAWT) differ in that their axes are perpendicular to the ground. This makes the wind from every direction appropriate, so the turbine does not need yaw power. The key components of the turbine can be set up on the ground, including the gearbox and the wind generator, simplifying the design and construction of the tower, minimizing the cost of the turbine. Vertical-axis turbines use an external source of energy to initialize blade rotation and since this is assisted only in one part of the world, the height of the tower must be decreased.

This lower power efficiency gives the horizontal-axis turbines the preference over the vertical-axis turbines (Tong, 2010). HAWT are used for commercial purposes therefore this research focuses on HAWT wind turbine (Burton et al., 2001). The below Figure 2-1, shows connection HAWT and VAWT.



Figure 2-1: HAWT and VAWT (Gururaja Murthy.D, 2014)

In this study HAWT Wind turbines are being used and the next section describes HAWT Wind turbine configuration in detail.

2.2.3.2 HAWT Configuration

There are three blades typically found in a modern large HAWT. The components of a modern, horizontal wind turbine with a transmission box in Figure 2-2 are shown.

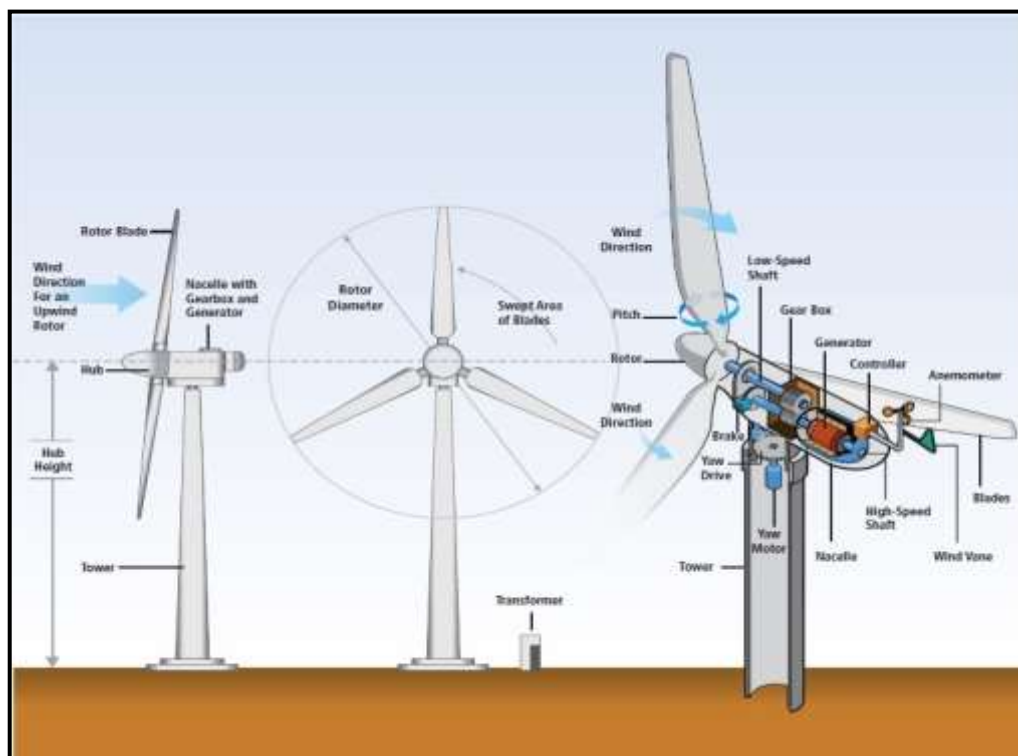


Figure 2-2: HAWT Housing Construction layout (Onwunta, 2014)

According, Burton *et al.*, (2001) rotor diameter gives the area consumed for available wind energy. The blades are connected to a hub, which is connected to a rotor shaft (some authors call it a Low speed shaft or main shaft) (Energy.Gov, 2013). Rotational speed will depend on blades connection, number of blades, and wind speed (P. C. Sen, 1997). Low speed shaft transfers kinetic energy to the gearbox. Gear box increases the speed from low speed shaft to high speed shaft. Brake slowing and halting turbine by converting kinetic energy to heat (Energy.Gov, 2013).

High speed shaft turns the generator to create electrical energy. Generator converts kinetic energy from the wind into electrical energy. Housing (some authors call it Nacelle) is suspended by tower and protects the wind system parameters hub, shafts, gearbox, brake, and generator. The tower height above the ground plays paramount role since the wind speed is directly proportional with height above the ground (Burton *et al.*, 2001).

2.2.3.3 Wind turbines capacity

Wind energy powered turbines can be classified in many ways such as in small to ultra-large turbines. Turbine with output of less several watts can be defined to be falling under the micro turbines since there is no clear definition of such turbines. Micro wind energy powered turbines are most suitable to remote places where there is no access to the national grid lines. These turbines are very crucial in developing countries since they can be used on per-structure setup to perform different functions. Micro turbines can be used in most areas around the globe because of their low wind energy start-up requirement and medium wind energy to maintain their operation (Tong, 2010).

Micro wind powered turbines can increase the supply of electricity but do not increase the transmission line's capacity.

Typical micro wind powered turbines have power output in the region of 100KW-1MW and can be utilized on-grid or off-grid for hybrid systems, village power and wind farms. Wind turbines having output power of up to 10MW can be categorised as large wind turbines. Large wind powered turbines are mostly suited at the off-shore wind farms and are currently of great interest in the research field and the international markets (Tong, 2010).

2.2.3.4 Classification of horizontal wind turbines

An additional classification of horizontal wind turbines can be described based on the configuration of the wind rotor in the direction of flow. The turbines may be wind turbines up or down. The upwind configuration is what is seen on most HAWTs where the rotors face the wind. This helps the flow field not to be skewed when the wind passes through the wind tower and the nacelle. The reverse is seen in a downwind turbine where the wind passes through the nacelle in front of the tower and then through the rotor blades. In this configuration, the rotor blades can be made more flexible and the tower strike would not have to be considered. (Tong, 2010).

The power supply of a wind turbine is influenced by the distortion behind the tower and nacelle by the unstable wakes. An additional cause of this unstable flow are aerodynamic losses and fatigue loads. The blades can also make higher pulse noises (Tong, 2010).

2.2.3.5 Wind turbines drivetrain

In a wind generation system, the wind turbines are classified as geared or direct drivetrains. A cross-stage geared drive wind has a gearbox to turn the low speed shaft into a fast rotation on the high-speed shaft to achieve high power output.

The benefits of using the drive system are lower costs, smaller weights and less reliability, increased noise levels and mechanical loss. The disadvantages are less reliability. The direct drive of the shaft on the other hand is directly connected to the blade rotor. Energy performance, durability and design simplicity are the benefits of this approach and costs and weight are the disadvantages (Tong, 2010).

2.2.3.6 Application of wind turbines

There are either off-grid or on-grid wind turbine applications. The former is the kind of wind turbine application that is found in residential areas, farms, and telecommunications. These are smaller wind turbines which can sometimes pose a challenge of storing the power generated from the turbines. The downside to using intermittent power sources of this kind is that they can drastically change at any given time. To mitigate this, batteries and generators are often used to stabilize the availability of the supply of the power produced by these turbines. In contrast, the larger sized wind turbines are used in grid tied applications where the storage of the energy or power used (Tong, 2010).

2.2.4 Wind power parameters

The wind power parameters, mathematical representation and graphic representations for wind power captured in this section are discussed. The wind turbine is a wind energy converter which draws energy from the swept area of the blades and, more power is obtained from the blades' diameter. The wind power is supplied by the kinetic energy per unit time of the moving air mass (Martin O. L., 2008). The mathematical representations are:

$$P_{air} = 0.5m*V^2 = 0.5*\rho*A*V^3 \quad (2.1)$$

From (2.1) the equation, P_{air} is wind power (in watt), ρ is air density, A is a swept field, (m^2), and V_{∞} is a wind velocity without any interference to the rotor, i.e. the velocity of wind at infinite distance from the rotor blades (Martin O. L., 2008).

The power available from the wind is given by the formula below (Martin O. L., 2008):

$$P_{air} = 0.5 \cdot \rho \cdot A \cdot V^3 \quad (2.2)$$

Equation (2.2), gives the available power in the wind and is reduced by a quantity called Power Coefficient C_P which is given by: (Martin O. L., 2008):

$$C_P = P_{wind\ turbine} / P_{air} \quad (2.3)$$

Therefore:

$$P_{wind\ turbine} = 0.5 \cdot \rho \cdot C_P \cdot A \cdot V^3 \quad (2.4)$$

Power Coefficient maximum value is defined by the Betz limit which states that a turbine can never extract more than 59.3% power from an air stream. The C_P values range between 25-45 % for wind turbine rotors. (Martin O. L., 2008). The tip speed is the tangential velocity of the rotor at the tip of the blades measured in m/s. Mathematically, it is the product of angular velocity, ω (rad/s) of the rotor and the tip radius R in m (Martin O. L., 2008):

$$\text{i.e. } V = \omega \cdot R. \quad (2.5)$$

Tip Speed ratio: It is defined as:

$$\lambda = \omega \cdot R / V \quad (2.6)$$

Solidity: Defines the proportion of solid with respect to swept area, i.e. high strength wind turbines are wind turbines with a greater number of blades and vice versa. Modern wind turbine electricity generation has low power rotors (Martin O. L., 2008).

Two important non-dimensional numbers (Lackner, 2009):

Tip Speed Ratio

Power Coefficient

$$\lambda = \omega * R / V$$

$$C_P = P_{\text{wind turbine}} / (16/27)0.5 * \rho * A * V^3$$

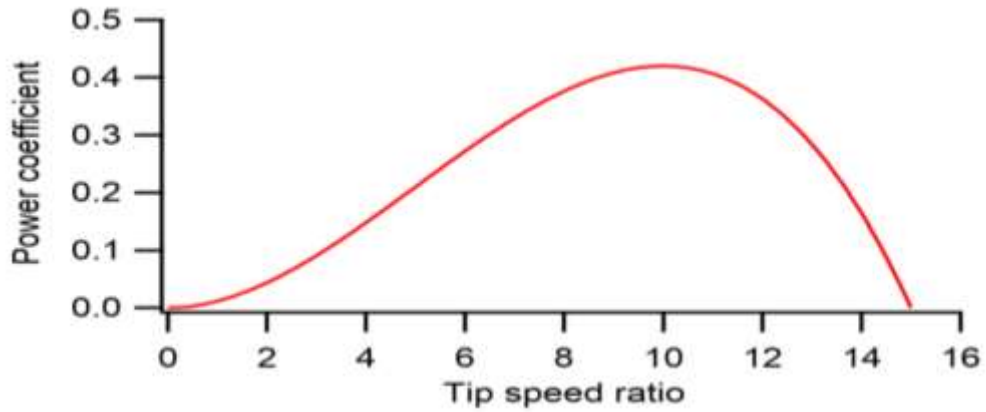


Figure 2-3 Power Coefficient as function of Tip Speed ratio (Lackner, 2009)

In Figure 2-3, a three-bladed rotor is shown graphically for the C_p as a function of the speed ratio of the tip. As the wind speed increases, the speed of the rotor increases, the maximum power extraction occurs at the optimum rate of tip speed. The rate of tip speed is not constant, causing undetected power, and the various designs have losses and inherent inefficiencies (Ragheb, 2014).

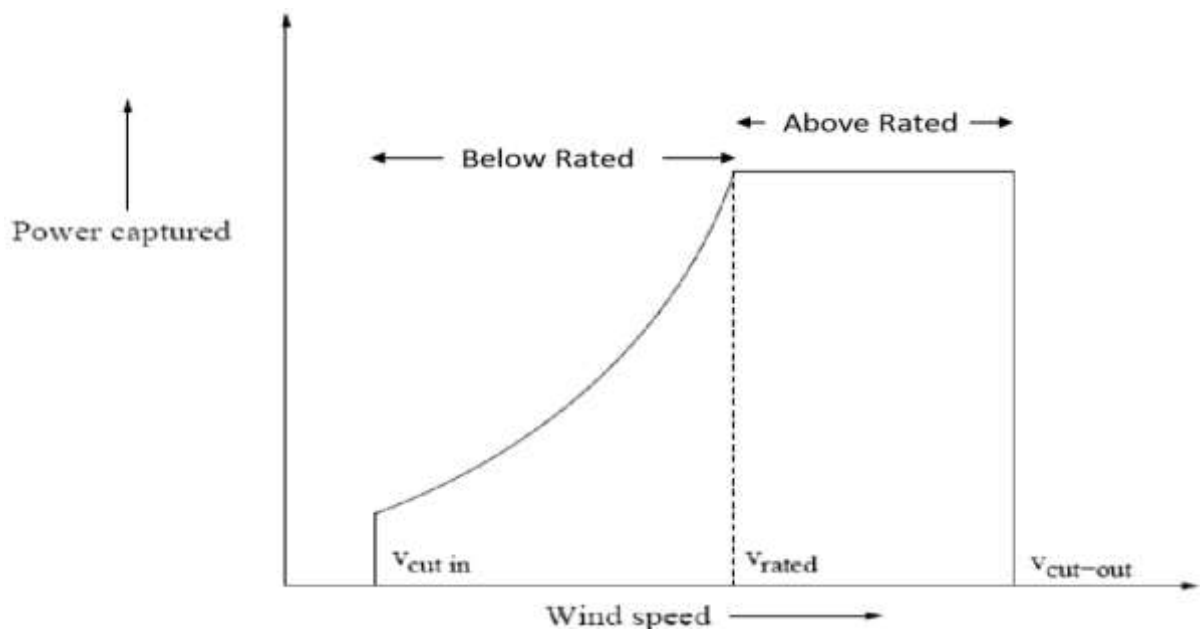


Figure 2-4: Power curve (Onwunta, 2014)

The output of the wind turbine varies with the wind speed and the wind turbine power curve. An example of this curve is shown in Figure 2-4. Measurements are typically taken from the field and the graphic power curves are measured. Cut-in speed occurs at low wind speeds and is noticeable as the wind turbine begins to generate usable electricity. The output power increases as the wind speed continues to rise until the output power reaches the rated power of the wind turbine. Instead, the speed of wind is said to have been rated at this point. At rated speed, the power control is enabled if the increase in the wind speed does not increase the power output. Cut-out speed happens when the wind is high, potentially damaging to the wind turbine, and the wind turbine must be shut down immediately to prevent damage to the wind turbine (Onwunta, 2014; Tong, 2010).

According to (Lackner, 2009), in practice, the rise in the wind rate causes the rotor to spin slowly, the aerodynamic torque increases, and the torque is increased so that more power is obtained. The amount of wind power that can be generated therefore depends on three factors: wind turbine blade aerodynamics; generator use, control systems synchronization (data input pitch control, generator voltage and current) for the mitigation of wind turbine load (Aerodynamics).

2.2.4.1 Wind turbine capacity factor

Wind turbines do not produce continuous electricity. The capacity factor thus accounts for the estimation of the wind turbine output for a given period, divided by its output if the turbine has worked for the whole time (e.g. daily, weekly, yearly, etc.). The average capacity factor is 0.25-0.30 and the excellent capacity factor is approximately 0.40. The average speed directly affects the wind turbine capacity factor (Tong, 2010).

2.2.5 Wind turbine generators and power electronics converters topologies

Various generator types and power electronics converters are the topologies used by the Wind Energy Conversion System. The two main generators are Synchronous Generator and Induction Generator, (Tripathy & Rourkela, 2014). The most different topologies for power translators are Soft Starter, Diode Corrector, Back-to - Back Convert, Multilevel Converter, Mattress, Resonant Converter and B-4 Converter (Gupta et al., 2013).

The research is however based on induction generators. Only induction generators with a back-to - back converter are examined.

2.2.5.1 Induction Generator

Induction machine is an alternating current (ac) electrical machine. It consists of stator winding and rotor winding with both windings carry ac currents. The induction machine can operate as induction motor or induction generator (P. C. Sen, 1997).

The induction machine runs as an induction generator when the rotor speed is higher than the synchronous speed and thus transformed the input mechanical energy as electricity from the primary mover (P. C. Sen, 1997).

According to, Tripathy and Rourkela, (2014) there are three types used in induction generators for WECS;

- i. Squirrel Cage Induction Generator (SCIG)
- ii. Wound rotor Induction Generator (WRIM)
- iii. Double Fed Induction Generator (DFIG)

2.2.5.1.1 Squirrel Cage Induction Generator (SCIG)

A SCIG is directly connected to an electric grid using a step-up power transformer (as seen in Figure 2-5). This constant-speed wind energy turbine can also limit power output when an active stall control is used. The advantage of having these kinds of constant-speed systems are low cost and simplicity, where the disadvantages and limitations are that a stiff grid with fixed voltage.

The frequency is needed, there is a difficulty in supporting different wind speeds and the structures need to be larger mechanically so that the mechanical structures can be supported when there are large wind gusts (Polinder, 2011).

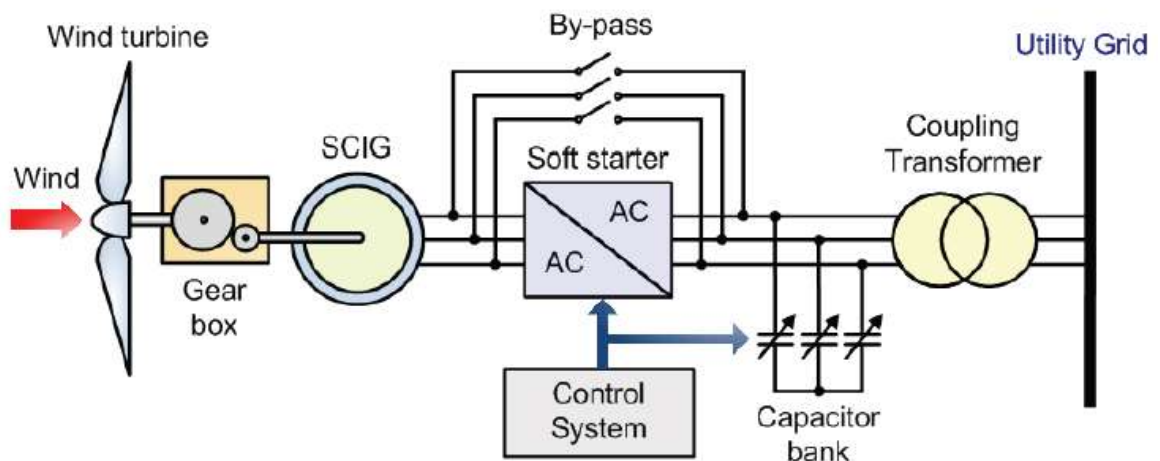


Figure 2-5: Squirrel Cage Induction Generator (SCIG) (Onwunta, 2014)

Starting the induction machine “across-the-line” poses another challenge in that the excitation field has a large reactive power and large currents are drawn by the machine whenever it is started. A soft starter is therefore used to minimise these effects, together with the use of capacitor banks within the turbine (Glushakow, 2007; Onwunta, 2014).

2.2.5.1.2 Wound rotor Induction Generator (WRIM)

The Danish Vestas Wind Systems manufacturer has used WRIG since the mid-1990s. This system is intended to include wind turbines with variable rotor resistance regulated by varying speed (structure shown in Figure 2-6) (Gupta et al., 2013; Tripathy & Rourkela, 2014).

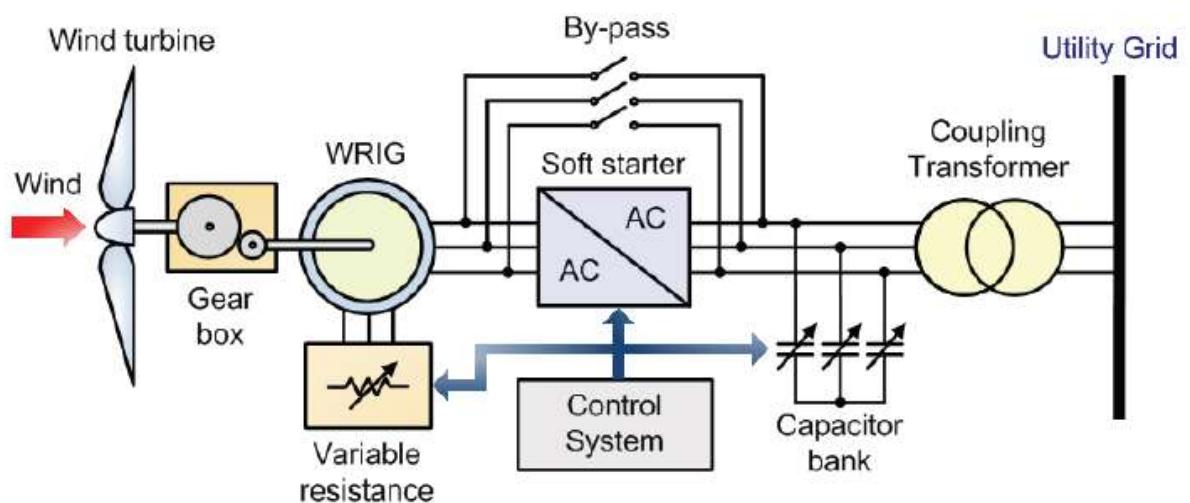


Figure 2-6: Wound Rotor Induction Generator (WRIM) (Onwunta, 2014)

To control the output power and the generator speed, the total rotor resistance needs to be varied. This is done by the direct connection of the generator winding stator to the grid and the series winding of the rotor with controlled resistance. Therefore, the range is between 0% and 10% higher than the synchronous rate. The power can then "expand" and slip by adding the rotor circuit resistance. When added to the rotor resistance, the turbine then needs to spin even faster to attain the same power output. Through the blade pitch mechanisms and the Turbine activity at the tip speed ratio, the speed can be controlled better, and the best energy capture achieved. The rotor resistance can lose power in the form of heat. (Gupta et al., 2013; Onwunta, 2014).

2.2.5.1.3 Double Fed Induction Generator (DFIG)

Wind turbine systems with variable speed are double-fed induction generators. This is the third type of Wind Turbine which, while the most expensive, is becoming increasingly popular with Type 1 and Type 2 turbines.

As shown in Figure 2-7, the stator winding is directly connected to the grid and the electronic converter that gives the rotor winding power is about 30 percent of the rated power rating. (Glushakow, 2007; Gupta et al., 2013; Onwunta, 2014).

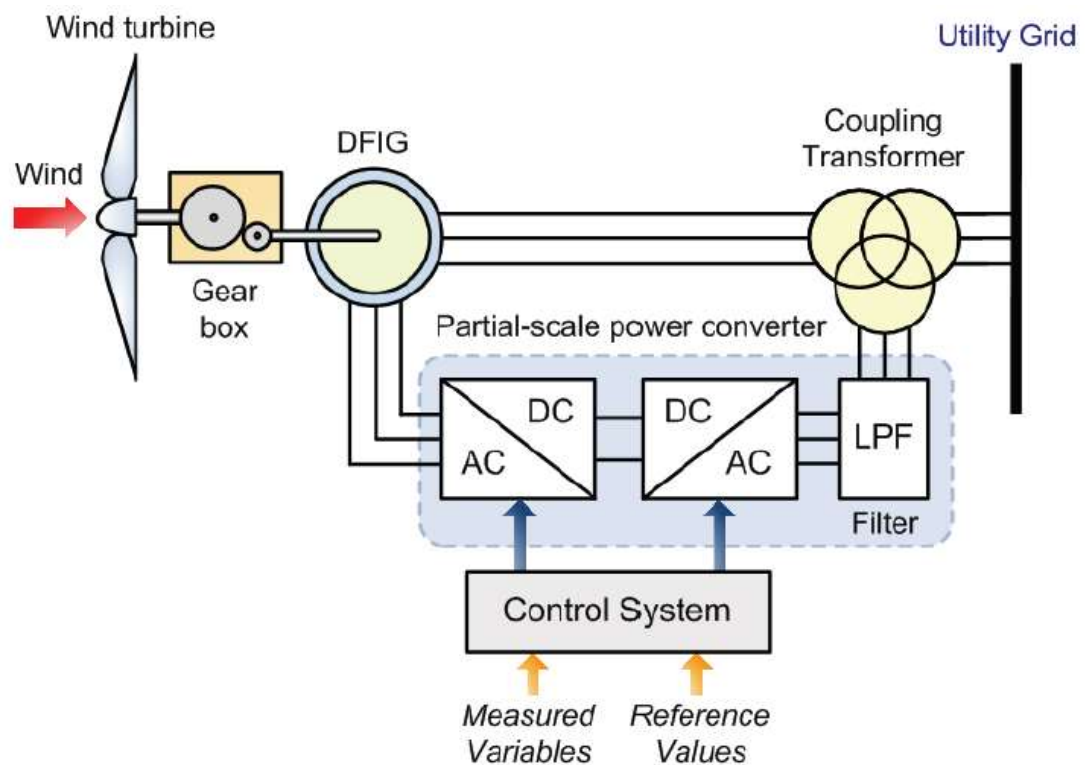


Figure 2-7: Doubly Fed Induction Generator (DFIG) (Onwunta, 2014).

However, slip rings must be used and this involves brushes and maintenance and, given that complex protection is needed in the event of grid faults, this may create a difficulty in the use of this type of wind turbine. What makes up for these drawbacks is that DFIG can provide separate real and reactive power controls that allow for more conventional synchronous control while still running asynchronous.

The advantage of using these control systems is that the devices can be comparatively more controlled during grid disruptions as the reaction of the torque generating rotor flux components is quicker (Conroy & Watson, 2009; Gupta et al., 2013; Onwunta, 2014). DFIG is commonly used type for large WECS and in this study, they will be used, therefore in this literature DFIG with back to back converter will be further studied in detail on the Grid connected system section.

2.2.6 Wind Turbines Control

Right control systems must be in place to ensure that wind turbines are efficient, secure, and capable of maximizing the capture of wind energy. The main control systems in modern wind turbines are pitch control, passive and active stall control, yaw control and others. Power management is critical to ensure that the wind turbine is able to withstand varying types of wind speed conditions where the turbine is likely to exceed its rated power output and potentially cause structural damage due to high wind speed conditions. The two main strategies for controlling power are pitch and stall control. (Korobatov et al., 2017; Leithead & Stock, 2016; Tong, 2010).

2.2.6.1 Pitch control

To achieve the correct certain rotor speeds and power output of wind turbines the correct blade angle should be optimized. This is a vital part in control of modern wind turbines. Optimizing blade angle also serves as the security system when there are higher wind speeds or in emergency situations. Backup batteries, mechanical energy storage devices or capacitors may be used to drive the blades to their feathered positions whenever there is a grid power failure (Murad et al., 2017; Tong, 2010).

Hydraulic actuators were previously used to control the blade pitch of all the blades at the same time.

The challenge with this technique is the wind speed being proportional to the height of the turbine tower, which means that the individual blades experience different wind turbulence depending on their position. This results in a need for techniques which can present individual blade control. The techniques employed currently allow for control of asymmetric and aerodynamic loads on each of the blades and can also support the larger, static, and more rigid structures of the tower (Murad et al., 2017; Tong, 2010). Each blade in this system is fitted with its own actuator, sensor, and controller. Hydraulic and electronic controlled systems are the two types of pitch control systems. Hydraulic control systems have traditionally been the most common due to high driving strength, lack of gearbox and high backup power. Figure 2-8 demonstrates how a hydraulic actuator uses a pitch mechanism to rotate a blade with its centreline (Korobatov et al., 2017; Tong, 2010).

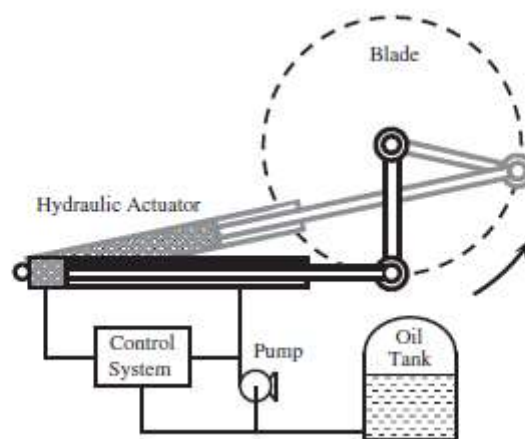


Figure 2-8 Hydraulic Pitch (Tong, 2010)

Electronic pitch control systems are the replacement for hydraulic pitch control systems. One of the benefits of this type of control system is that it has a limited effect on the environment compared to the hydraulic system that can spill or leak hydraulic fluid. Electronic control systems are much more powerful than the hydraulic system.

Figure 2-9 demonstrates how the engine is linked to the gearbox to lower the engine speed for more precise control. Both the responsiveness rate and the sensitivity of the blade pitch control can be increased by using electronic motors. The internal ring gear is connected to the roof of the rotor blade and the drive pinion is engaged. The belt-drive structure is used as an option in other wind turbines to change the pitch angle. Redundant pitch control systems have been suggested for use in large wind turbines to increase the stability of turbines in service. (Leithead & Stock, 2016; Tong, 2010).

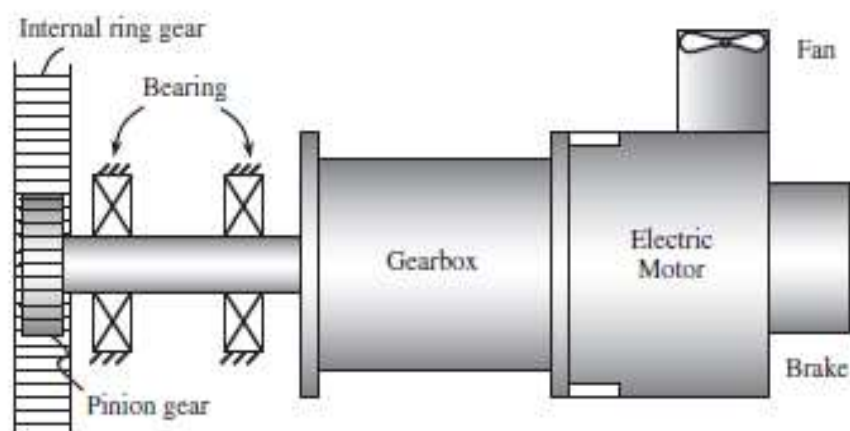


Figure 2-9: Electrical Pitch (Tong, 2010)

2.2.6.2 Stall Control

In addition to pitch control, stall control is another approach to wind turbines control and safety. The principle of the stop control system is that after rated rpm, power is controlled by the stalling of the blades. Control stables can be further broken down into passive and active control procedures. The key application of the passive stack control is wind turbines in which the blades are bolted at a set installation angle to the core. The power control system relies on the aerodynamic features on blades in a passive stall-regulated wind turbine. The turbine works near optimum efficiency at low to moderate wind speeds (Korobatov et al., 2017; Tong, 2010; N. Wang, 2018).

The turbine will be automatically operated at high wind speeds using stalled blades, which minimize the speed of rotation and the energy output to protect the turbine against extreme wind speeds (Tong, 2010).

A passive stall control system has a simple structure in comparison with a pitch control and avoids the use of a complex control system which leads to a highly reliable control system. Moreover, for stall operated turbines the power fluctuations are smaller. However, it does have some drawbacks, such as lower performance, the necessity of external turbine starting equipment, larger dynamic blade loads, nacelle and tower loads, reliable operational safety brakes (Tong, 2010; N. Wang, 2018).

This check technique was therefore used mainly in small and medium-sized wind turbines. With wind turbines in recent years joining the Multi-megawatt power range, the wind power industry has now dominated pitch regulation. For large wind turbines, the active stall control technology has been developed. The stalling blades along with a blade pitch mechanism are in an active wind turbine. As the blades are rotated at high wind speeds to their standing location, this control method is also known as a negative pitch control for pitch control systems in an opposite direction. (Tong, 2010; N. Wang, 2018).

The active controller controls the power output more precisely than the passive stall control and maintains the rated potential at high wind speeds. Thus, active stall control mode increases turbine costs with added pitch control function, decreasing operating performance. The pitch regulation is more advantageous with megawatts from the late 1990s than the traditional control of the markets for wind turbines. It has been stated that four times the number of stall-controlled turbines, and this trend will continue in the coming decades (Tong, 2010; N. Wang, 2018).

2.2.6.3 Yaw control

A horizontal wind turbine must be coordinated with the rotor wind via an active yaw control system to maximize the wind energy and to reduce the asymmetrical load on the rotor blades and tower. The lagoon system can be used electrically and hydraulically as wind pitch systems. During the earliest wind turbine development period, hydraulic logout systems were commonly used. Electric motors are used in modern wind turbines (N. Wang, 2018).

The Yaw control is normally a gearbox electric motor, an electric bull connected to the mast, a wind screen to provide the wind directions, a lay-out deck, and a brake to lock the turbine securely into the place of lay-off. Driving a heavy nacelle on a big turbine, with high driving loads, may be using two or more yaw engines. Laga error signals are used in the measurement of the lake 's average angle at a short interval. When the average yaw angle reaches the pre-set threshold, the Yaw motor is enabled to adjust the turbine to the wind direction. As a result, the measurement of wind direction with a high filtering is very small and slow (Korobatov et al., 2017; Tong, 2010; N. Wang, 2018).

2.2.6.4 Other control approaches

At the early stage of the turbine design, ailerons were used once to control the power output. This technique involves placing rotating flaps on the tip of the rotor blade. The ailerons adjust the blade lifting and drag properties and adjust the torque to allow control of the rotor speed and rotor power output. However, this system was less popular and was soon discontinued. The rotor can also be partially disconnected from the wind for power reduction. In practice, this yaw control technique is only used for small wind turbines (> 1 kW) (Tong, 2010; N. Wang, 2018).

2.2.7 Wind Farm

Wind farm is a site or location where multiple of wind turbines are integrated to produce electrical energy. There are two types of wind farm location which are on-shore and off-shore. On-shore refers to mounting turbines under earth and off-shore refers to mounting turbines underneath sea or ocean (Nate Richards, 2013).



Figure 2-10: On-shore and Off-shore (Ali Lorden, Drew Anderson, Luke Donahue, 2010)

The obvious differences between the offshore and onshore wind turbines have to do with the location being the best for how the turbines power outputs can be optimized. The advantages of using onshore wind turbines are primarily about cost and maintenance. It is easier to integrate these with already existing electrical networks and the convenience of having access to them when maintenance and repairs need to be done give them the advantage over offshore wind turbines.

Offshore wind turbines however can yield a greater output of energy as compared to the onshore turbines since they can receive greater amounts of wind (both in intensity and continuity). Another advantage to offshore turbines is that the environmental restrictions are more relaxed than onshore sites (Tong, 2010).

2.3 Electrical Energy Storage Systems (EESSs)

2.3.1 Background

Large, centralized, and highly predictable power stations supply traditional electricity grids. An inherent characteristic of such networks is that demand must always be balanced by supply. Supply balancing demand on a network typically involves backup power sources, such as an open-cycle gas turbine or a storage facility. Wind power is erratic, volatile, and potentially non-dispatchable (cannot be converted to 'on demand'). As a result, as the proportion of wind generation in the system increases, the need for such backup sources of power increases. To reduce fuel requirements, it is desirable that the backup source be a storage facility instead of more primary generation. The various options for electricity storage in this chapter will be discussed, including both large-scale centralized storage and small-scale distributed storage. (Tong, 2010).

Electrical energy storage systems are electrical technologies that store energy by absorption (charge) and discharge. Electrical energy can be saved in numerous ways, including mechanical, electromagnetic, chemical, thermal , and electrochemical (Zhao et al., 2015). Below Figure 2-11, shows how electrical energy are classified.

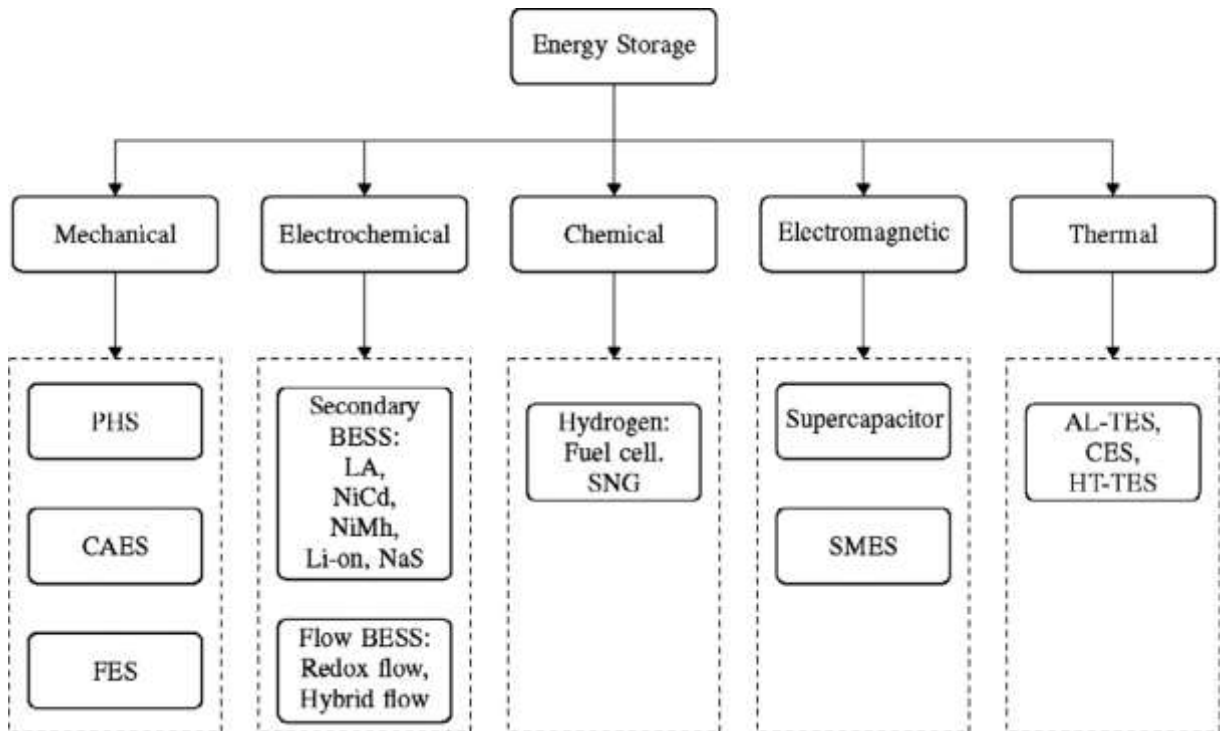


Figure 2-11:Energy Storage Systems Classification (Zhao et al., 2015)

According to research study of Zhao *et al.*, (2015) some of the other EESSs shown in the above Figure 2-11 they are either under development or theoretically developed, but still not commonly used: Fuel Cell (FC), Metal – Air (MA), Solar Fuel, Cryogenic Energy Storage (CES), SNG and Thermal Energy Storage (TES), below Figure 2-12: provides technical maturity of different types of EESSs showed on below bar chart.

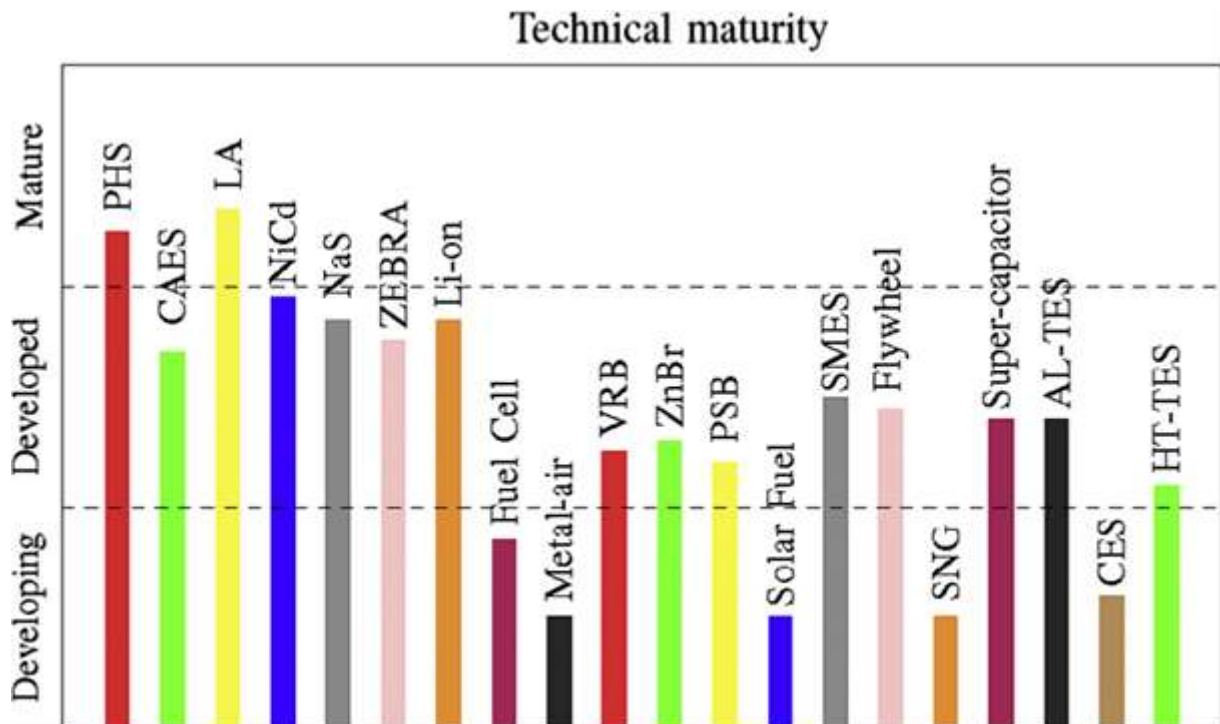


Figure 2-12: Technical maturity of EESS (Zhao et al., 2015)

As demonstrated on the above Figure 2-12, that some of EESS are still indeed either developed or technically developed. As mentioned in Chapter 1, in the section of the delimitation of the research, that this study will exclude thermal storage system, indirect storage systems, demand side management and smart electric vehicles. Then in this section, a brief description principle and capability of the commonly used EESS for large scale integrated, Wind Farm EESS for grid connection are presented below.

2.3.2 Pumped Hydro

PHES is the most innovative and highest available volume storage technology. In a single system built for this purpose, a pump and a turbine have been integrated. There are two large reservoirs situated at various elevations in the pumped hydro storage system and multiple pump turbine units (see Figure 2-13). Water is pumped from the lower to higher reservoirs during off peak, and there is a method of energy charging.

The water is discharged from the high to a low tank during release through the hydro-turbines attached to the generators, generating electricity (Zakeri & Syri, 2015). The power output of the running pumped storage systems at the top with more modern units ranges from 50% to 85%. However, this is now being enhanced with variable speed machines. The efficiency is limited by the efficiency of the pump / turbine unit used in the installations. Until recently, fresh water was used as a storage medium for PHES units.

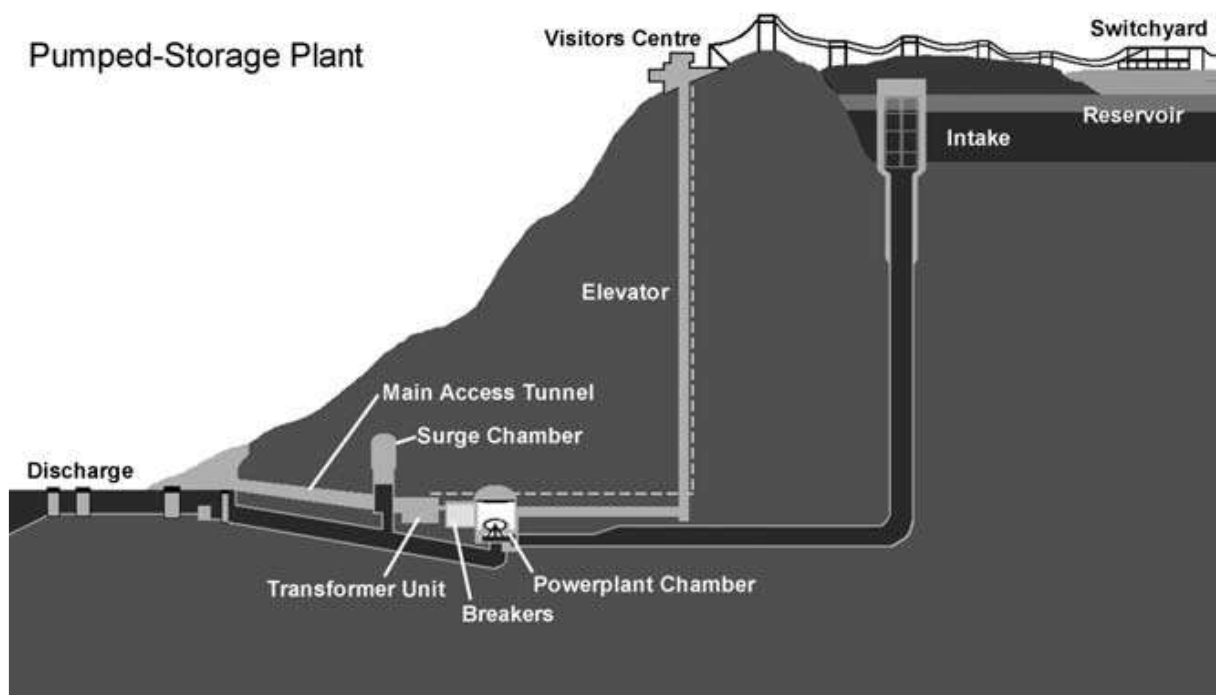


Figure 2-13:Pumped-hydroelectric energy storage layout (Tong, 2010)

2.3.2.1 Application

PHES also has a fast response time close to the large storage space, which makes them suitable for load-bearing applications because the plant can vary its effective burden in negative (generational) directions from full-name plate ratings in a positive (pumping) direction to full nominee plate ratings.

Equipment can react from full shutdown (or reverse-up) to full power for up to 10 minutes. In addition, when standby it can also reach maximum power within 10–30s. Further, PHES systems can now be used in pumping and generating modes for frequency regulations with the recent implementation of variable speed engines (The modes used in generation mode were always available) (Tong, 2010; Zakeri & Syri, 2015).

This helps PHES units to consume power more economically, making the facility not only more useful, but also enhancing its performance by about 3 percent and extending the service life of the facility. Due to its high-power capacity and ample download time, PHES may also be used for high and black beginning generations (start generations without the access of other units in the grid to a main frequency). Finally, during off-peak production, PHES supplies a load for base load generation plants which can prevent the cycling of these units to boost their lives and efficiency (Tong, 2010; Zakeri & Syri, 2015).

2.3.3 Compressed Air Energy Storage (CAES)

The CAES is a proven technology used for various industrial applications since the 19th century. Electrical compressors are used to compress air and hold it in a subterranean structure or in a vessel or pipeline system above ground (Salt Caverns, Rock Structures). When required the compressed air has been released into a modified gas turbine and combined with natural gas, burned, and extended. Consequently, CAES is pre-compressing and storing air in large storage tanks using electrical energy taken out of the grid to drive a motor (instead of the GAT). GT provides power during peak hours, releasing and using the compressed air from the storage plant during the GT period (see Figure 2-14) (Mahlia et al., 2014; Zakeri & Syri, 2015).

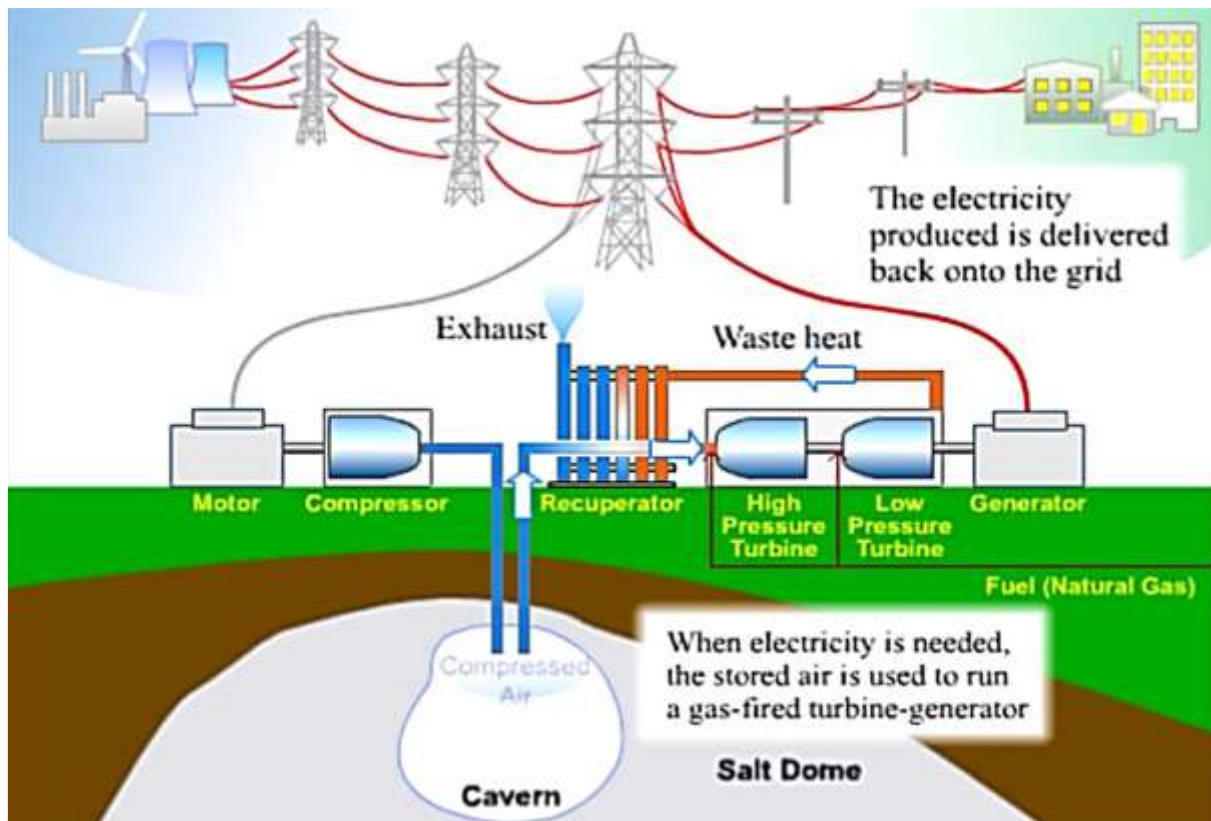


Figure 2-14: Compressed air energy storage facility (Mahlia et al., 2014)

This means that cheaper off-peak base energy can be used rather than costly gas to compress the air. As air is expelled from the cavern, however, it must be mixed before entering the turbine with a small amount of gas. Without gas applied, it would be troublesome to add a temperature and air pressure. The air temperature would be much too low for materials and connections to withstand if the pressure used alone were sufficiently strong for a substantial power output to achieve. The amount of gas needed to generate the same amount of natural gas can be generated by a GT that works with CAES simultaneously, 3 times as much power as a GT that runs alone (Mahlia et al., 2014; Tong, 2010).

CAES uses both electric power and coal, making it difficult to predict its performance. The efficiency of the entire cycle is calculated to be between 64% to 75%. In the 50-300 MW area, typical CAES plant capacity.

The life cycle of such plants is much longer than the current GT's and the charging / discharge ratio depends on the compressor size used along with the reservoir 's size and pressure (Tong, 2010).

2.3.3.1 Application

CAES is the only storage technology other than PHES that is incredibly large. CAES typically has a quick reaction time, with 0-100% in less than 10 minutes, 10-100% in 4 minutes and 50%-100% in less than 15s. It is therefore desirable to act as a broad sink for the supply and demand of bulk energy and can therefore carry out daily start-ups and shutdowns. Moreover, due to a reduction of the air density the standard GT experiences a decrease of 10 % of its efficiency by 5° C. To prevent them from suffering from this effect, CAES uses compressed air (Mahlia et al., 2014; Tong, 2010).

Traditional GTs are frequently exposed to excessive heat in part load operations and CAES systems do not. CAES can be used for auxiliary facilities, including frequency management, load monitoring and voltage control with this flexibility. As a result, CAES has become a major player in the energy storage sector in the wind industry. A variety of options, including mergers of a CAES plant with several wind farms in the same region, are being considered. To compress air from the CAES plant excessive off-power of these wind farms could be used. The Municipal Association of Iowa is currently preparing a similar project (Mahlia et al., 2014; Tong, 2010).

2.3.4 Flywheel Energy storage (FES)

The FES stored rotational energy in a massively spinning cylinder accelerated rotor. The principal components are a revolving cylinder in the compartment, bearings, and a shaft (which is composed of a rim fixed to a shaft).

To prevent wind loss, all the structure is packed into a vacuum jar. The rotor is speeds to a very high-speed during charging phase that can reach between 20,000 and over 50,000 rpm. By holding the spinning bottom constantly fast, the energy is stored in the flywheel. The flywheel releases energy during the discharge process and drives the unit as a generator (Kintner-Meyer et al., 2012; Tong, 2010). Below Figure 2-15, shows Flywheel energy storage device.

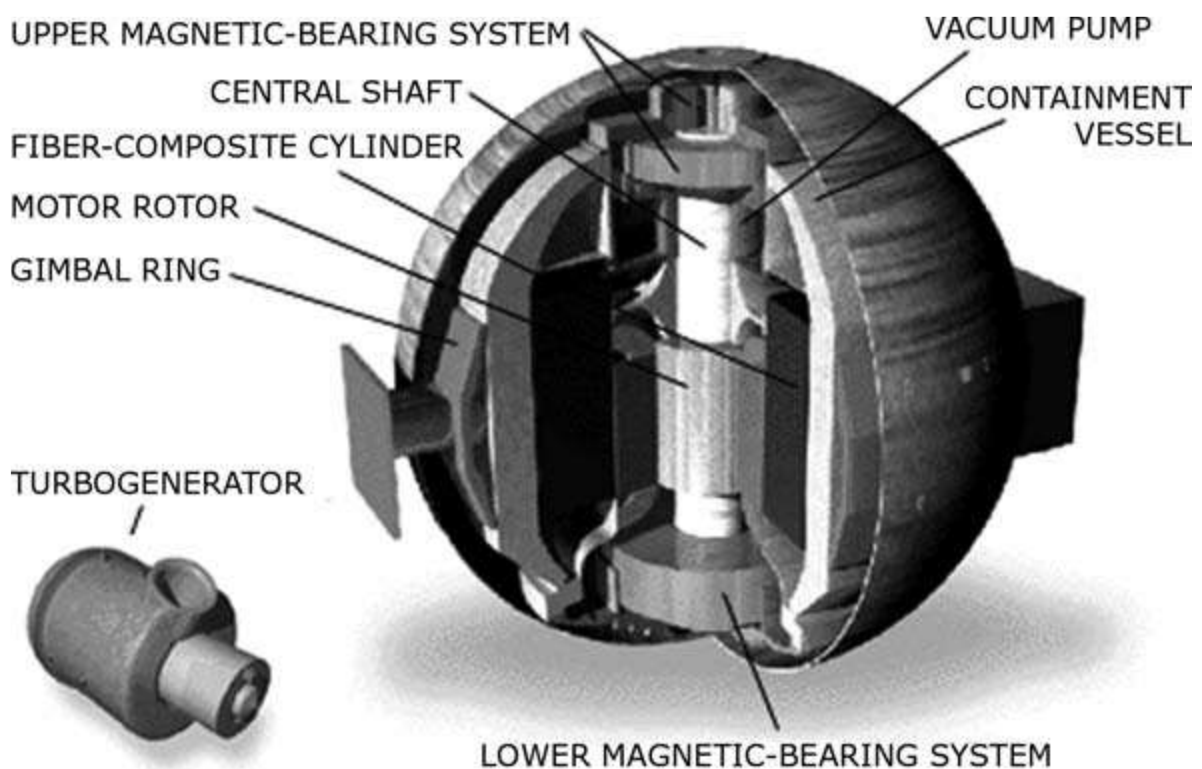


Figure 2-15: Flywheel energy storage device (Tong, 2010)

2.3.4.1 Application

The rotary energy is found in the accelerated rotor of the FES, a large rotary cylinder. A rotary cylinder in a room, a coater and a shaft are the main components. To minimize wind losses, the entire system is put in a vacuum box. The rotor is accelerated with a very high rate of charge between 20,000 and 50 000 rpm. At the point of recharge. The energy in the float is maintained by holding the rotating body at a constant rate.

During discharge the flight wheel releases energy and drives the machine as a generation (Kintner-Meyer et al., 2012; Tong, 2010).

2.3.5 Battery Energy Storage System (BESS)

For more than a century, conventional energy storage technologies have existed, including pumped or reservoir-based hydro-electric facilities and lead-acid batteries. The past decade has been marked by an increasing interest in both conventional and advanced technologies for energy storage. Advanced batteries (e.g. flow, lithium ion, sodium sulfur battery (NAS)), new mechanical systems based on compressed air and flywheels, and storage technologies based on thermal and gas (i.e. hydrogen and methane) have been given attention (World Energy Council, 2020).

In Flexible Alternating Current Transmission Systems (FACTS) applications, large Battery Energy Storage Systems (BESS) are increasingly being used to improve the system's voltage, frequency, oscillatory and/or transient stability and thus improve power supply reliability. Two parts consist of a battery energy storage system (BESS). First, a storage component that in an electrochemical process can store/restore energy. Secondly, a rectifier/inverter that can transform the DC voltage required for the grid from the storage component to the AC voltage and vice versa.

The rectifier/inverter is normally based on a pulse width modulation (PWM) and voltage-sourced converter (VSC). The problem with batteries is the vast variety of technologies and the diversity within one technology as well. So, no simple, precise model is available, valid for all batteries. With battery models, there are two principal challenges. The first issue is to get a model that is not too complex but sufficiently accurate. The second problem is to obtain from manufacturers the parameters or own measurements required for the model.

Only a model with suitable parameters can deliver good results (Fathima & Palanisamy, 2014; World Energy Council, 2020; Zakeri & Syri, 2015).

Lead-acid batteries are often common batteries in the industry. But many other types, such as nickel cadmium (NiCd), sodium-sulfur (NAS), nickel-metal hybrid (NiMH) and several types of lithium-ion, are also available. Each form has its own assets and disadvantages (World Energy Council, 2020).

In the form of chemical energy, the BESS stores electricity. A common secondary battery is a low-voltage or power cell collection which is connected to the required electrical features in parallel and in series. Each cell contains an anode, cathode, and liquid, paste or hard electrolyte. An internal chemical reaction loads the battery under both electrodes' potential. It is possible to reverse the reaction and unload the absorbed power from the battery. Three key types of BES are available. The lead acid (LA) is nickel cadmium (NiCd). They function as traditional batteries, but two electrodes are submerged in a large-scale electrolyte so as to create a chemical reaction whenever possible (Mahlia et al., 2014; Ohki, 2016; Tong, 2010).

2.3.5.1 LA battery

This is the energy storage unit most widely used. It is famous for its maturity, its relatively low costs, its long life, its fast reaction, its low self-dissipation (for some 140 years, ongoing research). These batteries can be used in short (second) as well as long (up to 8 h). The flooded lead acid (FLA) and valve regulated lead-acid (VRLA) are two types of LA batteries FLA consisting of two feather electrodes immersed in water (65%) mixture and sulphuric acid (35%) (Figure 2-16). The VRLA battery has the same pressure release valve as the FLA. This extracts air from the cells and prevents hydrogen ventilation.

Lower maintenance costs, lower weight, and lower battery space. These benefits are related to higher start-up costs and shorter lives.. (Ohki, 2016; Tong, 2010).

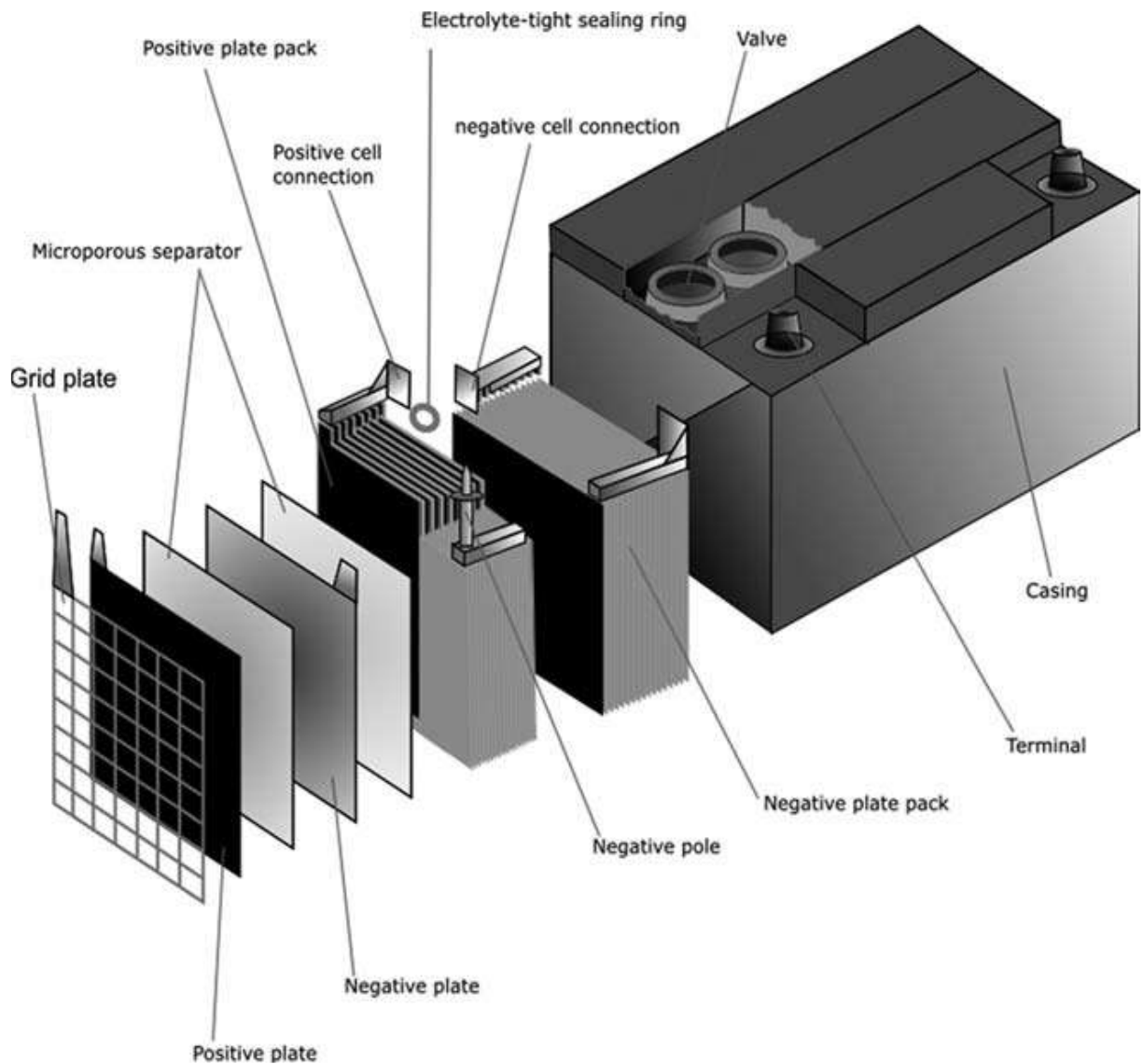


Figure 2-16: Lead acid battery (Tong, 2010).

LA batteries depend on electrode size and geometry for strength and efficiency. This ensures that the battery has a greater number of thinner electrode plates by adjusting the surface of each electrode to increase its strength. However, the weight of each electrode must be increased, and the battery must be stored with fewer and thicker panels. A solution must also be sought for each submission. In milliseconds, LA batteries can react with maximum energy.

Due to the depth of the discharge for around 5 years or 250-1000 recharge / discharge cycles, the performance average of DC / DC batteries during the regular operation is 75-85%. (Mahlia et al., 2014; Tong, 2010).

2.3.5.1.1 Application

Two key uses for FLA batteries (Tong, 2010):

1. Installation and starting, short power explosions e.g. car engine batteries
2. Deep period, long low continuous power

VRLA batteries are very common for backup power, stand-by power in telecoms and UPS systems. Today there are several LA storage installations running (Mahlia et al., 2014).

2.3.5.2 Nickel-cadmium (NiCd) battery

A NiCd battery consists of a nickel oxyhydroxide positive as the active material, and a non-metal cadmium electrode. The nylon spin-offs are separated (see Figure 2-17). Aqueous potassium hydroxide is an electrolyte that is not greatly altered during activity. The nickel oxyhydroxide is used to mix water and create nickel hydroxide with hydroxide ion during release. At the negative electrode, cadmium hydroxide is formed. The process can be reversed to charge the battery. However, the positive electrode can produce oxygen during loading and the negative electrode can produce hydrogen. This means that some ventilation and water supply, but less than is sufficient for a LA battery (Tong, 2010).

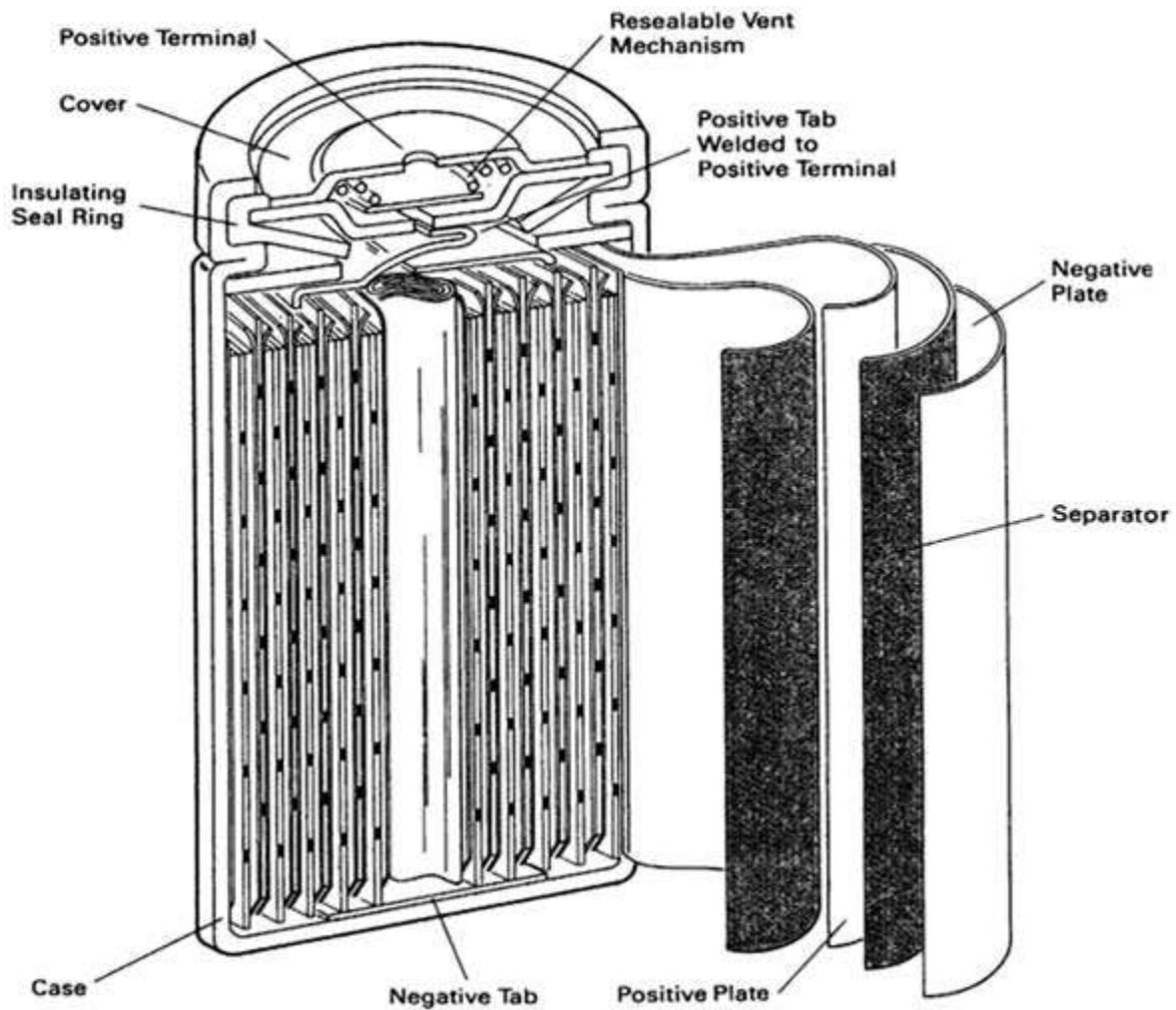


Figure 2-17: Nickel-cadmium battery (Tong, 2010)

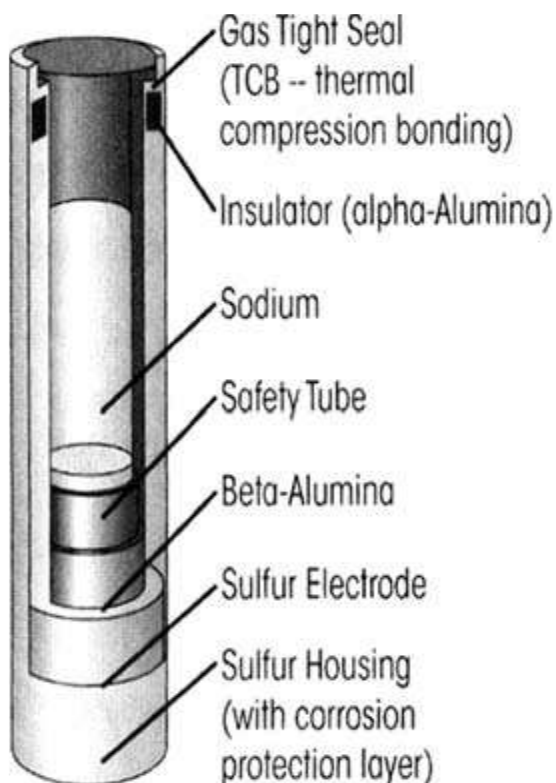
2.3.5.2.1 Application

NiCd sealed batteries are popular in commercial electronic products such as remote control, which are essential for lightweight, portable, and rechargeable power. Vented NiCd batteries are used for aircraft and diesel engines with high energy by weight and volume. Batteries from NiCd are ideal to provide stability in harsh circumstances and to protect the energy quality against voltage paths. Recently, due to their high temperature resistance, NiCd batteries have become popular for solar storage. However, during peak shaving applications they are not healthy, so that energy management systems are typically avoided (Mahlia et al., 2014; Tong, 2010).

2.3.5.3 NAS battery

Three times the power capacity, longer service life and lower maintenance are available for the NAS batteries. These batteries consist of a cylinder-electrical cell which contains a neutral electrode of molten sodium and a positive electrode of molten sulfur. The electrolyte used is solid β -alumina (Mahlia et al., 2014).

As the sulfur is released, and reacting with sodium polysulphide, sodium ions pass through the β -Alumina Electrolyte (see Figure 2-18). The reaction is reversed during the loading to decompose the sodium polysulphide and to turn sodium ions into a positive electrode. They are housed in a thermally isolated enclosure which must keep them above 270°C, usually at 320-340°C, to maintain battery molten sodium and sulphur to ensure enough electrolyte conductivity (Mahlia et al., 2014; Zakeri & Syri, 2015).



- **Low resistance, high efficiency due to**
 - Beta Alumina tube
 - Sulfur electrode design
- **High durability due to**
 - Corrosion protection layer
 - Sulfur electrode design
- **High energy density due to**
 - Cell properties and design
- **Intrinsic safety due to**
 - Incorporation of safety tube

Figure 2-18: Sodium-sulphur battery (Tong, 2010)

2.3.5.3.1 Application

NAS Batteries have shown potential with reasonably high overall efficiencies (75–85 percent), 2500–4500 lifecycles, an average 15yr life span and discharge time up to 7 hours in power quality and power transfer systems (Tong, 2010).

2.3.5.4 Flow BESS

The major forms of FBES are three: vanadium redox (VR); polysulphide bromide (PSB); and zinc-bromide (ZnBr). They all work the same way: two charged electrolytes, when a chemical reaction occurs, are injected into the cell stack, enabling a current to be accessed from the system if desired. In Tokyo, Japan, the power storage facility has been installed on 6MW 8h (see Figure 2-19) Sodium Sulphur (Mahlia et al., 2014; Tong, 2010).



Figure 2-19: 6 MW, 8 h Sodium-sulphur energy storage facility in Tokyo, Japan (Tong, 2010)

2.3.5.4.1 Vanadium Redox (VR) flow battery

The A VR battery comprises a cell, an electrical tank, a control unit, and a PCS (see Figure 2-20).

These batteries store energy by connecting two forms of vanadium ions to a sulfuric acid electrolyte; with V^{2+}/V^{3+} to a negative electrode; and with V^{4+}/V^{5+} for a positive electrode.

The cell stack size indicates the energy capacity (kW), while the battery capacity (kWh) is seen in the electrolyte volume (tank size). The two electrolytes fluctuate between the different battery tanks and enter a cell stack where H^+ ions are transferred between the two electrolytes through the permeable membrane. This mechanism leads to the isolation of the ionic form of vanadium in such a way that potential energy is converted into electricity. The process shall be reversed during recharge (Mahlia et al., 2014; Tong, 2010; Zakeri & Syri, 2015).

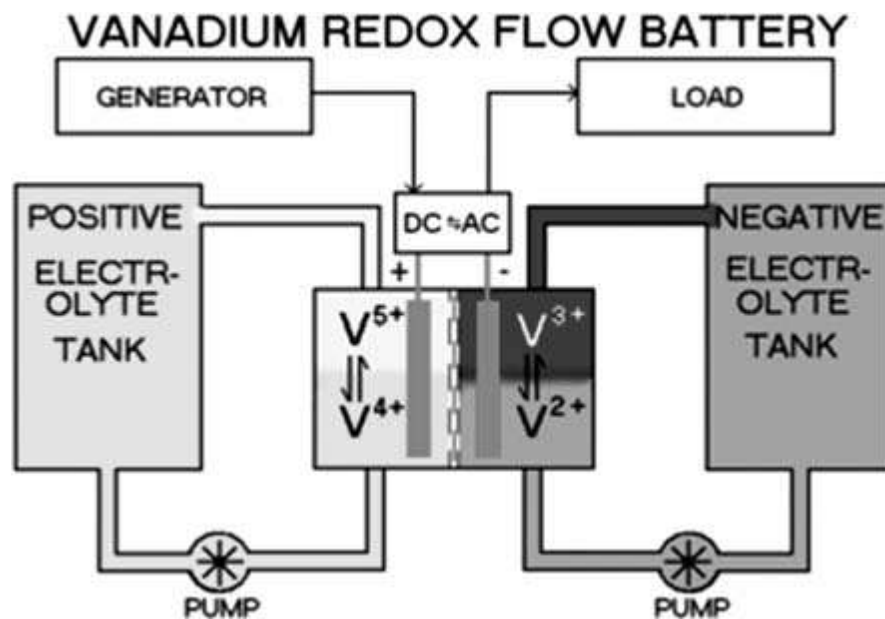


Figure 2-20: Vanadium redox flow battery (Tong, 2010)

A VR battery comprises a cell, an electrical tank, a control unit, and a PCS (see Figure 2-20). These batteries store energy by connecting two forms of vanadium ions to a sulfuric acid electrolyte; with V^{2+}/V^{3+} to a negative electrode; and with V^{4+}/V^{5+} for a positive electrode. The cell stack size indicates the energy capacity (kW), while the battery capacity (kWh) is seen in the electrolyte volume (tank size).

The two electrolytes fluctuate between the various battery tanks and join an input stack in which H⁺ ions are transmitted between the two electrolytes through the permeable membrane. This process leads to self-separation of the ionic form of vanadium in a way that transforms potential energy to electrical energy. This mechanism is reversed during reloading (Mahlia et al., 2014; Tong, 2010; Zakeri & Syri, 2015).

2.3.5.4.1.1 Applications of VR flow battery

Since power and energy capacity are disconnected, the VR flow battery is a versatile energy storage device. The unit can be used for all requirements for energy storage, such as UPS, load levelling, peak shaving, telecommunications, power, and incorporation of renewable resources. Due to the simplicity of flow piles, while it is extremely useful for many applications, there are numerous competing devices within each sector that perform better for their application. Therefore, while VR batteries can be regulated for a variety of applications, they are only taken into account when versatility is needed, such as renewable resources. (Mahlia et al., 2014; Tong, 2010; Zakeri & Syri, 2015).

2.3.5.4.2 Polysulphide Sodium Bromide (PSB) Flow Battery

PSB batteries work much like VR batteries. The same parts of a device are a cell stack, an electrolyte tank system, a control system, and a PCS (see Figure 2-21).

The positive electrolyte is sodium bromide, and the negative electrolyte used by the PSB flow batteries is sodium polysulfide. During the dumping process, the two electrolytes flow from their tanks to the cell in which the reaction occurs on a polymer membrane, allowing sodium ion movement (Mahlia et al., 2014; Tong, 2010; Zakeri & Syri, 2015).

Like VR batteries, self-separation takes place during discharge, and this mechanism is simply reversed to recharge the battery. The tension is around 1.5 V in each cell. The PSB batteries run from 20 to 40 ° C but, in the case of a plate cooler in the device, the wider range can be used. PSB fluid batteries have an efficiency of about 75%. The discharge ratio is 1:1 as for VR batteries, since during charging and misloading the same chemical reactions occur. It is calculated that the life period is 2000 cycles, but again this depends heavily on application. The power and energy capacities of VR batteries are isolated from the PSB batteries (Mahlia et al., 2014; Tong, 2010; Zakeri & Syri, 2015).

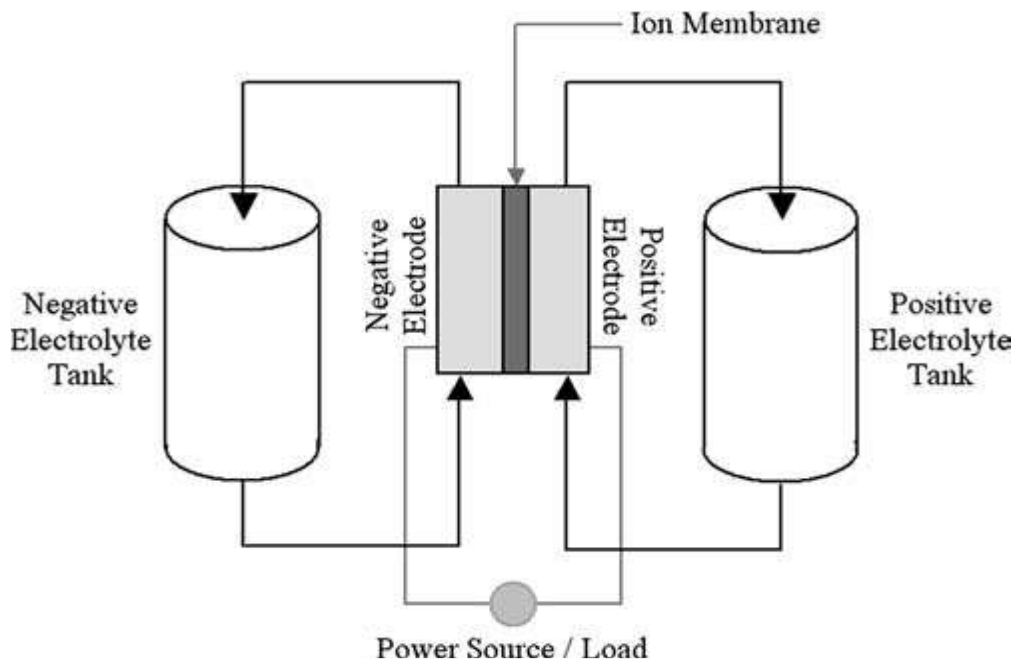


Figure 2-21: Polysulphide Sodium Bromide (Tong, 2010)

2.3.5.4.2.1 Application

PSB flow batteries, including charging, peak scrubbing and integration of renewable resources can be used for all energy storage requirements. But PSB batteries can react quickly and can react within 20 meters if electrolytes are loaded into pillars (from cells).

Under normal conditions, PSB batteries can recharge or discharge power at 0.1s. Therefore, PSB batteries are particularly suitable for response frequency and voltage control (Mahlia et al., 2014; Tong, 2010).

2.3.5.4.3 Zinc-bromine (ZnBr) flow battery

The flow batteries vary slightly from the flow battery VR and PSB. They have the same components, but do not function the same way: a cell stack, an electrolyte tank system, a control system, and a PCS (Figure 2-22). Zinc and bromine ions (which vary in their elemental bromine concentration only) flow to the cell stack when charging the electrolytes. The microporous membrane separates the electrolytes (Tong, 2010).

The electrodes in a ZnBr flow battery are a reaction substratum, unlike the batteries in the VR and PSB flow. With the answer, zinc is electrified on the negative electrode and a positive electrode, which is much like traditional battery action, produces bromine. To minimize the reactivity of the elemental bromine, an agent is added to the electrolyte. This decreases the bromine's self-discharge and increases device safety. The reaction is reversed during the discharge; zinc dissolves from the negative electrode and bromide is released from the positive electrode (Mahlia et al., 2014; Tong, 2010; Zakeri & Syri, 2015).

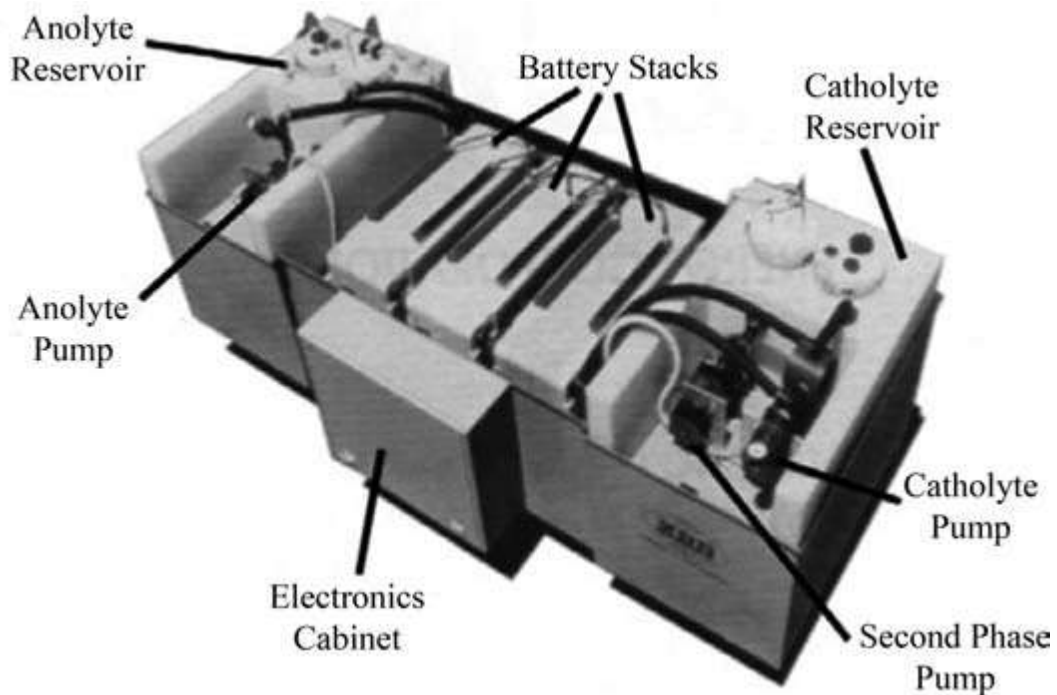


Figure 2-22: Zinc-bromine battery (Tong, 2010)

In a temperature range of 20–50 ° C, the ZnBr batteries will work. If required, a small chiller can remove heat. During action, no electrolyte is discharged and therefore the electrolyte has an eternal life. During activity, however, the membrane suffers from minor degradation, giving the device a cycle life of around 2000 cycles. Without any harmful effects, the ZnBr battery can be discharged 100% without any memory effect. The system 's performance is approximately 75% or 80%. Again, as during charging and unloading the same reaction takes place, the load / unload ratio is 1:1, although a slower rate is also used to improve performance. The ZnBr flow battery, with a cell voltage of 1,8 V, has the maximum power density among all flow batteries (Mahlia et al., 2014; Tong, 2010; Zakeri & Syri, 2015).

2.3.5.4.3.1 Application

Designed in parallel with three 60 cell battery plates, each with an actively working cell area of 2500 cm², is a 25 kW 50 kWh module for ZnBr flow batteries.

Even with a high-power density of 75–85 Wh/kg ZnBr batteries. In comparison with other traditional and flow batteries, such as the LA, VR and PSB, the ZnBr batteries are therefore relatively compact and powerful. ZnBr is also now targeting the backup market for renewable energy. The output variability in a wind turbine or solar panel can be alleviated and the frequency control can be given. ZnBr flow batteries, load control and micro turbines, solar generators, substations, and T&D grids have been used for the installations which currently have been completed (Mahlia et al., 2014; Tong, 2010).

2.3.6 Hydrogen Storage

Hydrogen (gas or liquid) chemical energy storage can store energy over long periods and can be extended without constraint in its place. Hydrogen can be used, processed, and transported to where appropriate as a carrier of electricity. There is no high self-discharge or output loss in the storage mechanism. Figure 2-23 (Ali, 2016), describes the essential elements of the hydrogen energy storage system (HESS).

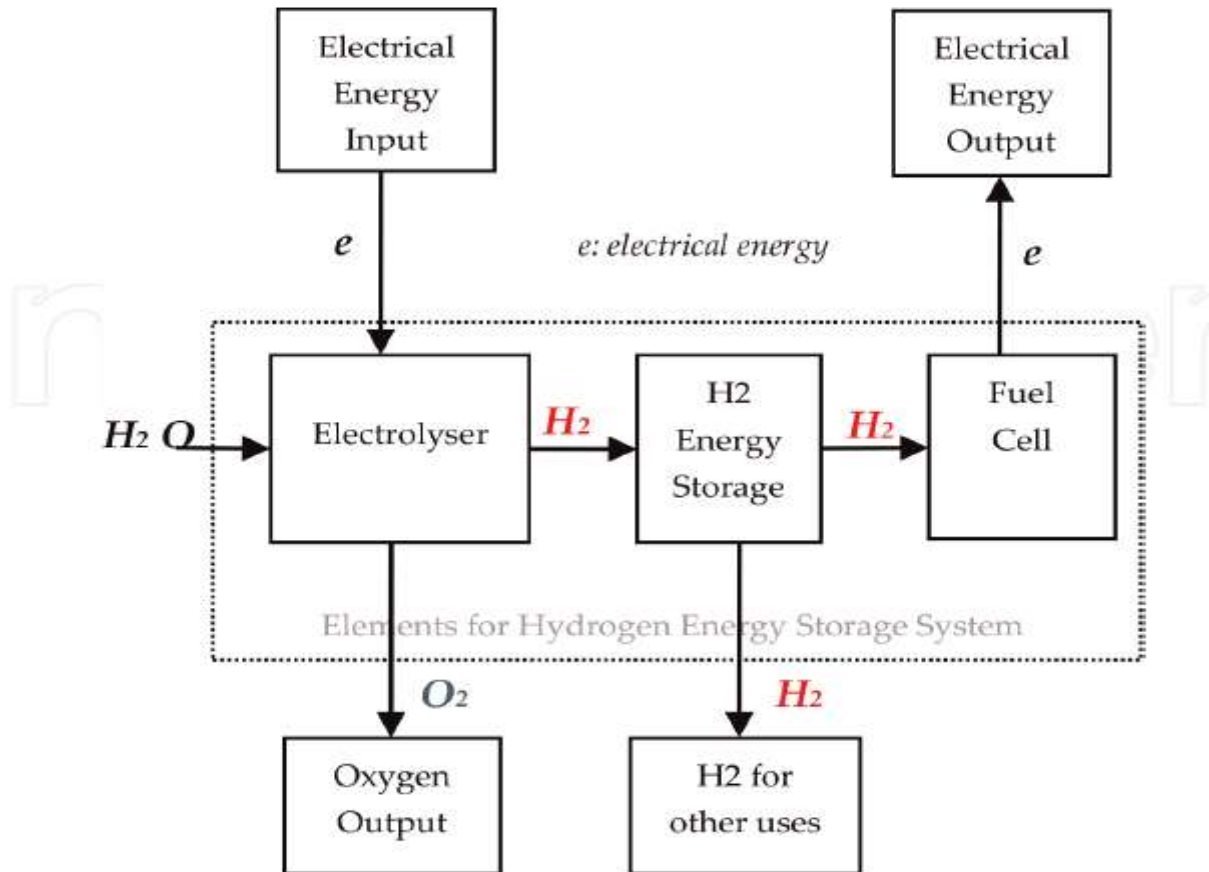


Figure 2-23: Basic elements of a hydrogen energy storage system (HESS) (Ali, 2016)

The electrolyser is utilized for converting electricity from a (usually renewable) source to hydrogen for storage. The hydrogen storage device can store hydrogen in many forms (pressure gas, metal hydride or liquid Dewar tanks). The hydrogen energy conversion system then converts the stored chemical energy into electric power, while at the same time water and heat are released as non-carbon by-products. As reported in installed projects, its typical average electrical converting efficiency is between 40 and 50 percent compared to up to 37 percent in a small combustion engine, which is widely used as a hydrogen energy conversion device. In addition, hydrogen processed for other purposes may be used, and hydrogen and oxygen gasses are thus marketed as commodities (Ali, 2016).

2.3.6.1 Application

Hydrogen can be sustained without decline for long periods. In the case of metal hydride storage technology, hydrogen can be adsorbed in a liquid or gas state, or in some cases in a solid shape. Hydrogen is connected to other gases, allowing fusion through a process known as the shift in the current natural gas grid market. Hydrogen may also be used as a reactive agent to chemical transformation of synthetic natural gas and oils. Many energy experts regard hydrogen to store wind, solar, wave and tide energy in excess from renewable energies. Demand for vehicle fuel is also visible in urban and remote rural areas (ESA, 2018).

2.3.7 Super-Capacitor (SC)

A dielectric insulator consists of two parallel plates consisting of condensers. (Figure 2-24). The plates have opposite load that store energy in an electric field. The energy inside the condenser is given by $E = (CV^2)/2$, whereby E is the energy contained inside the condenser (in J), V is the voltage, C is the feature found in $C = (A\epsilon_0 / d)$ where A is the area of the parallel sheets, d is the distance between the two condensers, and ϵ_0 is the free space permitting. ($8,854 \times 10^{-12}$ F / m) (Mahlia et al., 2014; Tong, 2010).

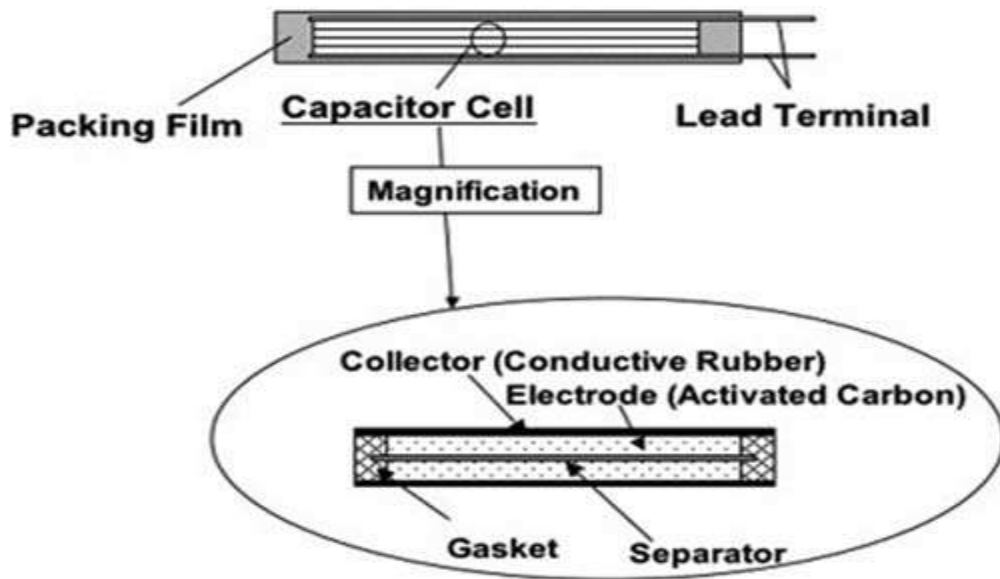


Figure 2-24: Supercapacitor energy storage device (Tong, 2010)

Consequently, voltage or capacitance must be raised to maximize the energy contained in a condenser. The maximum force on the power field restricts the voltage and the capacity is dependent on the dielectric constant (after the dielectric disrupts and the material begins to run). Supercapacitors for dielectric layers and electrodes are made with thin film polymers. The polarized liquid layers are used for raising the potential between ionic electrolyte conduction and a conductive electrode. They are available in sequence or concurrently. Energy storage system supercapacitors (SCES) usually have 20-70 MJ / m³ energy densities and an efficiency of 95%. (Tong, 2010; Zakeri & Syri, 2015).

2.3.7.1 Application

SCES is mainly attracted by its fast loading and unloading, coupled with its very lengthy life of 1 to 10⁶ cycles. For many small-scale (< 250kW) power quality applications it is a very attractive substitute. Supercapacitors are longer-lived than batteries, do not have any memory effect, display limited deterioration due to deep discharge, and do not warm up and create dangerous substances.

Thus, SCES is an extremely attractive choice for certain applications like electric vehicles, mobile phones, and load elevation tasks, although energy density is smaller. SCES is mostly used for milliseconds to second intervals, with downtime up to 1 minute pulsing power is used (Tong, 2010; Zakeri & Syri, 2015).

2.3.8 Superconducting Magnetic Energy Storage (SMES)

A SMES system comprises a superconducting spiral, a refrigerator, and a vacuum for keeping the spiral low (see Figure 2-25).

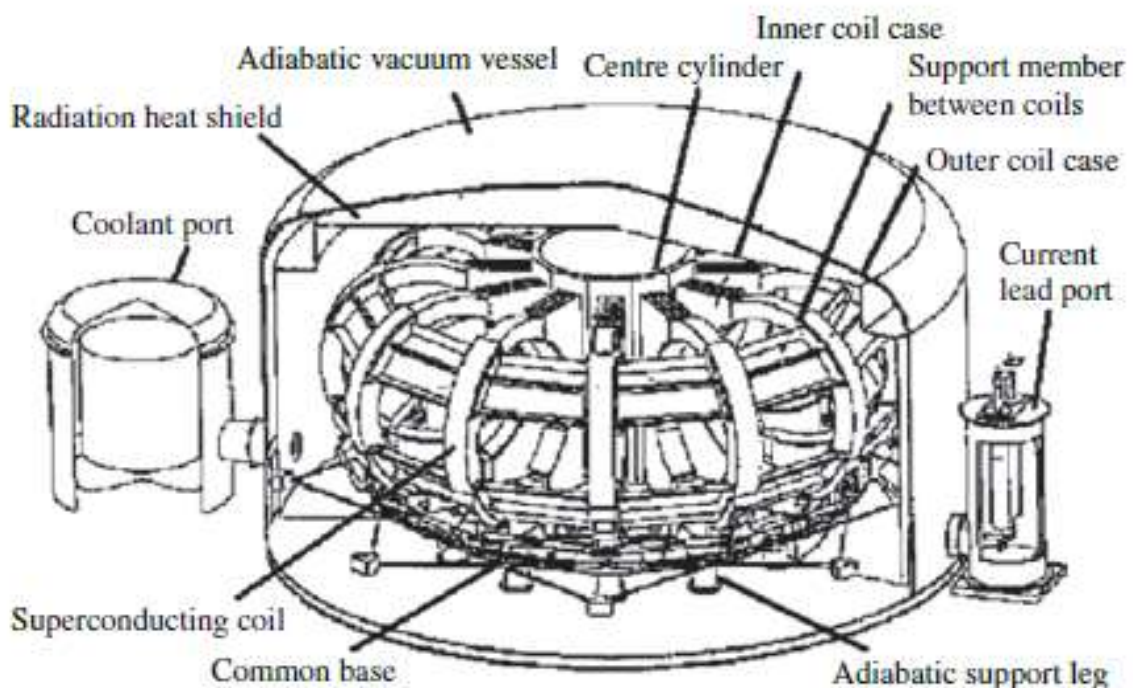


Figure 2-25: Superconducting magnetic energy storage device(Tong, 2010)

In the magnet field generated by a DC stream in the coil wire energy is stored. energy. The resistors of the filament as the currents pass through a wire usually distribute energy like heat. However, when the wire is manufactured from a supranational material such as led, mercury or vanadium, there is zero resistance, so that the conservation of energy requires virtually no loss. It should be kept at very low temperatures for this superconducting state within a material.

There are two kinds of superconductors: superconductive with low temperature that must be cooled to 0 to 7. The 2K superconductors with a temperature range from 10 to 150 K, but usually within 100 ± 10 K. There are two different kinds of superconductors. The stored energy in the coil (in J), EC, can be derived from $E = (LI^2)/2$, where L is the induction of the coil, and I is its current (Tong, 2010).

The material properties are thus extremely important as SMES designs are characterized by temperature, magnetic field, and current density. The overall performance of SMES is between 90% and 99%. SMES has very limited release times but typically takes less than 1 min for complete discharge and for very short periods. Unloading is possible in milliseconds if a PCS that can accommodate this is economical. SMES storage capacity can be up to 2 MW, but the main attraction is its cycling capacity. SMES devices can run on thousands of load / unload cycles without any magnet degradation giving it a lifetime of 20 + years (Mahlia et al., 2014; Tong, 2010).

2.3.8.1 Application

It is suitable for the industrial power quality markets thanks to the high capacity and instantaneous SMES discharge speeds. It protects equipment against rapid abrupt voltage slides and stabilizes fluctuations in the network, due to unexpected shifts in customer demand, lightning strike, or operating switches.

SMES is also a valuable network improvement solution, with some reports reporting that it can up to 15 percent increase the capacity of a local network. However, SME is unsuitable for dailies like peak reduction, green uses, and generation and transmission delays due to the high energy usage of the refrigerator system. (Mahlia et al., 2014; Tong, 2010; Zakeri & Syri, 2015).

2.4 Grid Integration of Wind Farm and BESS

2.4.1 Background

The grid connected wind farms cause fluctuation of power and redistribution of the reactive power, which leads to voltage imbalance at times. The grid stability and safety are therefore seriously threatened. Therefore, a power system combined with a significant amount of wind power must maintain dynamic stability and stable operation. Recent developments in storage technology offer an incentive for the use of renewable energies (RES) energy storage systems (Abhinav & Pindoriya, 2016; Sheng et al., 2005).

The researchers have used BESS to fix these issues. During wind shortage or increased load demand, BESS may provide the additional active power support. When demand decreases or the active power of the wind generator is more than necessary, the same can be used to charge the batteries. BESS will thus help to maintain a balance of the output and voltage, and in turn reduce power oscillations, frequency fluctuations and increase the wind power shipment which will also supports the wind farm owners from an economical point of view (Rao et al., 2013; T. Weber et al., 2010; Zou & Zhou, 2011).

In terms of its positions for the various stakeholders: the wind farmed owner, the network operator and the energy user, BESS applications for incorporating wind power can be summarized and categorised. But we will just look at the side of wind farm and grid (Schaffarczyk, 2014; H. Wang et al., 2013) .

2.4.2 Wind farm Integration with BESS

Wind power integration is primarily a problem, including power interference, ramp speed and a decrease in wind output.

The task of BESS on the generating side is to boost the wind farm's smart grid efficiency to dispatch wind power to regulate it like traditional power plants. Furthermore, restricted transmission capacity shall be efficiently used (Branco et al., 2018; Schaffarczyk, 2014; West & Baldwin, 2013).

2.4.2.1 Time shifting

Because of the stochastic characteristics of wind, wind energy output is a non-disposable resource, and it also has anti-peak characteristics, such as high wind power during off-peak demand or low wind power in high demand.

The time change is to store extra wind power during low demand times and is ready to ship power during high demand periods into the grid. With wide demand differences between high and off-peak, the advantages of storing energy would be higher. To perform the role of time change, vast amounts of energy are essential to the BESS facility for substantial periods (from hours to days). Moreover, storage quality is also a crucial element in the economical functioning of time shifts, as large losses are associated with an inefficient storage system (Schaffarczyk, 2014; W. Wang et al., 2016).

2.4.2.2 Output smoothing

The wind energy inherently variable nature can cause frequency and voltage fluctuations. The BESS allows these variations to be smoothed out to stabilize the system. Therefore, the BESS output power must be quickly regulated such that excess energy is consumed during output spikes and energy is released during output decreases. For the smoothing function, the ramping capacity is therefore very necessary.

The production smoothing in the plant decreases the demand for electricity quality and system auxiliary services (Abhinav & Pindoriya, 2016; W. Wang et al., 2016).

2.4.2.3 Transmission utilization efficiency

Wind resources are often far from available high-capacity transmission lines in rural areas. The energy generated cannot be transferred to the load due to the transmission constraints. Further BESS can mitigate congestion, postpone or prevent improvements to transmission and distribution (Branco et al., 2018; Schaffarczyk, 2014).

2.4.3 Grid Integration with Wind Farm

The grid connect ability guidelines or consumer regulations are the basis for the grid operators' technical access requirements and summarize the important points for the grid generation plants. In particular, the roles of network operators, erectors, planners, and customers are specified. Together with Part 19 of the energy Management, the technical link requirements (TCCs) of the grid operator are valid and must be written in Germany. The link guidelines and application rules are generally relevant for connecting new generating plants and those where significant improvements are made (i.e. repowering) (Schaffarczyk, 2014; Tande, 2003).

In high voltage, high and medium voltage grids, wind turbines must also be enabled to engage in static and dynamic grid support. The slow changes in voltage can be preserved to tolerable limits by supplying reactive power conditions with a static frequency stability in normal operations. Dynamic grid support avoids the unwanted turn-off of major power supplies and, when component failures occur on the maximum and maximum voltage grids, the resulting grid collapses.

Wind turbines with ties in the medium voltage grid must also be able to provide system services, as these turbines have an immediate or long impact on the maximum voltage grids (Schaffarczyk, 2014; H. Weber & Kleimaier, 2009).

In future, the static tension stability must also be accomplished by plants that feed low-voltage grids. As they are required to contribute to the maintenance of low-voltage grid voltage during normal grid service, this has an immediate impact on plant design. Dynamic grid support is not required when generating installations that feed into the low-voltage grid. Independent certified institutions should provide for the verification of the appropriate electrical properties of WTs and wind farms (T. Weber et al., 2010).

(Abhinav & Pindoriya, 2016) notes the project-specific electrical characteristics and guideline-conforming actions of all grid-based wind turbines, the internal wind turbines linked to the grid and other components such as compensation system and grid connecting lines (also the full connecting system); A test of the voltage changes, the grid reaction, the short-circuit strength and the Grid's operating media design is needed for a connection evaluation. Furthermore, long term flickering, harmonics, tone frequency reactions, tap control and complex grid support systems need to be controlled.

2.4.4 Grid Integration with Wind Farm BESS

The grid operator is currently expected to supply ancillary services by the BESS to reduce instability and volatility across the whole grid instead of loads or wind farms. Net variability and instability are less due to the spatial distribution of wind energy. The need for the entire service is therefore reduced (Schaffarczyk, 2014). At present, the main methods for dealing with uncertainty issues are stochastic optimisation, fuzzy optimisation and robust optimization (Hosseini et al., 2020; Shi et al., 2020).

Fuzzy optimization usually depends on human experience. Robust optimisation is more widely used in line with the actual phenomenon. Stochastic optimisation does not depend on human experience nor with the actual phenomenon, but it describes uncertain parameters as discrete or continuous functions of probability density (Hosseini et al., 2020). Stochastic optimisation requires the distribution of the probability of unknown parameters and has been widely employed to deal with uncertainties in some areas of, (1) power system planning, (2) comprehensive stochastic optimisation model for optimizing the electric power system of wind farms, (3) the investment of components, (4) the system efficiency, and (5) the system reliability such as power transmission planning and capacity expansion planning (Banzo & Ramos, 2011).

For example, (Sperstad & Korpås, 2019) investigated stochastic optimization for integration of renewable energy technologies in district energy systems for cost-effective use and discovered uncertainty of energy loads and power generation from renewable energy resources heavily affects the operating cost. (Ghasemi et al., 2018), introduced a two-stage stochastic programming approach to optimal design of distributed energy systems.

Thus, this research proposes a stochastic model for optimizing the wind farm battery energy storage system, by considering network future components planning, the system efficiency, and the system reliability. (Abhinav & Pindoriya, 2016) provide the BESS applications for Active and Reactive power are listed in below Table 2-1.

Table 2-1: Application of BESS (Abhinav & Pindoriya, 2016)

Objective	Technique/ Algorithm	ESS type	Time frame
Power Oscillation Damping/ Power Fluctuation Mitigation/ Output Power Smoothing	Adaptive Linear Neuron based power tracking	BESS	Steady state
	Fuzzy logic based adaptive Kalman filter	Li-ion battery	Steady state
	Fuzzy logic	SMES, VRB, Ultra-capacitor	Steady state
	Bacteria Foraging	BESS	Dynamic
	Spectral analysis, MPPT technique	Lead-Acid battery	Steady state
	Neural network	Super-capacitor, lead-acid battery	Steady State
	Output power reference waveform tracking	BESS with Super-capacitors	Steady state
	Coordination control of HESS	BESS with SFES	Steady state
	Two-time scale coordinated control	Super-capacitor hybrid system	Steady state
	Hierarchical Structure based control	BESS	Steady state

	RSC and GSC control	BESS	Dynamic
	State machine based Supervisory control	Lead-acid battery	Steady state
Frequency Regulation	Fuzzy Logic	SMES and VRB	Steady state
	SOC feedback control	BESS	Steady state
	Pitch angle control for turbine and H-∞ controller for BESS	NAS battery	Steady state
Dispatchability Improvement	Stochastic coordinated predictive controller	NAS battery	Dynamic
	Statistical analysis of wind power forecast	Li-ion battery	Steady state

Stochastic model predictive control	NAS battery	Steady state
SOC feedback control	Dual Battery ESS	Steady state
Artificial Neural Network	Zinc–bromine flow battery	Steady state
Dispatch Based on Wind-Power Forecast	Super-capacitor HESS	Steady state

Two scale dynamic programming scheme	Li-ion battery	Steady state
Wind power generation shifting and ramp-rate limiting	NAS battery	Steady state

APPLICATION OF BESS FOR REACTIVE POWER MANAGEMENT: SUMMARY

Objective	Technique/ Algorithm	ESS type	Time frame
	Fuzzy logic based supervisory control	Flywheel ESS	Steady state

Reactive Power Support	Hysteresis current control	BESS	Dynamic
	Stall-controlled wind turbines	Synchronous machine based ESS	Dynamic
Voltage Stability	Hybrid control strategy	Lead-acid	Dynamic
Low voltage ride through (LVRT)	Fuzzy logic	SVC with VRB	Dynamic
	Bi-directional control converter	-	Steady state

2.4.4.1 Energy arbitrage/load levelling

The electricity price varies sometimes, usually hourly, on the electricity market. The BESS can be used to store low-cost off-peak power and pollution at higher rates. This will lower the exposure to market risk from volatile peak prices and control high cost energy imbalances (Abhinav & Pindoriya, 2016; Zheng et al., 2015).

2.4.4.2 Frequency regulation

The grid operator must provide modern wind farms with frequency control. With high wind penetration level, it is theoretically feasible to provide frequency response from a wind farm using additional droop power. It can cause wind turbine fatigue and instability (Schaffarczyk, 2014). The use of the BESS is an optimal solution. The active power controller of the BESS can be equipped with a local drop control loop to the primary frequency control. The drop control aims to adjust the active power output proportionally to the difference in frequency. The active power control is created through the centralized Automatic Generation Control (AGC) for the secondary frequency control (Abhinav & Pindoriya, 2016; Zhang et al., 2014).

2.4.4.3 Inertia emulation

The grid inertia decreases the variability of the frequency and makes the grid less susceptible to sudden changes in output. The inertial instantaneous response defines the frequency change rate (ROCOF). Added BESS could increase a grid's obvious inertia significantly. Adding the additional loop to the active ESS power control (Schaffarczyk, 2014; Zhang et al., 2014).

2.4.4.4 Oscillation damping

In an interconnected system, sudden timeline power change might result in frequency oscillations between 0.5 and 1 Hz.

It may lead to the failure of many machines' synchronization. An efficient method of control is to simultaneously manage the inherent power changes and improve the reliability of the system for a large wind farm. The damping controller is applied. The BESS should be used for the oscillation of the device. The power deviation from the tie line is used as a feedback signal to generate the converter control phase portion. (Y. Liu et al., 2014; Schaffarczyk, 2014).

2.4.4.5 Voltage control support

The variable wind power will degrade the stability of the grid voltage. The BESS can be setup to maintain a local voltage level with a sufficient reactive capacity. The full-scale converter connected to the grid will provide this service. (Schaffarczyk, 2014; Zou & Zhou, 2011).

2.4.4.6 Low Voltage Ride Through (LVRT) support

The LVRT capability of WTGs should be preserved during grid-specified serious failures by grid codes. In addition, some grid codes need WTGs to provide the maximum reactive current during certain defects. To compensate for the losses related to the supply of the reactive fuel, the converter should draw real strength. No power can be drawn from the grid during serious defects. The voltage of the DC drops, and the switches of the converter are blocked. In these situations, DC tension during failures may be assisted by the BESS. (Abhinav & Pindoriya, 2016; Zou & Zhou, 2011).

2.4.4.7 Reserve application

Because of the wind power error forecast, more emergency support reserves are needed. The reserves would normally be categorized in major, secondary and tertiary reserves based on the response time (Y. Liu et al., 2014; Schaffarczyk, 2014).

2.4.4.8 Emergency power supply/black start

The BESS can be used in case of severe failure to restart a shutdown state without the assistance of the electric grid to control the power system (Abhinav & Pindoriya, 2016; Y. Liu et al., 2014).

2.4.4.9 Transmission utilization efficiency

The BESS will help grid operators use the transmission system resources effectively, update the transmission system to reduce transmission costs and alleviate the local wind energy dependence challenges. (Abhinav & Pindoriya, 2016; Y. Liu et al., 2014).

2.4.5 Grid Code Power Quality Parameters

2.4.5.1 Voltage variation

Voltage variation occurs at different set point in a power system. Generating, the transmission and distribution process play an important role influencing voltage level and changeability in the power system. The main factor is the ability to change the load and accidental load changeability in a distribution system imposes requirement concerning voltage stability maintenance. The reactive power and Active power produced needs to be considered to minimise the voltage instability in power system network. When reactive power consumed is bigger than generated, voltage decrease and vice versa. Highlighted below are reasons for voltage variation in power system(Eskom, 2013):

- Changing loads slowly
- Switching on/off essential power system elements
- Producing self-excitation from the generator
- Swinging of synchronous machines

According to (Eskom, 2019), the grid code of South Africa requirements, the following needs to be met all times concerning the system voltage stability; Wind farms shall be designed to operate with the specified voltage range limit (see Table 2-2 and Figure 2-26 below).

Table 2-2: Minimum and maximum operating voltages (Eskom, 2019)

Nominal [U_n] (kV)	Min [U_{min}] (pu)	Min [U_{max}] (pu)	Min [U_{max}] (kV)
132	0.90	1.0985	145.0
88	0.90	1.0985	96.7
66	0.90	1.0985	72.5
44	0.90	1.08	47.7
33	0.90	1.08	35.8
22	0.90	1.08	23.9
11	0.90	1.08	12

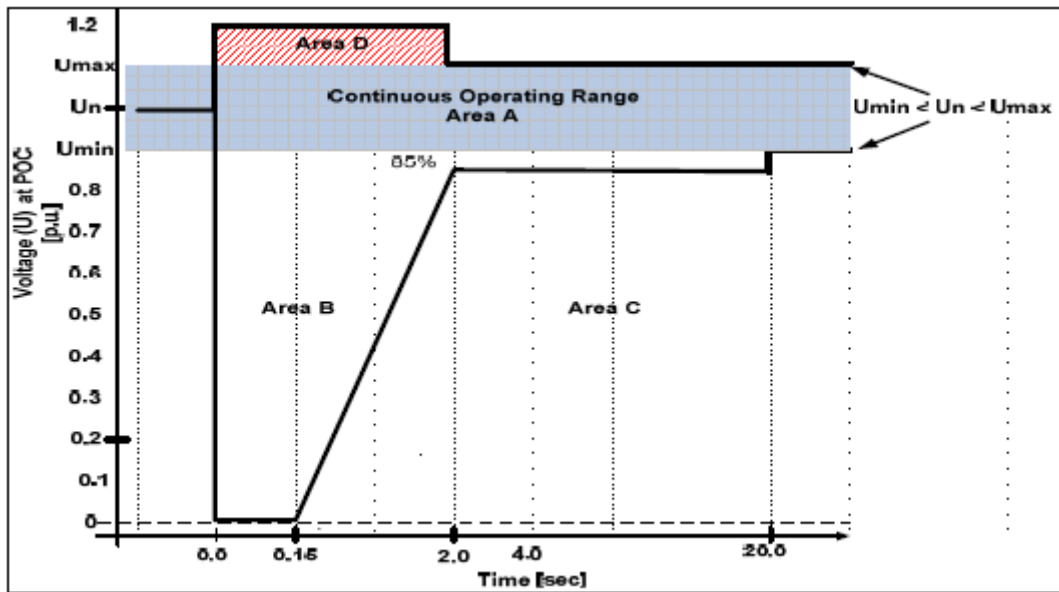


Figure 2-26: minimum and maximum operating voltages (Eskom, 2019)

Wind energy farms shall withstand the voltage changes at the Point of coupling under normal and abnormal conditions (POC). When the voltage change in the system network is $110\% < V < 120\%$, The Wind turbines are required to withstand the change for 2 seconds before disconnecting (see Table 2-3 below) (Eskom, 2019).

Table 2-3: Maximum disconnection times (Eskom, 2019)

Voltage range (at the POC)	Maximum trip time (seconds)
$V < 50\%$	0,2s
$50\% \leq V < 85\%$	2s
$85\% \leq V \leq 110\%$	Continuous operation
$110\% \leq V \leq 120\%$	2s
$120\% \leq V$	0,16s

When immediate voltage drops or dips, wind farms shall then provide maximum voltage support by supplying controlled amount of the reactive current to ensure stabilization of the system.

2.4.5.2 Frequency variation

The frequency is the fundamental component of power quality in a power system network and it requires the centralized control as it is being shared by all the points in the power network (Shepherd & Zhang, 2011). According to (Angelo, 2008), “The frequency control and maintenance within allowed limits requires the existence at the system operator level important power reserves that can be called automatically to assure a balance of the set-point frequency value power consumption and generation”.

Frequency can then be sustained in the whole system at the set point value by ensuring the effective control of the generation and consumption in each zone of the system through the system operator and other neighbouring zone systems. According to grid code requirements under normal operating condition, when the frequency on the National Interconnected power systems (NIPS) is higher than 51.2 Hz for longer than 4 seconds, the wind farm shall be disconnected from the external grid or frequency is 47 Hz for longer than 200ms, the Wind farm may be disconnected (see Figure 2-27) (Eskom, 2019; Ochani et al., 2019).

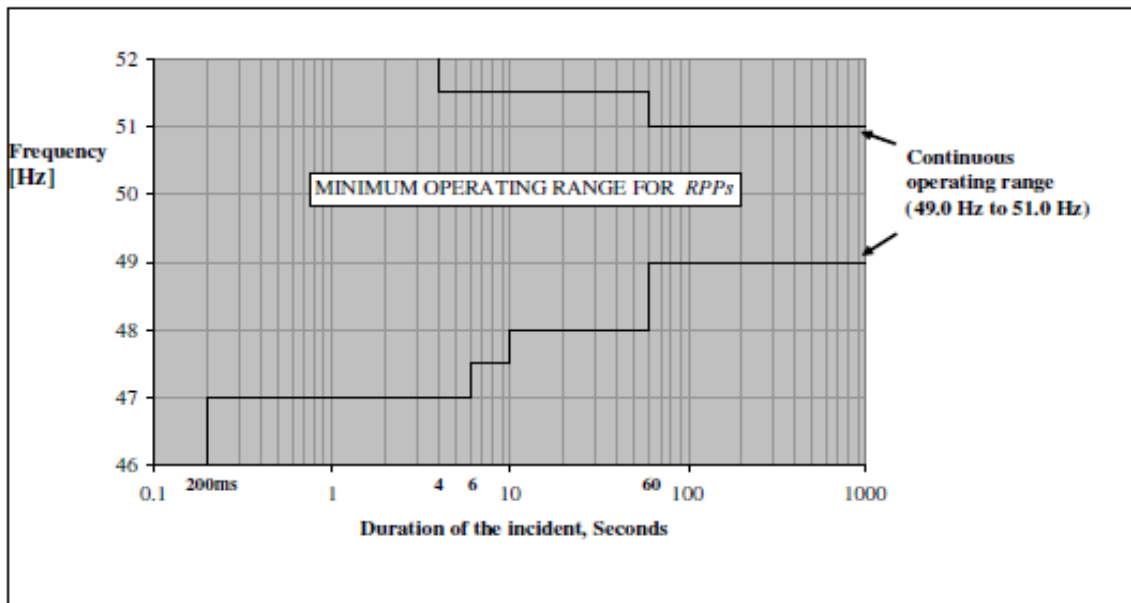


Figure 2-27: Frequency operating range (Eskom, 2019)

2.4.5.3 Static synchronous compensator (STATCOM)

STATCOM is a shunt and versatile AC transmission system (FACTS) that is used to counteract reactive power in a grid, stabilizing grid voltage and improving the system power transmission, based on (Farhad et al., 2015). Recently, the most power flow controls, and damping systems oscillation have been used in FACTS-based applications. They can also be used to increase the ability of transmission lines, to regulate stable state voltage, to provide transient power support to avoid failure and to oscillate damp power.

The FACTS equipment in wind energy systems can be used to maximize the overall power system's transient and dynamic stability. STATCOM consists of the FACTS family of equipment that can efficiently be used in a wind farm to provide transient supportive voltage to avoid failure of the system. Power transfer is system voltage dependent and FACTS is used to enhance interconnection stability between the AC electrical systems.

STATCOM has a PCC voltage regulator capability and can then generate a reactive potential and inductivity (Arulampalam et al., 2006; Farhad et al., 2015). Figure 2-28 illustrate integration of Wind turbine with STATCOM.

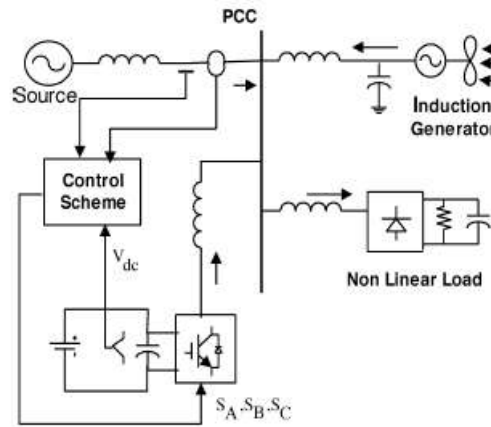


Figure 2-28: Wind turbine with STATCOM (Farhad et al., 2015)

The STATCOM consists of the DC capacitors which are used to store energy, the high frequency semiconductor switches, and inductor for system connection. STATCOM system ensures grid code compliance of wind energy farm in all operations which enables it to meet grid code requirements.

2.4.5.4 Static Var Compensator

Based on the findings of (Shuchuang, 2015), the static Var compensator can be used for the reactive power compensation in Wind energy Farm.

When Connecting SVC in Wind farm feeder or busbar station can control power factor to a Unit in the point of connection (see Figure 2-29, showing SVC connected between Wind Farm and Grid).

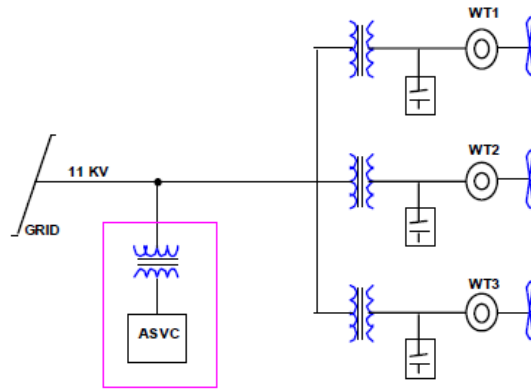


Figure 2-29: SVC connected to wind farm (Shuchuang, 2015)

SVCs can be used to generate high power for wind farms using a multi-level IGBT (Gate Switching off Thyristors) inverter. The Var compensators will then keep the transmission network load voltages within the reach and increase the power transmission capacity of the lines while preserving the power system stability (Arulampalam et al., 2006; Shuchuang, 2015).

2.5 Control of integrated Systems

2.5.1 Background

An integrated power system that includes thousands of components and devices that are to be controlled is huge and very complex. The challenge is to constantly change the electricity supply to accommodate the system users' ever evolving needs. At the lowest available cost, high reliability must be maintained. There should be a constant observation of the physical limitations of each part of the network, such as the generators, transmission lines and substations (Shepherd & Zhang, 2011; Varbanov & Klemeš, 2010).

Device service involves (Ochani et al., 2019; Shepherd & Zhang, 2011):

- Node voltages within desirable limits.

- Always set the frequency of the system to keep all generating units synchronised, including wind generation.
- Verify that the system can stand up to unplanned failures or loss of major elements or recover from them.

The following items describe the technological aspects to ensure stable machine working (Kintner-Meyer et al., 2012; Shepherd & Zhang, 2011):

- Control of voltage and transmission of reactive electricity. It requires deployment of reactive power generation machines or / and equipment.
- Frequency control through the modification of some generating units in response to fast device load fluctuations.
- Changing the generation and charge distribution to meet the demand trends for daily load.
- Keeps the spinning reserve sufficient, normally online and synced to the device, to react quickly to the failure of a major drivetrain such as a wind generator.
- To handle an extra generating capacity replacement, which can be added relatively rapidly if a wind power supply shortfall is substantially unforeseen.

The precise load forecast is the principal cornerstone of the reliable machine operations even if it is never 100 % accurate. The dynamic load prevision strategies and realistic experience both help to minimize confusion. While wind variability makes the performance of each wind turbine very much unpredictable, then when the effects of transmission grid and system operations come in, many turbines have a general performance.

The presence of many wind farms at various locations leads to a smoothing effect at the level of available wind generation. In addition, the larger the distances between the various wind farms, the larger the luxury (Kintner-Meyer et al., 2012; Ochani et al., 2019; Shepherd & Zhang, 2011).

2.5.2 Effect of Integrated Wind Generation on Steady-State

If electricity flows through a grid, the voltages at different points (often referred to as 'nodes') are different. Figure 2-30, a conceptual schematic, contains a transmission grid, the grid of distribution through which a wind farm is linked and several charges. The device voltages at the different transformer terminals must be kept within the design limit and often automatically voltage regulated. The most impedances in power systems are resistive – inductive and can be defined by serial resistance inductive elements in an analogous circuit due to transmission lines and transformers. (Shepherd & Zhang, 2011; Varbanov & Klemeš, 2010).

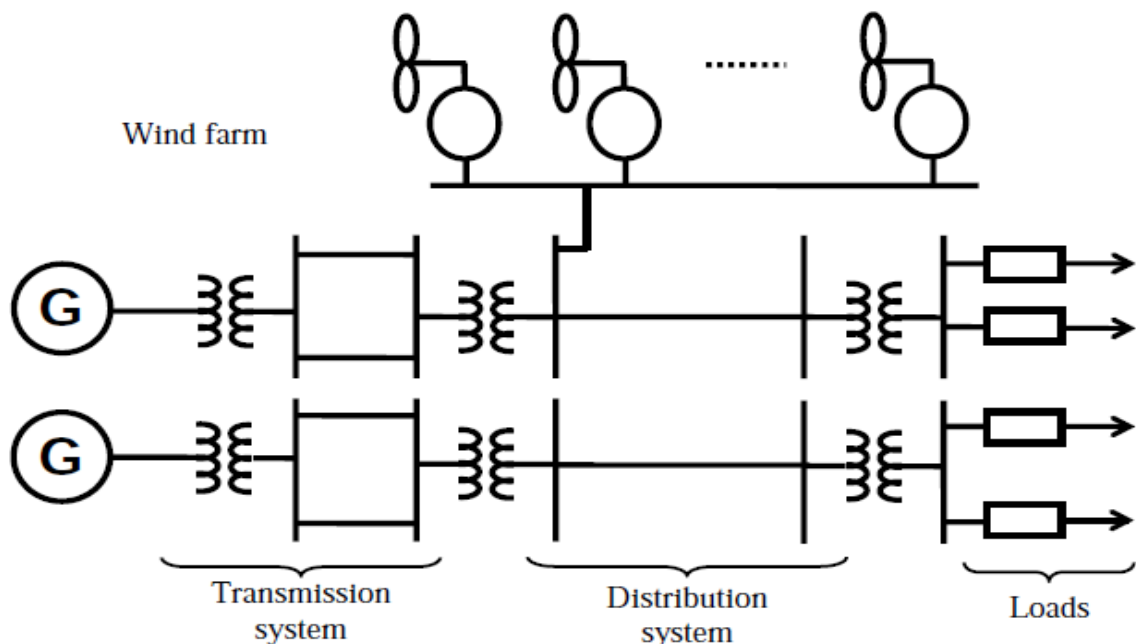


Figure 2-30: The electrical power system incorporating a wind energy farm (Shepherd & Zhang, 2011)

In Figure 2-31, an analogous circuit shows a radial circuit connecting the wind turbine to the fixed voltage stage. The induction generator generates real P power for the fixed voltage DC bus of the V_b power system in the configuration for the wind generator Figure 2-31. The induction generator produces Q -leading reactive volt amps (VARs) to a power factor of about 0.92. The condenser bank absorbs or absorbs part of the VARs supplied by the induction generator (Shepherd & Zhang, 2011).

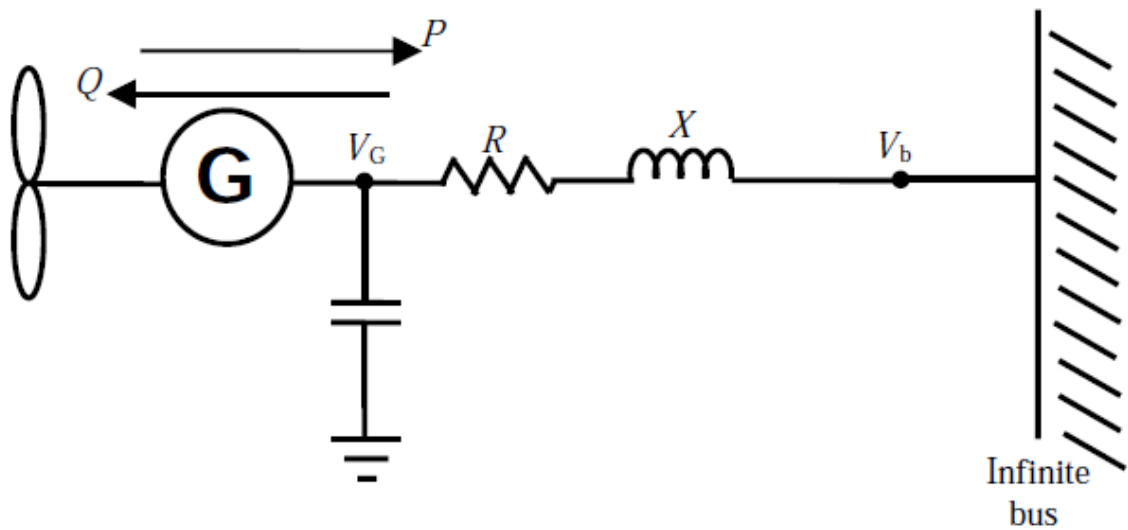


Figure 2-31: The fixed-speed wind generator connected to a fixed voltage point (Shepherd & Zhang, 2011)

2.5.3 Effect of Integrated Wind Generation on Dynamic

Irrespective of the mode of output, all electrical power systems are subject to instantaneous changes of state and thus to transient voltage. The most common change is due to incidents involving switching out or major components, such as a large load, a transmission line, or a generator. The most frequent shift. The changes listed create changes to the impedance of the system instantly, or even to the level of active power and reactive power demand.

This is preceded by an interrupt voltage transience, which may take the form of a sharp voltage spike or a sudden shift in the level accompanied by an oscillatory decay or an increase in voltage (Shepherd & Zhang, 2011).

2.5.3.1 Lightning strikes

The transmission and distribution facilities are subject to lightning strikes in every electrical power system. This flash can lead to severe injury, loss of equipment and danger for workers. The light elevation is very steep, with a rising time of approximately $1\mu\text{s}$ and is normally below $10\mu\text{s}$ (Glushakow, 2007; Shepherd & Zhang, 2011; Tingfang & Xin, 2010).

The voltage wave passes through the device unless protective equipment stops or deviates to earth (ground). Since a lightning voltage can reach as high as several megavolts, it is likely that the impact of a strike is very severe. Particular issues occur with the safety of wind turbines and wind farms (Glushakow, 2007; Shepherd & Zhang, 2011; Tingfang & Xin, 2010).

Usually, the turbines are mounted on the tops of high towers and on hilltops that contain high-resistivity terrestrial devices. For the use of 50/60-Hz current and lightning strikes containing high-frequency components, a wind farm earthing device is needed. The descriptions of the earthwork used are given in several reference documents but are beyond the reach of the current text (Glushakow, 2007; Shepherd & Zhang, 2011).

2.5.3.2 Voltage flicker

The hopper blades move through the eye of the tower, upstream and downstream, on each rotation of the wind turbine. This causes the blades to lose their wind power. During the effective shadow time there is a bending moment in each rotation.

The passing frequency of the blade is typically 1–2 Hz at normal rotational rates for high power turbines, which is the rotor velocity time of the number of blades (Thiringer, 2007). It also causes the cyclical flexing force at the blade root which may ultimately result in a fatigue failure of the propeller blade if the bending force is adequate in frequency and magnitude. Cyclic change in force on the propeller blade represents a minor difference in the torque given to the turbine and functions as a small stirring of the generator output voltage.

The ripple voltage would be noticeable in the flicker of the lights if the generator supplied the light with the electric load. This flicker is obvious in the human eye, even at the 25 Hz frequency that is generated simultaneously in some North American cities and can also be very annoying (Abhinav & Pindoriya, 2016).

The human eye is most likely to be changed by around 10 Hz. In wind engineering, the word "flicker" was imported to describe circular voltage disruptions caused by the shadow effect of the wind turret and other switching events. The transient voltage variations are also defined in the flicker criteria. Many nations are developing guidelines to measure flicker and maintain restrictions on appropriate voltage adjustments in flicker and phase. The magnitude of the wind turbulence flicker depends on the slope of the current capacity v. the generator's reactive energy characteristics, power pitch v. the turbine 's wind characteristics, wind speed and power turbulence. As embedded winds may start and stop on a regular basis, the flickering effects that result can become relevant. Flicker is typically much less a problem for fixed-pitch, standing-controlled machines than for square-controlled machines (Shepherd & Zhang, 2011; Thiringer, 2007).

2.5.3.3 Harmonics

The frequency converter is necessary to be introduced between the generator and the system is connected to due to the changing frequencies of the produced changing voltages. The recent systems makes use of IGBT(Isolated gated bipolar transistor) to achieve the desired results of acting as a switch known as PWM (Duffey & Stratford, 1989).

In this harmonic order, the inductive components of the impedance system are more contrary to the harmonic flow than is the case in the simpler inverter form, which generates low-level harmonics due to phase wave voltages. The flow of simple harmonic currents can then be reduced by increasing the loss of power in the conductors and spuriously tampering with the safety relays (Balda et al., 1994).

The presence of harmonics in system currents and voltages exists in non-sinusoidal waveforms. This is a critical problem for the electricity authorities to lay down strict, legally enforceable guidelines on the number of harmonics allowed at the key points of the system. Harmonic distortion is specifically investigated in relation to an individual called Total Harmonic Distortion (THD) (P. C. Sen, 1997; Shepherd & Zhang, 2011; Zakeri & Syri, 2015).

2.5.3.4 Self-excitation of induction generators

Normally parallel attached condensers compensated for the fixed-speed induction generator and the magnetizing current from the attached unit through the computer stator windings. When the induction generator is removed from the unit, its voltage and frequency will be lost simultaneously. This condition, also referred to as 'islanding,' causes serious difficulties by generating power above the defined voltage or/and frequency limits as well as the power supply to the system defect.

The generator will start to accelerate when the load is removed as it is disconnected from the system network. The resulting increase in the frequency of the voltages produced is then followed by an increase in the pace. The loss of the equivalent circuit system connection can be decreased to Figure 2-32 showing only the dominant impedances of jX_m magnetic circuit generator and the impedance for external power factor correction jX_c (Gupta et al., 2013; Zhao et al., 2015).

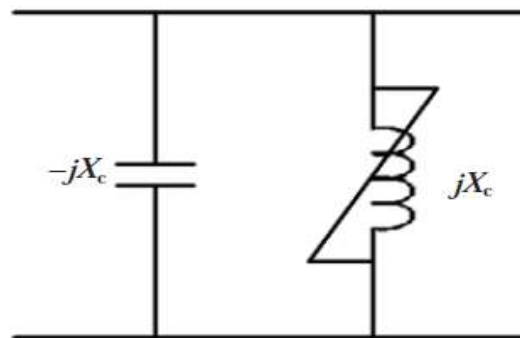


Figure 2-32: Equivalent circuit of a disconnected induction generator (Shepherd & Zhang, 2011)

Self-excitation occurs when a capacitance of the correction power factor is equal to the generator's non-loading reactive power. Thus, as the energy oscillates between the magnetic field of the generators and the power factor correction condensers, it may generate excessive voltage levels that are enough to destroy the connected equipment. Compensated wind turbines have a fast-acting relay safety, if it should be disconnected, to detect and shut off the turbine. (Duong et al., 2010; Shepherd & Zhang, 2011; X. Y. Wang et al., 2005).

2.5.4 Control operation of Grid integrated ESS Wind Farm

The design of the wind farm with internal DC connection and energy storage is shown in Figure 2-33. Figure 2-34 displays the electrical equivalent device diagram.

Inside the wind farm, the grid side converter controls its power output as a function of the grid conditions during the control of the grid frequency.

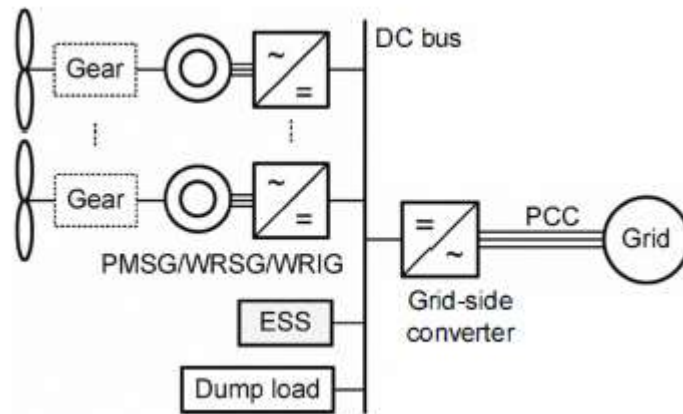


Figure 2-33: Structure of wind farm with internal DC connection and energy storage (Tran & Khambadkone, 2012)

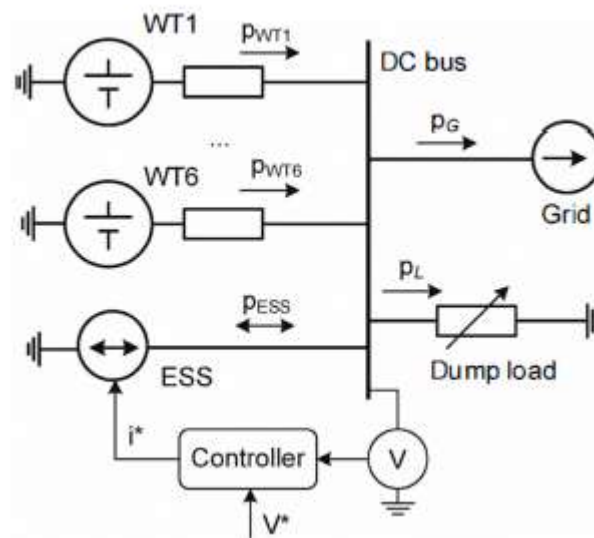


Figure 2-34: Equivalent diagram of wind farm with internal DC connection and energy storage (Tran & Khambadkone, 2012)

The grid converters follow the strategies derived from the secondary frequencies which includes power delta control and power balance or dead band from the primary frequencies.

The above stated point can therefore act as a non-varying power load towards the DC bus of the wind energy farm. Internal power fluctuation is caused by the failure of a single turbine along the network even though lesser power is still delivered to the grid.

The above mentioned fact causes the instability within the wind energy farm. The braking resistor (BR) or the dump-load is thus used in order to stabilize the operation of the wind energy farm since it operates on a N-1 turbine principle (Anca D. Hansen et al., 2002a; Logue & Krein, 2001; Tran & Khambadkone, 2012; L. Wang et al., 2009).

The above-mentioned method has a disadvantage of inability to stabilization of the system and the power waste. Another solution is the use of energy storage to boost device damping. Control in however does not understand the energy storage dynamics. Moreover, a state-of-the-art model of all wind farm components guarantees design complexity.

Energy storage system (ESS) is presented by a simple dynamic control principle to produce a stable wind energy farm. ESS controls parameters are provided with reference to the small and large signal stability. The simulated results shows stability of the wind energy farm when there is constant power load (L. Wang et al., 2009; X. Y. Wang et al., 2005).

A. Criterion for small-signal stability

The load side current perturbation is given by the following equation when the small bus voltage V_b (X. Y. Wang et al., 2005):

$$i_{\Sigma load} = i_L + i_G + i_{ESS} \quad (2.7)$$

Where i_L , i_G and i_{ESS} are grid, dump, and energy storage system disturbances, respectively. Positive criterion for small-signal stability in load side disturbance is (X. Y. Wang et al., 2005):

$$P_{\Sigma load} = v_b i_{\Sigma load} > 0 \quad (2.8)$$

Dynamic impedances at the load side in the wind energy farm are as follows(Tran & Khambadkone, 2012; X. Y. Wang et al., 2005):

$$Z_L = \frac{v_b}{i_L} \quad (2.9)$$

$$Z_L = \frac{v_b}{i_G} \quad (2.10)$$

$$Z_{ESS} = \frac{v_b}{i_{ESS}} \quad (2.11)$$

The small signal criterion is then reflected as the total impedance load ($Z_{\Sigma load}$) and is positive. (Tran & Khambadkone, 2012; L. Wang et al., 2010):

$$\frac{1}{Z_{\Sigma load}} = \frac{1}{Z_L} + \frac{1}{Z_{Grid}} + \frac{1}{Z_{EES}} > 0 \quad (2.12)$$

B. Criterion for large-signal stability

In the wind energy farm, Direct Current bus voltage (v_b) is expected to not vary at any rated voltage V_b , Voltage deviation Δv_b is therefore expected to be zero (Duong et al., 2010; Tran & Khambadkone, 2012).

$$\Delta v_b = v_b - V_{b, rated} = 0 \quad (2.13)$$

When $\Delta v_b \neq 0$, occurs during large disturbance and the below relationship is expected

$$p_{bus} \Delta v_b < 0 \quad (2.14)$$

whereby P_{bus} is the bus power, which discharges or charges the bus capacitor C_{bus} .

For wind energy farm, we have the below relationship:

$$p_{bus} = P_{\Sigma WT} - P_L - P_{ESS} - P_{Grid} \quad (2.15)$$

$P_{\Sigma WT}$ is total power from wind turbines. P_L , P_{ESS} , P_{Crid} are load power, ESS power and grid power, respectively. Condition (2.14) ensures that DC bus voltage is maintained at its rated value. The condition for large-signal stability is then:

$$H_{\infty} = \lim_{t \rightarrow \infty} p_{bus} \Delta v_b < 0 \text{ for } \Delta v_b \neq 0 \quad (2.16)$$

2.5.4.1 Selection of dynamic control structure

The stabilization of the wind power plant, the dynamic control of the energy storage system, must be able to generate the relevant dynamic impedance for the energy storage system. Based on the impedance criterion, the magnitude of the ESS dynamic impedance Z_{ESS} must be smaller than Z_{CPL} , which ensures stability under continuous power loads. (Tran & Khambadkone, 2012; L. Wang et al., 2009):

$$|\tilde{z}_{ESS}| \ll |\tilde{z}_{CPL}| \quad (2.17)$$

Multiple controls strategies are analysed below:

A. Power control configuration:

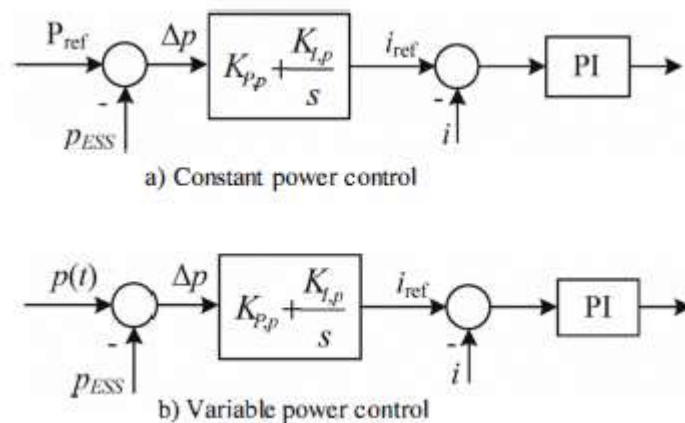


Figure 2-35: Structure of power control strategy (a) Constant power control (b) Variable power control (Tran & Khambadkone, 2012).

The power control has the primary loop as a current control and secondary loop as a power control, shown in Figure 2-35. By the assumption of dynamics of current loop being negligible, we then have (Luta, 2014) (Logue & Krein, 2001):

$$i = K_{P,p} \Delta p + K_{I,p} \int \Delta p dt \quad (2.18)$$

1) The non-varying power control: For constant power control

$$di = -K_{P,p} dp + K_{I,p} (P_{ref} - p) \quad (2.19)$$

$$dp = d(vi) = vdi + idv + dv \cdot di \approx vdi + idv \quad (2.20)$$

Neglecting $K_{I,p}$, we have:

$$\tilde{z}_{ESS,p} = \frac{dv}{di} = -\frac{1}{K_{P,p}i} - \frac{v^2}{p} \quad (2.21)$$

The dynamical impedance $IZ_{ESS,pl}$, increases and the condition in (2.11) cannot be fulfilled as the voltages v rise and the power p is connected to the reference F_{ref} . Constant power control, if the power comparison P_{ref} for the ESS is smaller than the PCPL constant power load, is called a power buffer. The volatility arising from a constant electricity load reduces.

The voltage of the bus and instability are increased when the P_{ref} is higher than the P_{CPL} by a constant power imbalance. $P_{ref} = P_{CPL}$, which requires fast contact, performs the power balance. Variable power control: Instead of the P_{ref} constant power relation, the variable power relation $p(t)$ is used on the variable power control scheme to avoid power differences. Usually, instant power $p(t)$ is chosen as a power differential between wind turbine power and grid power.

This approach is to set reference $p(t)$, such that the power criterion set in condition is fulfilled (2.14) when the DC Bus Voltage is different from its rated point of operation. (Duong et al., 2010; L. Wang et al., 2009, 2010). Otherwise, there are broad voltage differences due to the difference in power from the current power reference. In the controller design in Ref this condition was not specified.

Furthermore, as the $p(t)$ immediate power relationship tends to change, stability improvement depends on how the $p(t)$ relationship is formed. It can be unstable if ESS power PESS has complex limits and cannot readily track different $p(t)$ systems. This problem was not discussed in Ref. Finally, the efficacy of this control mechanism depends on the time necessary for measuring and transmitting the immediate power reference. (Duong et al., 2010; L. Wang et al., 2009, 2010).

B. Constant current control

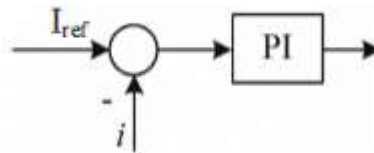


Figure 2-36: Structure of constant current control strategy

Constant current control only has a primary loop as current control, as seen in Figure 2-36. If the current loop dynamics are trivial, we have (Duong et al., 2010; Tran & Khambadkone, 2012; X. Y. Wang et al., 2005):

$$di \rightarrow 0 \tag{2.22}$$

Therefore:

$$\tilde{z}_{\text{ESS},i} = \frac{dv}{di} \rightarrow \pm\infty \quad (2.23)$$

Condition in (2.24) is not satisfied. Therefore, constant current control for ESS cannot stabilize system. Non varying voltage control:

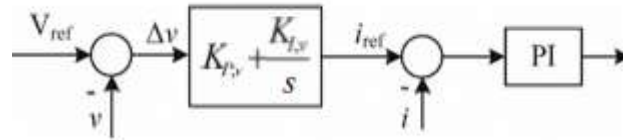


Figure 2-37: The configuration of constant voltage control strategy

The voltage control without difference has a primary loop as the power control and a secondary loop as the voltage control. If the current loop dynamics are trivial, we have (Duong et al., 2010; Tran & Khambadkone, 2012):

$$i = K_{P,v}\Delta v + K_{I,v} \int \Delta v dt \quad (2.24)$$

$$di = -K_{P,v}dv + K_{I,v}(V_{\text{ref}} - v) \quad (2.25)$$

By not considering $K_{I,v}$, we have:

Condition can be achieved in (2.17) if $K_{p,v}$ is high enough. In addition, the continuous voltage control system with complete $K_{p,v}$ and $K_{I,v}$ pipelines will continue to ensure stable system operation at constant power load (Arulampalam et al., 2006). Consequently, constant voltage control is chosen as the dynamic ESS control.

2.5.4.2 Dynamic Control of ESS stabilization of Wind Farm

The anticipated dynamic control strategy is based on the constant voltage control structure, but the gain of voltage controller is adjusted to satisfy presented stability criteria (Anca D. Hansen et al., 2002a).

$$K_P = \left| \frac{1}{\tilde{z}} \right| = \left| \frac{\tilde{i}}{\tilde{v}} \right| \quad (2.26)$$

A. Small-signal stability

Based on the previous data, since the power from the wind farm to the grid through the grid conversion system is regulated by grid conditions, for instance, the grid serves as a constant power load in the internal DC bus of the wind farm during its continuous operating power to support frequencies regulation.: Where $P_G = \text{const}$. We have (Tran & Khambadkone, 2012; L. Wang et al., 2009):

$$\tilde{p}_G = v_b \tilde{i}_G + i_G \tilde{v}_b + \tilde{v}_b \tilde{i}_G = 0 \quad (2.27)$$

Neglecting $v_b i_G$, we have:

$$\tilde{z}_G = \frac{\tilde{v}_b}{\tilde{i}_G} = -\frac{v_b}{i_G} = -Z_G = -\frac{v_b^2}{p_G} < 0 \quad (2.28)$$

The grid is then negative and has the same size as its input. The complex input impedance. When the dump load is passive, the dynamic impedance is equal to the passive (C. H. Liu et al., 2012; Tran & Khambadkone, 2012):

$$\tilde{z}_L = \frac{\tilde{v}_b}{\tilde{i}_L} = \frac{v_b}{i_L} = Z_L \quad (2.29)$$

The dynamic impedance of the ESS must meet the small signal stability criterion (Tran & Khambadkone, 2012):

$$\frac{1}{\tilde{z}_{\text{ESS}}} > -\frac{1}{\tilde{z}_L} - \frac{1}{\tilde{z}_G} \quad (2.30)$$

When the dump load is not used: $\tilde{z}_L = Z_L = \infty$, we have (Duong et al., 2010; Tran & Khambadkone, 2012; L. Wang et al., 2009):

$$K_P = \frac{1}{\tilde{z}_{ESS}} > -\frac{1}{\tilde{z}_G} \quad (2.31)$$

B. Stability of Large signal

$$p_{ESS} = v_b i_{ESS} = v_b \left(K_P + \frac{K_I}{s} \right) \Delta v_b \quad (2.32)$$

The bus power is then given by the following:

$$p_{bus} = p_{\Sigma WT} - p_{Grid} - p_L - v_b \left(K_P + \frac{K_I}{s} \right) \Delta v_b \quad (2.33)$$

As PEWT, $p_{\Sigma WT}$, p_{Grid} and p_L are bounded, then by applying the Final value Theorem, we have the following relationship:

$$H_\infty = \lim_{t \rightarrow \infty} p_{bus} \Delta v = \lim_{s \rightarrow 0} s p_{bus} \Delta v = -K_I v_b (\Delta v)^2 \quad (2.34)$$

When $H_\infty < 0$ when $\Delta v_b \neq 0$ to satisfy large-signal stability condition, we have:

$$K_I > 0 \quad (2.35)$$

The dynamic control strategy of an energy storage device for a stable wind farm operation that does not require an immediate reference to energy is explained in this section. The parameters of small signal stability and large signal stability are proposed to assess the stability of the device. The dynamic control system is chosen for the stability of the wind farm against the constant load of power introduced by the grid.

Simulated results have shown that the wind farm will operate against a constant power load operating as a grid under the proposed control scheme or under wind turbine failure conditions. (Duong et al., 2010; Tran & Khambadkone, 2012; L. Wang et al., 2009).

2.6 Conclusion

This chapter discusses the range of characteristics required to dynamically monitor the wind farm 's grid relation. The BESS noticed that numerous applications demands both active and reactive power control. BESS can provide support to frequencies, reduce the energy fluctuations, and sustain an unreliable supply of non-varied local grids, and help preserve the overall system reliability and protection. The additional active power support from BESS helps to increase shipping reliability and robustness of the system. In addition to the other technologies listed above the potential for improving the future penetration of renewable energy sources is great for all energy storage systems in this Chapter. In the next chapter, a case study will be discussed.

CHAPTER 3. CASE STUDY OF WIND FARM IN SOUTH AFRICA

3.1 Introduction

The study is of a Wind Farm situated in 35 km NE of Malmesbury, in the Western Cape of South Africa. The Wind Farm has a total of 46 wind turbines. Each turbine has a hub height 100m, concrete towers, 3 Blade, Double Fed Induction Generator (DFIG), Hydraulic Pitch control, 12kV with an out power 3MW totalling up to a capacity of 138MW. Connected to a 132 kV Distribution network at Windmeul Substation (Wellington), Germanischer Lloyd (GL) Certified and Grid Code Compliant. The initial construction started in March 2013 and Commercial Operation Date July 2014. The owners are Acciona (54.9%), Royal bafokeng Holdings (25.1%), Soul City (10%) and Gouda Wind Energy Community Trust (10%) (Johan.kroes, 2012). Below is the Cape Town wind farm and Acciona wind turbine (Johan.kroes, 2012).



Figure 3-1: Cape Town wind farm and Acciona wind turbine (Acciona Windpower, 2011)

3.2 Wind Turbine Description

The AW 3000 wind turbine has a three-blade upwind rotor with regulated pitch and variable speed with an automatic yaw system.

The turbine is covered with a fiberglass reinforced polyester nacelle cover that protects it from the weather, as well as helping to prevent noise emissions. The rotor consists of three variable pitch blades, three pitch bearings, and a hub. Power is transmitted from the hub, through the low speed shaft, to the gearbox, and to the generator with a fibre-composite flexible coupling that absorbs any possible misalignment between the components. The yaw system of the turbine consists of six yaw motors with gear reducers which drive a toothed yaw bearing attached to the top tower section. The yaw bearing has ten hydraulically actuated brakes to help maintain the orientation of the turbine. In addition, the yaw motors have integrated electric brakes that are applied in the absence of electrical power (Acciona Windpower, 2011).

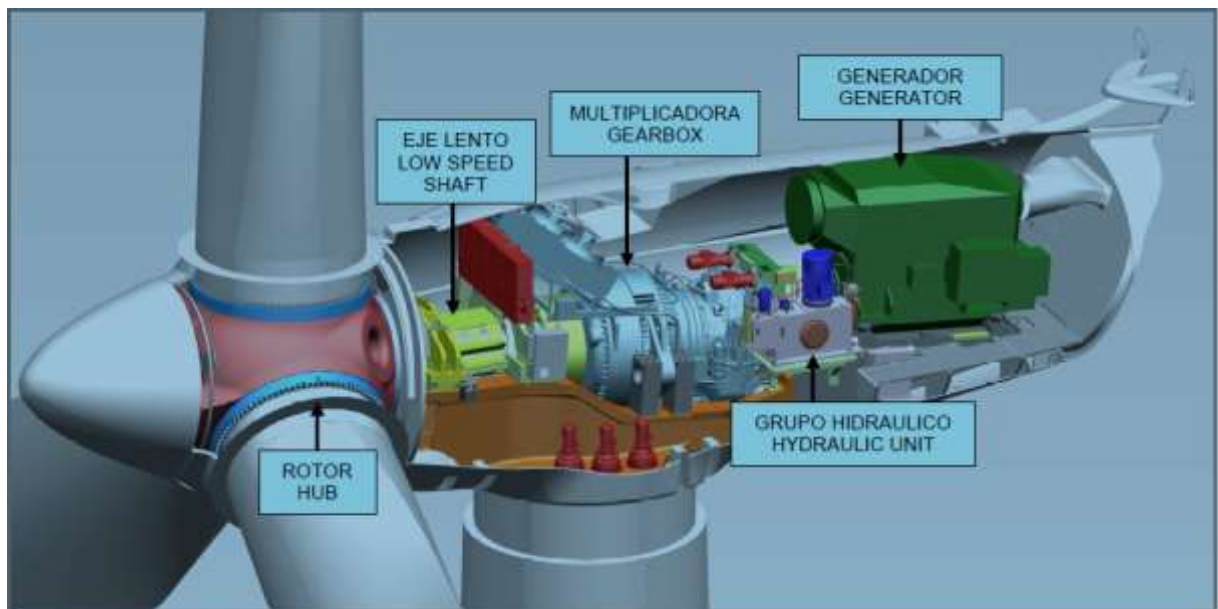


Figure 3-2: AW 3000 wind turbine (Acciona Windpower, 2011)

For low temperatures, the turbine AW3000 has installed a low temperatures Kit. This Kit is made from the following elements (Acciona Windpower, 2011):

- Unit heater: 2 in the tower base (GROUND) and 10 in the Nacelle.
- Spring return actuator for the generator's hatch.
- Motor and pump to heat the hydraulic unit oil.

3.2.1 Rotor

The function of the turbine's rotor is to capture energy from the wind. It is comprised of the hub, blades, and the nose cone (Acciona Windpower, 2011).

3.2.1.1 Blades

The blades are designed to rotate clockwise and are manufactured of fiberglass reinforced polyester. They are secured to the hub bearing with a ring of studs. This bearing with the pitch system allows the blade to rotate longitudinally about its axis (Acciona Windpower, 2011).

3.2.1.2 Hub

The hub, made of nodular cast iron, transmits the captured wind energy through the main shaft. The inside of the hub is hollow and houses the components used for pitch control (Acciona Windpower, 2011).

3.2.1.3 Cone

The nose cone for the turbine is made of fibreglass reinforced polyester and protects the hub from the weather (Acciona Windpower, 2011).

3.2.2 Pitch System

The pitch system used in the AW3000 turbine is a hydraulically actuated variable Pitch system, independent for each blade.

This system consists of (Acciona Windpower, 2011):

- 3 hydraulic cylinders to move the blades upon their axes.
- 2 hydraulic accumulators for each cylinder.
- 3 manifold blocks to actuate each cylinder.
- 3 pitch position sensors.
- 1 pressure distribution block.
- Electrical junction box.

The main functions of the pitch system are (Acciona Windpower, 2011):

- Safe return of the blades to the feathered position (90°) in case of hydraulic or electrical failure.
- Maintain the pitch angle of each blade determined by the turbine controller.

The speed at which the pitch position changes is controlled to avoid fatigue of the turbine.

3.2.3 Yaw System

The yaw system is composed of the following parts (Acciona Windpower, 2011):

- Wind sensor.
- Absolute position and cable twisting sensors.
- 6 yaw motors with gear reducers.
- 2 frequency converters.
- 10 hydraulic brakes.

The wind sensor collects the information regarding the prevailing wind direction and sends it to the PLC which interprets the information and sends the appropriate signals which drive the yaw motors (with gear reducers) to turn the yaw ring gear, thereby rotating the nacelle CW or CCW depending upon the wind direction (Acciona Windpower, 2011).

Each gear reducer is coupled to an electrical motor, which is fed a signal from a yaw frequency converter. The signals are supplied in a manner to provide a smooth start to the motor. The motors contain an electric brake, which is actuated independently from the motor for safety reasons.

In the case that there was no hydraulic pressure or electric power due to a failure or outage, this would not result in the turbine being freely moved by the wind. The yaw system includes an active braking system, which has ten hydraulic brake callipers, which maintain the nacelle's orientation when the yaw gears are not rotating the ring gear (Acciona Windpower, 2011).

The Yaw system of the turbine has three different purposes (Acciona Windpower, 2011):

- To keep the rotor positioned towards the prevailing wind, in RUN, STANDBY and STOP modes.
- To control the twisting of the tower cables.
- To detect the wake effect during RUN mode.

3.2.3.1 Positioning

As previously mentioned, the wind sensor provides the predominant wind direction. Before orienting of the turbine, the hydraulic pressure must be within operational limits.

To move the nacelle, the electric brakes in the yaw motors are released, the hydraulic yaw brakes are then released. Once the hydraulic callipers have been released, voltage is then applied to the yaw motors to move the nacelle to the desired direction (Acciona Windpower, 2011).

3.2.3.2 Cable twisting

The power, supply, and control cables installed in the tower are designed to twist during the orientation of the nacelle. The twisting of the cables is controlled by the PLC through the absolute position and cable twisting sensors.

The PLC monitors and manages the information and when the number of rotations of the nacelle reaches an established limit, the PLC rotates the nacelle in the correct direction to untwist the cables (Acciona Windpower, 2011).

3.2.3.3 Wake condition strategy

When each wind farm is laid out, it is necessary to determine which turbines will be stopped when they enter a wake condition.

For these turbines, the position sectors and the specified low wind conditions must be defined in which these turbines will switch from RUN to STANDBY. The sectors are defined with an imaginary line extending to the north from the turbine being defined. The range of these sectors must be parameterized in relationship to the adjacent turbine. The absolute position sensor defines the position of the nacelle and the conditions for operation (Acciona Windpower, 2011):

- -The turbine is in RUN mode if the signal does not equate to a prohibited sector.
- The turbine switches from RUN to WAKE when the turbine is in a prohibited sector.

3.2.4 Gearbox Cooling and Lubrication Gearbox System

The gearbox of the turbine transmits the torque from the rotor to the generator. The gearbox is equipped with separate lubrication and cooling systems. This system has the following function (Acciona Windpower, 2011):

- Forced lubrication of the bearings and gears.
- Control oil flow depending upon the temperature of the oil.
- Maintain the recommended oil temperature defined by the manufacturer of the gearbox.
- Continuous filtration of the gearbox oil.

3.2.4.1 Lubrication System (recirculation)

The gearbox cooling and lubrication system is enabled in RUN and STANDBY modes and is equipped with the following parts (Acciona Windpower, 2011):

- A pump activated by an electric motor.
- Mechanical pump.
- Oil pressure switch on the gearbox inlet.

3.2.4.2 Cooling System

The gearbox cooling system is managed by the PLC which continuously checks the PT100 sensors that monitor temperature of the oil and bearing (or bearings) in the gearbox. Cooling is achieved with the following parts (Acciona Windpower, 2011):

- 2 Intercooler motors.
- 2 Intercooler fans.

3.2.4.3 Filtration

- Filter 10µm-50µm.
- Filter obstruction switch.
- Micro filter.
- A manifold block mounted directly on the gearbox.

3.2.4.4 Control

Other devices related to the gearbox are (Acciona Windpower, 2011):

- PT100, oil gearbox temperature sensor.
- PT100, bearing gearbox temperature sensor.
- Heater, single-phase resistance type.

3.2.5 Generator

The generator transforms the rotational kinetic energy from the gearbox into electrical energy (Acciona Windpower, 2011).

3.2.5.1 Generator Type

The electric generator has 6 pairs of poles, with the stator connected to the grid, and the rotor connected to the slip rings.

The generator is a doubly fed asynchronous type which is connected through the slip rings to the frequency converter which monitors and controls the magnitude and frequency of rotor current, to establish the desired torque values and rotational speed. With the controller, it is possible to control the phase displacement and therefore, the power factor. As a result, equipment for adjustment of reactive power is not necessary.

The connection of the turbine to the electrical grid is soft and electrical losses are decreased. The generator is protected against short circuits and overloads (Acciona Windpower, 2011).

3.2.5.2 Temperatures

The PLC monitors the generator temperature, which is active in the Run, Pause and Stop modes. To control and monitor the temperatures, the generator is equipped with the following components (Acciona Windpower, 2011):

- Temperature sensors (PT100) located in the stator and bearings.
- Electric cooling fan.
- Internal resistance heaters.

The generator fans are located on the driven end of the generator. They blow the air from the nacelle through the generator, thus cooling the generator windings and the slip rings. The fans are activated when the generator is coupled and in STOP as well as other conditions. The fans are not activated in FAULT and EMERGENCY states. The electric fans for the generator have other secondary functions (Acciona Windpower, 2011):

- Cool the nacelle.
- Cool the hydraulic unit oil.

The resistance heaters located in the stator windings and in the slip ring compartment are used to reduce the exposure of the windings to humidity.

3.2.6 Hydraulic Power Unit

The AW3000 turbine hydraulic system has been designed to provide and control the necessary pressure to the yaw and pitch systems. Their functions are (Acciona Windpower, 2011):

- Control of the blade pitch angle during normal turbine operation.
- Bring the blades to the safe (feathered) position (90°) in the event of electrical fault or insufficient pressure.
- Activate the Yaw brakes.
- Activate the disc brake (high speed shaft).
- This system consists of two independent hydraulic units:

3.2.6.1 Pitch hydraulic unit

This unit provides hydraulic pressure for the main accumulator and for the blade accumulators, cylinders, and lock pins. This hydraulic unit is active in STOP (Acciona Windpower, 2011).

3.2.6.2 Brake hydraulic unit

This unit provides hydraulic pressure to the Yaw brake accumulator, high speed shaft brake accumulator, Yaw brake callipers, and the high-speed shaft brake callipers. This hydraulic unit is activated from STOP. There is also a manual hydraulic unit that has the following functions (Acciona Windpower, 2011):

- Apply braking to the high-speed shaft through the brake callipers.
- Activate the low speed shaft locking pin.

3.2.7 Rotor Locking and Braking System

The rotor locking and braking system consist the following (Acciona Windpower, 2011):

3.2.7.1 Aerodynamic braking system

The blades are used to apply aerodynamic braking to the turbine.

The turbine can be stopped during operation completely by aerodynamic means by moving the blades into the feathered position. The turbine speed is reduced without overloading the gearbox or connected systems.

3.2.7.2 High speed shaft braking system

The brake system is composed of a brake disc and two hydraulic callipers that are connected to the flexible coupling on the gearbox output shaft. The turbine's high-speed shaft brake is applied only in the three following instances (Acciona Windpower, 2011):

- When one of the emergency buttons is pushed.
- When applying the braking command from the generator through one of the manual modes of the maintenance screen.
- When the turbine goes through test, to calculate the initial pole angle before connecting to the grid.
- With the manual hydraulic unit.

3.2.7.3 Rotor locking systems

The rotor locking will be performed whenever wind conditions permit. The turbines rotor can be locked from two places (Acciona Windpower, 2011):

3.2.7.3.1 Rotor locking from low speed shaft

The rotor locking system for the low speed shaft consist of (Acciona Windpower, 2011):

- Manual hydraulic unit.
- 1 cylinder and lock pin.
- 3 locking sectors.

The low speed shaft locking system has a locking pin that engages any of the 3 locking sectors when hydraulic pressure from the manual hydraulic unit is supplied (Acciona Windpower, 2011).

3.2.7.3.2 Rotor locking from high speed shaft

A brake disc and hydraulic callipers are connected to the gearbox high-speed output shaft for braking of the turbine. In addition, there are holes in this brake disc that allow the high-speed shaft to be mechanically locked. The callipers can be manually actuated with the manual pump or automatically by pressing one of the emergency buttons.

After actuating the brakes to stop the rotor, align the holes in the calliper and brake disc to allow installation of the locking pin. Finally, insert the lock pin, screwing it into the brake calliper (Acciona Windpower, 2011).

3.2.8 Safety System

The AW 3000 Safety System fulfils the requirements established in the Germanischer Lloyd IV Non marine technology, Part 1 The Safety System monitors the sensors and hardware with the software in the control system and is connected to the relays from the Safety System. Both the Safety and Monitoring Systems are supplied with low

voltage power from the low voltage side of the transformer. When the Safety System is not powered, the wind turbine goes to a safe position where the blades are in a feathered orientation which provides minimum resistance to the wind (Acciona Windpower, 2011).

3.2.8.1 Safety system description

The Safety System consists of discrete hardware sensors connected to the monitoring circuit of a master safety relay. AW3000 has three different control cabinets according to the different distributed control areas (Acciona Windpower, 2011):

- Power Converter cabinet located on the base of the tower.
- Ground controller cabinet located on the base of the tower.
- Top controller cabinet located on the Nacelle.

To integrate a global safety system, a safety relay is placed in each of these cabinets. One is the master, located in the Ground Controller, and the other two are configured as slaves. Every time the safety system is triggered, the safety relays will open, setting the condition in the PLC (Acciona Windpower, 2011).

3.2.8.2 Safety system sensors

The sensors included in the turbine's safety system are the following (Acciona Windpower, 2011):

- Over speed TOG.
- Overcurrent relay.
- Vibration sensor.
- Emergency button.

- Emergency relays.
- Yaw Sensor.

The five emergency buttons also activate the safety system, energizing the brake valve for the high-speed shaft. Upon depressing any of the emergency buttons in the nacelle, the high-speed shaft brake is applied immediately and when any in the ground are depressed, the high-speed shaft brake is applied in 60 seconds (Acciona Windpower, 2011).

3.2.9 Sensors

The PLC controls the functions of the AW 3000 turbine which are equipped with a number of sensors that monitor the turbine's important functions, providing the necessary information to the PLC (Acciona Windpower, 2011).

3.2.9.1 Environmental Sensors.

The AW3000 wind turbine is controlled in various environmental conditions with the following sensors. Two, FT702LT acoustic resonance sensors (anemometer and wind direction) with RS485 communication (Acciona Windpower, 2011):

- i. Nacelle temperature sensor.
- ii. Environmental temperature sensor.

3.2.9.2 Speed sensors

The turbine incorporates various speed sensors that monitor and oversee, through the PLC, the speed of various elements of the turbine. These sensors are (Acciona Windpower, 2011):

- Generator incremental encoder.

- Inductive rotor sensor.
- Inductive TOG sensor.
- Inductive generator sensor.

The analysis of the sensors provides the information to set speed alarms and permissions for other subsystems which rely upon the speed of the turbine. The relationship between the Inductive sensors found in the rotor and the generator are related to the gearbox ratio. Therefore, the sensors can protect the turbine from possible over speed conditions (Acciona Windpower, 2011).

3.2.9.3 Vibration sensor

The control of the turbine vibrations is carried out by a Vibration Monitor sensor (PCH1026). The PCH vibration sensor has two accelerometers, one in the X and one in the Y direction as required by Germanisher Lloyd. The vibration control is independent from the control system and is constantly monitoring the level of vibrations. The sensor is specially designed to detect low frequency vibrations.

The vibration sensor is integrated into the safety system. As soon as the vibration level reaches a predetermined value, the safety system opens and the turbine's operating mode changes to EMERGENCY (Acciona Windpower, 2011).

The vibration sensor offers protection through the PLC and hardware protection. In addition, the sensor includes internal monitoring with testing of all its internal sensors (Acciona Windpower, 2011).

3.2.10 Control System

The AW 3000 turbine is a variable speed wind turbine with a generator and controller capable of delivering any level of required torque (within set limits) in the generator.

There are two types of control: torque control and pitch control. The program uses the speed set point to enable one type of control and disable the other. This ensures that pitch control is active and torque control is inactive for speeds above the nominal set point and for speeds below, the opposite is true. The use of one or the other depends upon the speed of the wind (Acciona Windpower, 2011).

At low and moderate winds, the rotor speed is monitored varying the generator torque in such a way that maximum wind energy is captured by turning the blades to the maximum position to gain the most energy from the wind. (Torque control). With strong winds, the generator will reach nominal speed as well as the nominal torque value. Pitch control is used to regulate the rotor speed. The torque is inversely proportional to the speed. So, to maintain the nominal power, the torque demand varies about the nominal speed set point (Acciona Windpower, 2011).

3.2.11 Frequency Converter

The frequency converter is composed of (Acciona Windpower, 2011):

- i. Power Converter:
 - Grid side converter (rectifier).
 - Rotor side converter (inverter).
 - DC-link capacitors.
 - Converter control circuits:
 - IGBTs control cards.
 - Communication devices.
 - Measurement devices.

- ii. Active crowbar and passive crowbar:
 - Protects the converter against the overvoltage. Cooling Systems.
 - Temperature measuring system.
 - External cooling system (water).
- iii. Connection of the grid side converter:
 - Bus preload contactor.
 - Direct power supply contactor.

3.3 Grid connection

Connection to the grid and the auxiliary circuits are composed of the following parts (Acciona Windpower, 2011):

- 12KV Switch gear cabinet.
- Auxiliary services transformer 1200/690/400 VAC 630 KVA.

3.4 Conclusion

In this chapter a case study has been introduced and followed by the wind farm electrical and operation indispensable guide for the safe and efficient operation of the AW 3000 series wind turbine designed and made by ACCIONA WINDPOWER.

This chapter contains important information for operating the AW 3000 series wind turbine safely, competently, and profitably. Following the guide will help to avoid dangers, reduce periods of inactivity and repair costs, increase functional safety, and prolong the life of the turbine. The next chapter presents the system modelling and simulation of the case study (Acciona Windpower, 2011).

CHAPTER 4. SYSTEM MODELLING AND SIMULATION

4.1 Introduction

The network diagram of integration system in this study is illustrated in Appendix 1. The wind farm network consists of 46 wind turbines, 12kV with an out power 3MW totalling up to a capacity of 138MW. The 46 wind turbines, 12kV are all parallel connected to three step-up 50MVA transformer of 132/12 kV. The grid model consists of a 132 kV, 50 Hz, 40 KVA grid supply point.

4.2 BESS for Wind Farm Grid Connected

In simulation research, due to the absence of a common battery model, different software programs may be used. There are certain problems, for example, they represent only the characteristic of battery charging or discharge. In other words, available models can not represent battery behaviour in any situation, including charge, discharge, and storage time. It was implemented into a form of generic battery model. The data sheet from this specified battery model shows the manufacturer's battery discharge characteristic curves. But a detailed battery scheme is not shown by this approach (Zareifard, 2017).

Each battery type has a different mathematical model based on its chemical and physical characteristics. However, a model has not yet been released which can be used for all types of batteries. We therefore suggest in this chapter a standardized model that can be used for all batteries.

A battery model that considers energy leaks and the charge / unload rate is important to achieve a good estimate of the performance of the wind power station. One of the benefits of this model is that it considers the energy leak not only when the battery is charged and discharged, but also when it contains energy (Zareifard, 2017).

Owing to its compatibility when combined with the wind farm in contrast with other battery technologies, the battery that is used in the simulation is the NAS (sodium sulphur). High performance (89%), high power capacity and long lifetime with 100% discharge depth (DOD) up to 2500 cycles. The data on the NAS battery is therefore obtained from the company NGK insulators (NGK Insulators, 2020).

4.3 Battery Model

When the battery is simulated in the model of wind power plant energy, such models do not correspond to energy models. Therefore, in our later control design we are looking for an energy model with the features of this energy storage system. Before we go through the design part of the analysis, we need to see the battery characteristics.

4.3.1 Analysis of the battery Charging and discharging

In general, changes inside the battery, including charging, discharge, and storage, depend on chemical reactions that differ under the following conditions (Zareifard, 2017):

- Charge State
- Capacity of battery storage
- Charging or Discharge rate
- Temperature of the environment

Each of these conditions should therefore be considered to have a comprehensive model.

As we introduce a generic battery energy model, we split battery behaviour over three main periods (Zareifard, 2017):

- i. Period of charge
- ii. Duration of discharge
- iii. Duration of storage

The battery has different behaviour during each of the above cycles, which must be evaluated before developing a model.

- i. Charging mode

During the charge of the battery, energy is converted within the battery. Based on the parameters of the ambient temperature, charge rate, battery capacity and charge status, a certain amount of energy entering the battery is absorbed. For example, the inner resistance of the battery causes some losses which result in the dumping of a fraction of energy (Zareifard, 2017).

- ii. Discharging mode

The battery is extracted from the battery during the discharge process like charging, ambient temperatures, charge rate, battery capacity, battery charge and battery loading. These effects are not, however, identical to charging based on empirical results of any kind of battery. The percentage of lost energy in the discharge phase is found to be greater than the charging time under the same terms (Taghi & Fard, 2017). The data from the producer must be provided in their catalogue to obtain an exact overview of the characteristics of the battery during charging and discharge. Therefore,

we use these data in our design and the following section describes it. Temperature impact on the battery charging and discharging is studied (Zareifard, 2017).

iii. Storage mode

Owing to the chemical reactions within the battery, any energy will lose if there is no charging or discharge in the battery. Factors that significantly depend on the form of battery and the materials that are generated by it depend on the rate of this deduction. The battery's output is heavily influenced by temperature change and has in all above circumstances been investigated. Figure 4-1: shows the battery capacity impact of the temperature.

The standard ambient temperature of 25°, as shown by experimental findings, would achieve the highest efficiency of the battery (Taghi & Fard, 2017).

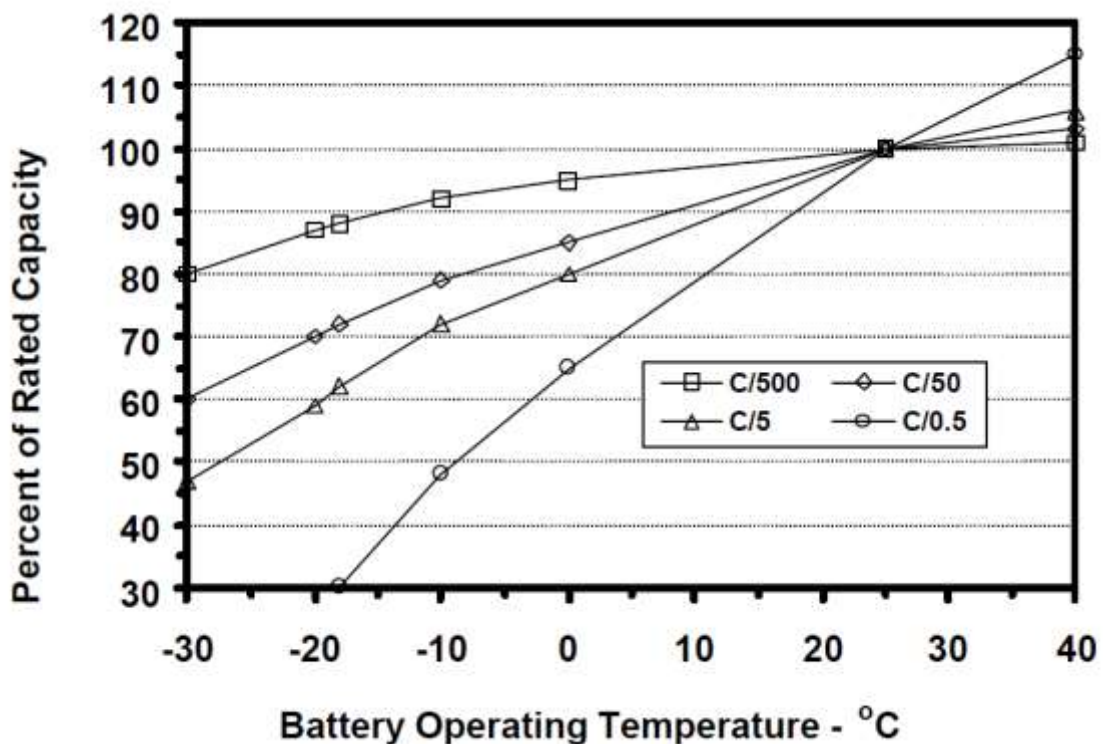


Figure 4-1: Effect of temperature on battery capacity (Zareifard, 2017)

4.3.2 Modelling battery energy storage for wind power plant application

A simple and applicable model is one of the key issues in the modelling of renewable energy plants as it is detailed. Battery energy storage is a key part of the wind power plant, although a practical model helps the control designer to control and optimize the performance of the real plant more easily. There are several models for battery storage, as stated previously in the introductory section and the literature review, each of which constitutes a battery. In this study, we are going to adopt a generic model based on all the battery properties explained in the previous section. The new model can be used to identify certain parameters that must be defined for any type of battery (Zareifard, 2017):

$$x(k + 1) = f(x(k)) + g(x(k); u(k)) \quad (4.1)$$

Functions f and g are specified accordingly:

$$f(x) = g(x)x \quad (4.2)$$

and;

$$g(x,u) = \begin{cases} \beta(x)Mc & \text{for } u > Mc \\ \beta(x)u & \text{for } 0 \leq u \leq Mc \\ -\gamma(x)u & \text{for } -Md \leq u < 0 \end{cases} \quad (4.3)$$

With following constraints

$$\begin{cases} f(x(k)) \leq x(k) & \forall x(k) \\ g(x(k), 0) = 0 & \forall x(k) \\ g(x(k), u(k)) \leq u(k) & \forall x(k), u(k) \end{cases} \quad (4.4)$$

Table 4-1 defines parameters of battery model.

Table 4-1: Parameters of Battery Model (Zareifard, 2017)

Parameter	Description	Unit
α	Battery self-discharge rate	%/day
β	Charging efficiency	%
γ	Discharging efficiency	%
M_c	Maximum charging threshold	MW
M_d	Maximum discharging threshold	MW

The battery energy and energy supplied to the battery is $x(k)$ and $u(k)$ in (4.1). The battery is charged using a positive input energy ($u(k)>0$) and a negative input ($u(k)<0$). Functions f and g are determined by exterior results from various types of batteries, including lead acid and sulfur sodium (NAS) based on charging, discharge, and storage modes. In function f , when battery power is stored, records the state loss. The self-discharge rate in batteries ($0 < \alpha(x)<1$) varying by x is called a loss rate (Zareifard, 2017).

The energy of the battery is absorbed by energy supply ($u(k)$) and energy in the battery ($x(k)$). The energy is displayed in (4.3). For positive input energy, the battery is charged with $\beta(x)$ until it is saturated at M_c . The same pattern is noted in the discharge phase. $\mu(x)$ is the speed of discharge and variable is the parameter. The variable-dependent parameter is x , α , β . The relationship entre x and these coefficients is generally the other way around. That idea is because it meets the maximum potential of a high share of energy lost within the battery.

The relationship between α , β , and β and x will be determined by experiments on a specific battery form. Since the battery's actual behaviour is nonlinear and we are looking for a model that shows this way (Zareifard, 2017).

4.3.3 BESS model for Sodium Sulfur (NAS) battery

For this study, we selected a battery NAS (sodium-sulfur) due to its compatibility with other battery technologies when incorporated into the wind turbine. First, the NAS battery was deployed to control the energy in 'load elevation' and 'peak shaving' and firstly it was used in Japan. As a result of technological advancement in the battery industry, NAS has been developed in a way that improves power efficiency in the demand segment in a large-scale manner (Zareifard, 2017).

We choose NAS type of battery in our analysis for three key reasons (Zareifard, 2017):

- i. Long duration

NAS batteries have shown to be more suitable for large-scale use, such as installation in wind turbines, among other batteries. In the other term, because of their per-unit volume, which are higher than the lead acid batteries, the NAS batteries can provide three times more energy than the lead acid battery. This function is shown in Figure 4-2.

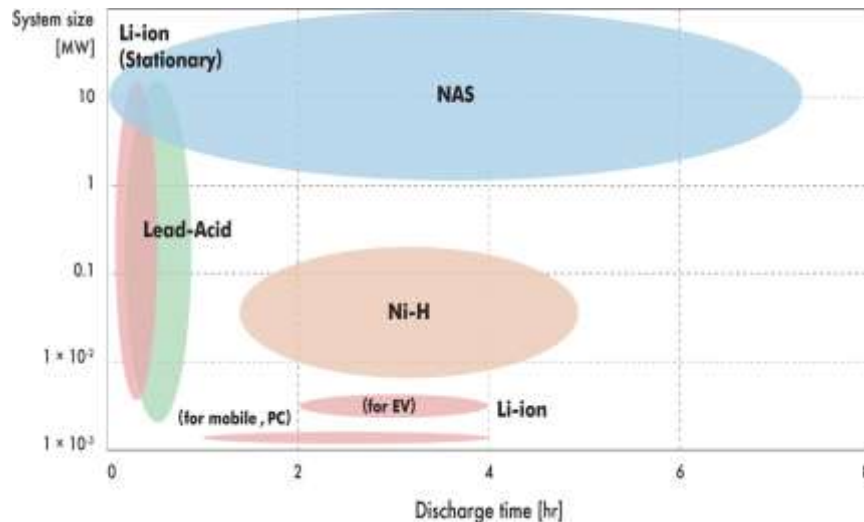


Figure 4-2: Comparison between system size and battery discharge time (Zareifard, 2017)

ii. High power

NAS batteries are compatible with wind and solar (10-100 mW) large-scale plants. NAS is the best choice in terms of its reliability and compatibility to control wind power in large scales.

iii. Expectation of long life

Another characteristic of this battery is its high energy capacity and 'long-duration' as it is 100% DOD and can last up to 4500 cycles (NGK Insulators, 2020). The standard wind energy plant fitted with the battery NAS is shown in Figure 4-3. We derived our model parameters for this battery based on the data collection from the NAS battery catalogue of the manufacturer including patterns in charging and discharging and other factors including temperature impact. We use this model in our control designs to simulate the case study. To simplify the model, we assume that all α , β and α are constants for all x in this study scenario. Table 4.2 describes battery model parameters.



Figure 4-3: A sample of 51MW and 34MW capability built-in NAS with a capability of 245 MWh (Zareifard, 2017).

Table 4-2: NAS Model Battery Parameters (Zareifard, 2017)

Parameter	Description	Total Units
α	Battery self-discharge rate	0.98 %/day
β	Charging efficiency	0.95 %
γ	Discharging efficiency	1.05 %
M_c	Maximum charging threshold	-37 MW
M_d	Maximum discharging threshold	54 MW

Therefore, the nonlinear NAS battery model is as follow:

$$x(k + 1) = f(x(k)) + g(x(k), u(k)) \quad (4.5)$$

Which based on the battery model parameters in Table.4.2, functions f and g are defined as:

$$f(x) = 0.98x \quad (4.6)$$

$$g(x,u) = \begin{cases} 0.95 Mc & \text{for } u > Mc \\ 0.95u & \text{for } 0 \leq u \leq Mc \\ -1.05u & \text{for } -Md \leq u < 0 \end{cases} \quad (4.7)$$

4.4 Nonlinear Control of Wind Farm BESS for Grid Connection

Different application of MPC strategies have been applied for wind farm active power control, voltage control and frequency control. In (W. Liu & Liu, 2020) study, the hierarchical model predictive control (HMPC) method of wind farm BESS for frequency regulation during black-start (BS) is proposed, which consists of two control modes: frequency regulation mode and re-serve recovery mode; The study of (Dang et al., 2010), provides a novel model prediction control (MPC) based control strategy for BESS, is presented aiming to minimize the equivalent operating cost of BESS during each control step. The study of (Hu et al., 2021), provides a comprehensive review of model predictive control (MPC) in individual and interconnected microgrids, including both converter-level and grid level control strategies applied to three layers of the hierarchical control architecture.

The study of (Jadidi et al., 2020), looked at fault effects due to common power loss malfunctions in solar photovoltaic arrays in the presence of microgrid uncertainties and disturbances. In the study, a model predictive control strategy (with a 24-hour prediction horizon) is proposed to reduce the operational cost of microgrids. achieved a smoothing goal to reduce the action of the BESS using Model Predictive Control (MPC) to ensure the overall results were smooth. In short, the common purpose of the above control algorithms is to reduce the output of wind farms to a large extent.

In the areas of renewable energy production and control, MPC is used widely with good results (Yang et al., 2016). In this section, a model MPC-based control system and a non-linear battery energy storage model will be developed to achieve a smooth wind power generation via controlled wind energy storage in batteries about battery power and battery constraint use (Zareifard, 2017).

The objective of the control is to maximize the BESS power supplied to the grid using predicted wind power by smoothing output. We take a battery model as a non-linear one. A scheme diagram of the entire structure is shown in Figure 4-4.

As this figure shows, battery energy storage (P_c) offsets the gap between fluctuation in wind power (P_w) and smooth transmitted power (P_g) (Zareifard, 2017).

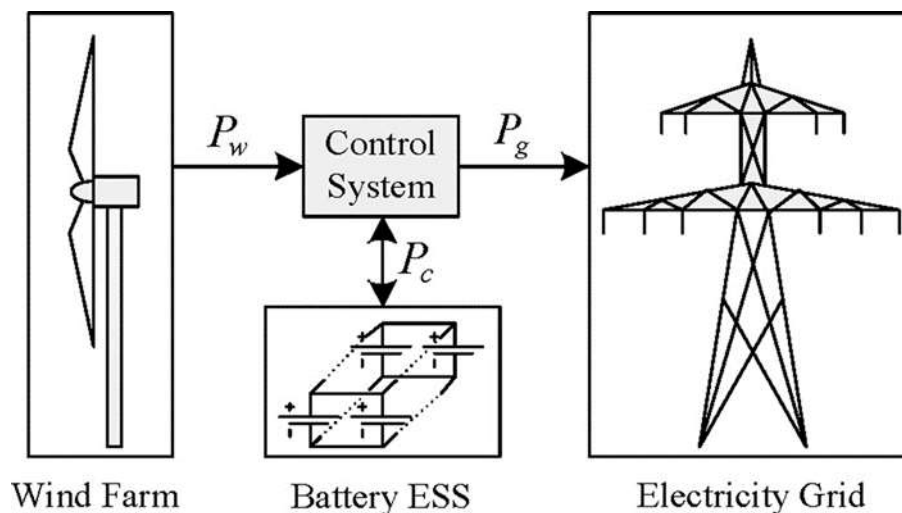


Figure 4-4: Wind farm battery ESS connected to the Grid

4.4.1 Control System Design Description

This research adopts the following models for wind energy storage:

$$\begin{cases} x_1(k+1) = r(k) - u(k) \\ x_2(k+1) = f(x_2(k)) + t_d \cdot g(x_1(k), u(k)), \end{cases} \quad (4.8)$$

With the function below:

$$J = \sum_{k=N_0}^{N+N} ((r(k) - u(k))^2 \rightarrow \min \quad (4.9)$$

Subject to these restrictions

$$0 \leq u(k) \leq c_3 \quad (4.10)$$

$$-c_4 \leq u(k) - u(k-1) \leq c_4 \quad (4.11)$$

$$0 < c_2 \leq x_2(k) \leq c_1 \quad (4.12)$$

$$-c_5 \leq x_1(k) \leq c_5 \quad (4.13)$$

In brief and related references in these studies, physical principles of constraints of the proposed method have been clarified.

In 4.8, $r(k)$ denotes the performance of production of the farm as the quantity of energy being sent to the grid, $x_1(k)$ indicates the error between actual and smooth electricity, $x_2(k)$ is the battery state of charge. Battery energy storage is loaded for positive values of $x_1(k)$ ($x_1(k) > 0$) and loaded for negative ones ($x_1(k) < 0$). This method has placed certain constraints suggested by (c_1) , (c_2) , (c_3) , (c_4) , (c_5) . To maintain the system's smooth performance from 0 to the rated wind power value (c_1) , limit (4.10) is defined. The degree of smoothing is defined by restriction (4.11). The difference between two consecutive quantities of smooth wind power is defined. The restriction (4.12) is chosen to prevent battery overload or load and c_5 in (4.13) constitutes the maximum battery charging / unloading capacity. In (4.10), t_d the coefficient is i.e., $t_d = 5\text{min}/60\text{min} = 1/12$ (Zareifard, 2017).

4.4.2 Proposed Prediction Model

The prediction system for wind farms is linked to the energy storage system to increase the overall system efficiency. We have a method of estimation for short-term wind power in this regard. This model is composed of two stage wind speed and direction projections, the projected wind speed, and the estimated power production in the first phase and in the second phase (Zareifard, 2017).

i. Prediction of wind speed and direction

Since there is a direct relationship between the two parameters of wind speed and direction, an accurate forecasting system should be in place to represent the efficient operation of the wind turbine system. The model used in this study is therefore designed to simultaneously predict wind speed and direction. To achieve this goal, the data obtained from a wind farm is firstly translated into wind vectors as shown in Figure 4-5. The trade-off between the horizon of prediction / control and the accuracy of the control should be stated. When the number of prediction steps is increased, the wind power prediction fault size of the arrays in the MPC calculations will increase dramatically. The processor will thus be burdened, and time delays would occur. Thus, in simulations, we used number of phases as 3.

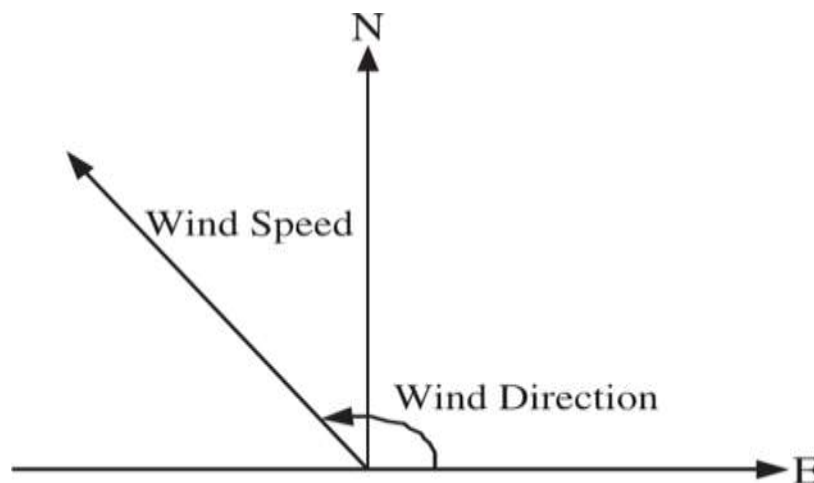


Figure 4-5: Representation of wind vector (Zareifard, 2017)

4.4.3 Controller Design

MPC is based on a solution to an online problem with optimum control when a receding horizon approach is used to solve a transparency optimal control problem over a certain future interval in all current statuses $x(k)$ at a time k , considering current and future limitations. The MPC algorithm calculates the open-loop sequence of the treated variables in a way that optimizes the plant's potential behaviour.

Then the first optimization value is introduced into the farm. The current state $x(k + 1)$ repeats this operation at a time $(k + 1)$. The ability of the MPC to cope with limitations, its functional use and optimization online are some of the main benefits (Zareifard, 2017). Optimization method in this study for minimizing (4.8) is dynamic programming algorithm subject to the system model (4.9) and constraints (4.10), (4.11), and (4.12) with a given initial condition for (x_1) and (x_2) . We first implemented a function to use the dynamic programming procedure (Zareifard, 2017):

$$V(x_1, x_2, m) := \frac{\min}{u(\cdot)} \sum_{k=N_0}^{N+N} (r(k) - u(k))^2 \rightarrow \min \quad (4.14)$$

r is the predicted wind power in (4.14). This is the product of a complete search procedure, since we can take all x_1, x_2 for all $0 \leq m \leq N$, with a small positive step $\varepsilon > 0$, since we calculate $-c_5 \leq x_1 \leq c_5, c_2 \leq x_2 \leq c_1$. DigSILENT solves the problem of optimization at each stage.

4.5 Dynamic Control of Wind Farm BESS for Grid Connection

There are two main components to the adopted control system:

- i. An active reference generator block and
- ii. A controller block based on MPC.

This controller is a new insight into the wind farm power control issue integrated with the device BESS by using this real-time reference generator in the design of the proposed control system.

The benefits of the control system proposed are:

- Optimization in real time and physical limitations of device overall behaviour with MPC,
- Updating the reference signal according to machine states and forecast price and wind power estimates, and
- Increased management of the electricity market with the BESS wind farms while retaining the power signal ramp inside predefined barriers.

It is also seen that the performance of the battery has greatly affected the wind farm. The choice of a suitable battery quantity for a wind farm may thus boost performance. Based on the parameters in the adopted framework, we test our controller with various scenarios.

Finally, we calculate the battery capacity and parameter values to optimize the benefit for a specific wind farm. We equate the results with other potential conditions, such as linear and nonlinear control to demonstrate the strength of the proposed technique. The dynamic system is simulated in Western Cape of South Africa using actual wind farm data from Malmesbury.

4.5.1 Dynamic model of the system

We suggest the following wind power storage system control model in this report (Taghi & Fard, 2017):

$$\begin{cases} x_1(k+1) = r(k) - u(k) \\ x_2(k+1) = f(x_2(k)) + t_d * g(x_1(k), u(k)), \end{cases} \quad (4.15)$$

$$y(k) = x_1(k) \quad (4.16)$$

Where x_1 or $P_g(k)$ are the power sent to a grid in Figures 4-4, $x_2(k)$ is the battery capacity at phase k , $r(k)$ the unregulated wind power output, $u(k)$ or pc the power control signal is a positive ($u(k) \geq 0$) signal and the battery is charged and discharged respectively for negative $u(k)$ values. T_d is a MW to a MWh conversion factor. Functions f and g are described in (4.15) as representing the battery's nonlinear behaviour:

$$f(x) = \alpha(x)x \quad (4.17)$$

and:

$$g(x,u) = \begin{cases} \beta(x)Mc & \text{for } u > Mc \\ \beta(x)u & \text{for } 0 \leq u \leq Mc \\ -\gamma(x)u & \text{for } -Md \leq u < 0 \end{cases} \quad (4.18)$$

With these limits:

$$\begin{cases} f(x(k)) \leq x(k) & \forall x(k) \\ g(x(k), 0) = 0 & \forall x(k) \\ g(x(k), u(k)) \leq u(k) & \forall x(k), u(k) \end{cases} \quad (4.19)$$

Functions f and g are presented to respond to the actual battery activity during the charge or discharge and storage time. Based on function described in (4.17). The chart of the proposed control system was shown below, Figure 4-6.

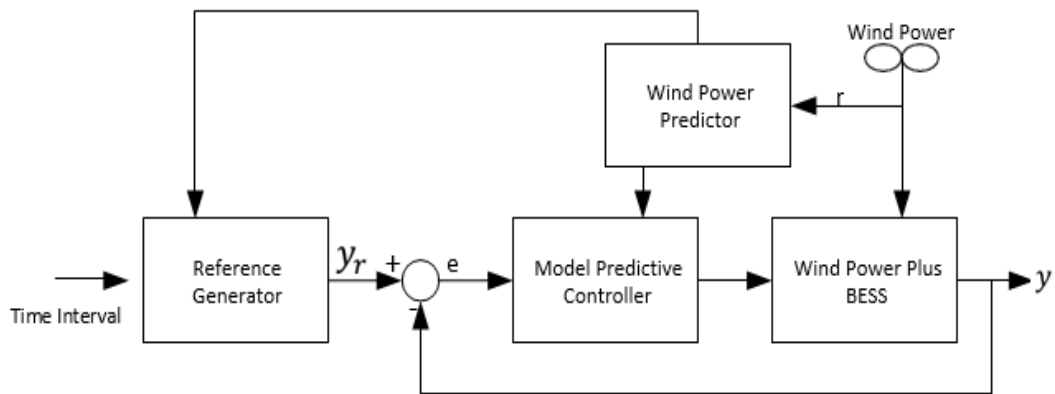


Figure 4-6: Proposed control system block diagram (Taghi & Fard, 2017)

The α coefficient is loaded on the battery. In condition (4.18), g also means the charge and discharge process when the power signal $u(k)$ is sent to the battery. Due to derived experimental data from a battery type, parameters (α , β and μ) are calculated.

In this analysis both α , β and α for simplicity are constant for all x . As previously stated in the 4.3.2 battery model, the charging and unloading technique of a battery is based on the strategy proposed. In relation to the introduction, the novelty of this work is twofold. Whether the integrated battery storage systems are dynamically controlled:

- i. Mitigating variations in the range of wind farms and
- ii. Preserve grid link power stability

The model proposed is an additional battery model that covers energy losses, as described in this section. The battery model parameters in Table 4.1 of the earlier section of the battery model are described.

4.5.2 Reference Generator

The reference signal or target output should be defined for any closed-loop control system, in accordance with the desired system specifications and control objectives.

We therefore propose to establish the reference signal via a decision-making method. The dynamics of our reference generator are as a battery state fraction and wind power expected. Mathematically, the decision-making mechanism is expressed (Zareifard, 2017):

$$y_{\text{ref}}(k) = \begin{cases} r(k) + (2w - 1) x(k) & w \geq 0.5 \\ r(k) + (2w - 1) (x_{2\text{max}} - x_2(k)) & w < 0.5 \end{cases} \quad (4.20)$$

Where $y_{\text{ref}}(k)$ is the power signal reference, $r(k)$ is the wind power forecast, and $x_2(k)$ is usable battery power. w is the Battery Plus Wind Power decision weight and is represented by,

$$w = \frac{1}{1 + e^{-\lambda}} \quad (4.21)$$

It is the best nonlinear exponential parameter function. Two key principles underlie the proposed decision system:

- i. When the wind power is low, we supply the grid with electricity (with less storage and more supplies) and Wherever possible.
- ii. Whenever the wind is high, we save as much energy as possible into the battery (it means more storage and less grid delivery).

We consider that a fraction of the energy available (battery + wind) is supplied to the grid for implementation of our decision-making method, and that is specified by $(2w-1)$.

"Weight function." We name it.

4.5.3 Wind Power Prediction Model

To increase the overall efficiency of the control system, a wind farm prediction system is combined with the energy saving system.

Here we have a method of estimation for short-term wind power. The science of forecasting weather using atmosphere patterns and statistical techniques is the numerical weather prediction (NWP). At the input of the atmosphere mathematical models, existing weather conditions are used to forecast the weather (Khalid & Savkin, 2013). The model proposed consists of two stages:(1) wind speed and direction prediction model and (2) the direction dependent power curve model. The prediction of wind vectors and, consequently, predictions of speed and direction are achieved using multiple observation points in the first stage. The second stage, using direction-dependent power curves, converts the predicted wind speed to the predicted output power. Figure 4-7 represent a schematic diagram of the device weather (Khalid & Savkin, 2013).

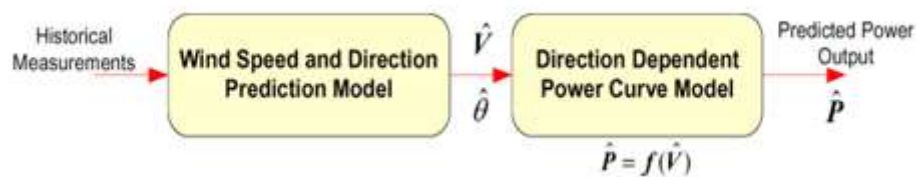


Figure 4-7: NWP Model scheme schematic (Khalid & Savkin, 2012)

The advantages of the proposed solution are based on the use of many observation points leading to performance improvements.

The NWP model data further improved marginally for a 10-minute wind speed forecast. The final wind power forecast was thus substantially improved (Khalid & Savkin, 2013). Data from NWP are collected from the wind farms in the Western Cape of South Africa and are expected to provide ideal wind speed data for ten minutes. The data collected to study the generation magnitude and losses produced by the wind farm were considered in the parcels and thoroughly discussed in section 4.3.5 Simulation.

4.5.4 Dynamic Controller design

MPC is based on the solution of an optimal online control problem where a retrograde horizon approach is used in order to solve an optimum control problem for any current $x(k)$ status at k for a potential open loop interval taking the constraints of present and future conditions into account.

The MPC algorithm measures an open loop sequence of manipulated variables such as the plant's potential behaviour. The first optimization value is then introduced into the factory. The status $x(k+1)$ of this process is repeated at time $(k+1)$. The MPC's ability to comply with limitations, its use in practice, and online optimization are some of the key advantages. Figure 4-6 shows the layout of the proposed control system. The proposed system control law in (4.15) will therefore be accomplished by minimizing the costs feature as follows (Zareifard, 2017):

$$J = V \sum_{k=N_0}^{N+N} \left(y(k) - y_{ref}(k) \right)^2 \rightarrow \min \quad (4.22)$$

Where N is the horizon of the forecast. The dynamic programming algorithm subject to the device model (4.15) and following constraints is the optimisation mechanism in this minimization analysis (4.22),

$$x_{2min} \leq x_2(k) \leq x_{2max} \quad (4.23)$$

$$-U_{max} \leq u(k) \leq U_{max} \quad (4.24)$$

$$0 \leq x_1(k) \leq c_1 \quad (4.25)$$

for all $k \in 0, \dots, N - 1$ with a given initial condition for (x_1) and (x_2) as $(x_1(N_0))$ and $x_1(N_0)$ respectively. There are some constraints which imposed by this system that indicated by (4.23), (4,24) and (4.25).

The limit (4.23). The constraint (4.24) is chosen to avoid overloading or under loading of the battery i.e., the BESS cannot be discharged less than x_{2min} or charged above x_{2Max} , because the battery cannot exceed or be overloaded by the loading of a battery. U_{max} in (4.24) reflects the maximum battery loading or unloading capacity. To keep the output of the system between 0 and rated value of the wind power (c_1), constraint (4.25) is introduced.

We first implemented a function to enforce a dynamic programming procedure:

$$J(x_1, x_2, M) := \min_{u(\cdot)} \sum_{k=N_0}^{N+M} (y(k) - y_{ref}(k))^2 \quad (4.26)$$

Where M is control horizon. We calculate this equation by complete search method, since $0 \leq x_1(k) \leq c_1$, $x_{2min} \leq x_2(k) \leq x_{2max}$, we can take all x_1, x_2 with some small step $\varepsilon > 0$ for all $0 \leq M \leq N$. For simplicity, the MPC algorithm uses wind energy estimation to be similar and equal to three ($N = M = 3$) in a control horizon.

We take it for granted first:

$$\left\{ \begin{array}{l} J(x_1, x_2, M) := \min_{u(\cdot)} \sum_{k=N_0}^{N_0+M} (y(k) - y_{ref}(k))^2 \\ = \min_{u(\cdot)} \{ (y(N_0) - y_{ref}(N_0))^2 + \dots + (y(N_0 + M) - y_{ref}(N_0 + M))^2 \} \end{array} \right. \quad (4.27)$$

Thus, we presume:

$$\left\{ \begin{array}{l} J^*_{N_0, M} = \min \{ J^*_{N_0, M-1} + J_M \} \\ J^*_{N_0, M-1} = \min \{ J^*_{N_0, M-2} + J_{M-1} \} \\ J^*_{N_0} = \min \{ J_{N_0} \} \end{array} \right. \quad (4.28)$$

We assume that we want to optimize $J(x_1, x_2, M)$:

$$\left\{ \begin{array}{l} J^*_{N_0, M} = \min \{ J^*_{0, M-1} + J_M \} \\ J^*_{N_0, M-1} = \min \{ J^*_{0, M-2} + J_{M-1} \} \\ J^*_{N_0} = \min \{ J_{N_0} \} \end{array} \right. \quad (4.29)$$

To calculate $J^*_{N_0}$, we search all x_1, x_2 in full, taking into account the constraints that have been established to find $y(N_0)$ for all $-U_{\max} \leq u \leq U_{\max}$ with small steps from our proposed models (4.1).

After we have found an optimal value for $J^*_{N_0}$, we will go to the next step to find $J^*_{N_0+1}$ and find $J^*_{N_0+M}$ again. The optimal signal control sequence $u^{\text{opt}}(k)$, is found for $k = \{N_0, \dots, N_0 + M\}$ at the end of the optimization cycle.

$$u^{\text{op}} = \{u^{\text{op}}(N_0), u^{\text{op}}(N_0 + 1), \dots, u^{\text{op}}(N_0 + M)\} \quad (4.30)$$

The first value of the sequence ($u^{\text{op}}(N_0)$) is then selected as the first optimization value and implemented in the plant. This process is repeated ($k+1$) and the new step N_0 is $N_0 + 1$, and according to the model, the present state is $x(k+1)$. For our entire path, this procedure is repeated. DigSilent solves the problem of optimization at every stage.

4.6 Simulation

The simulation of integrated Wind Farm BESS is the focus of this section. The simulation is conducted on a DigSILENT simulation software package. The scope, data collection, battery selection type, modelling and result and discussion are outlined in following subsections.

4.6.1 Scope

The scope includes modelling and Simulation of the following parameters:

- i. The wind farm network consists of 46 wind turbines, 12kV with an out power 3MW totalling up to a capacity of 138MW. The 46 wind turbines, 12kV are all parallel to three step-up 50MVA transformer of 132/12 kV.
- ii. The BESS of NAS with 42 enclosure package and battery modules, consisting of 1 680 NAS modules, each rated at 30kW and 216kWh, and with a total rated of 50.4 MW and 201.6 MWh.
- iii. The grid model is consisted of a 132 kV, 50 Hz, 40 KVA grid supply point.

4.6.2 Data Collection

The real wind farm data is used to model the proposed system of control in DigSILENT software. The data obtained from the wind farm network in this simulation consists of 46 wind turbines with 12 kV of output 3MW with a total of 138 MW. Different wind measurements were carried for each month through the year 2016 to 2019. The wind data obtained includes hourly and monthly average wind speeds for each hour in the month. Calculations were performed on these data for each month to obtain the duration in hours for each 1 m/s speed range selected. The total wind speed range was divided into 1 m/s speed ranges taking the ranges: 0-1, 1-2, 2-3, 3-4, and so on. For each month, average wind speed, percentage of occurrence of each wind speed, power density for each wind speed and the total energy available in wind are calculated. Below Figure 4-8 and Figure 4-9 demonstrate a graphical representation of hourly and monthly energy production is demonstrated.

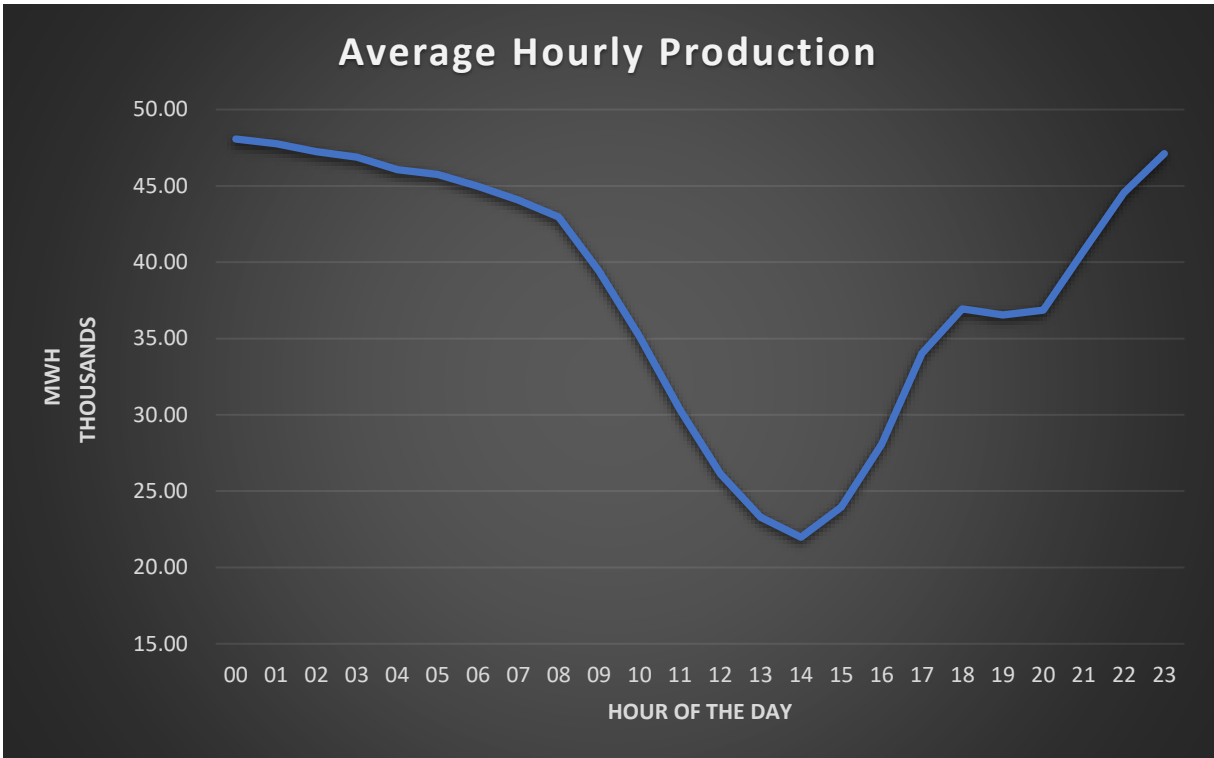


Figure 4-8: Hourly Energy Production (Acciona Windpower, 2019)

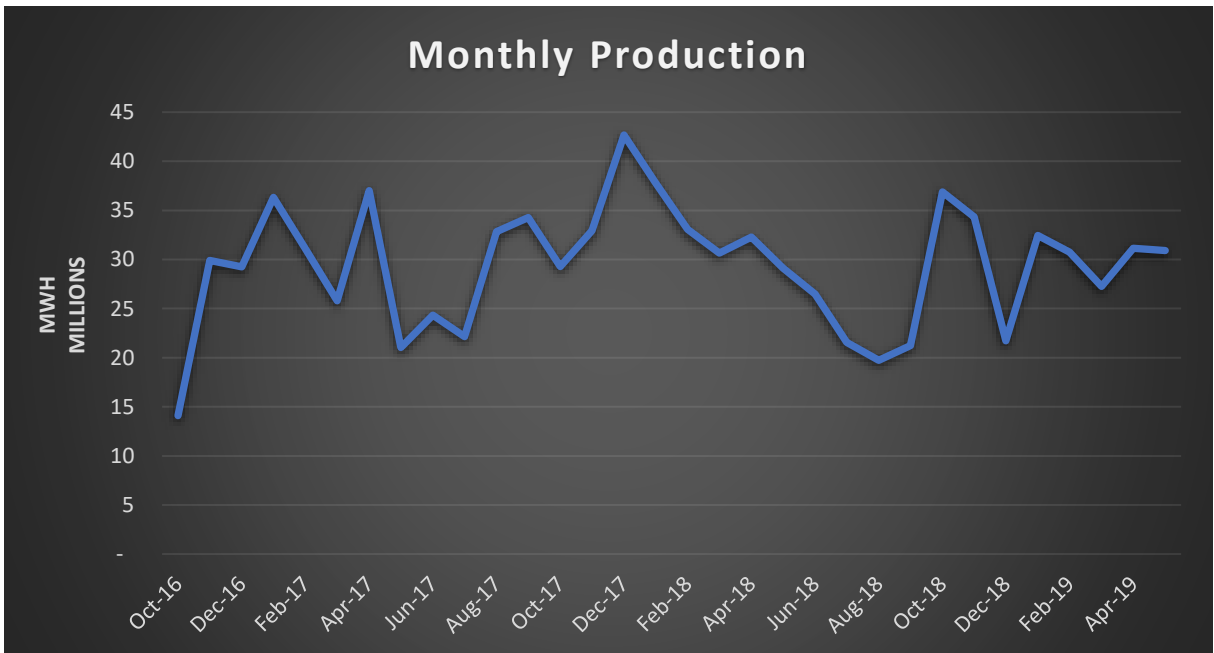


Figure 4-9: Monthly Energy Production (Acciona Windpower, 2019)

Table 4-3 shows the average wind speed for period of year 2016 to 2019 months and energy available in the wind for each month. Table 4-4 shows the average wind speed for year 2019 only for each month and energy available in the wind for each month.

**Table 4-3: 2016 to 2019 January to June production average and Capacity factor
(Acciona Windpower, 2019)**

Month	Monthly Production	Daily Average	Hourly Average	Unit	Capacity Factor
January	26415.7	852.11	35.5	MWh	25.7%
February	22835.5	815.6	34	MWh	24.6%
March	22766.3	734.4	30.6	MWh	22.2%
April	20377.6	679.3	28.3	MWh	20%
May	16414.7	529.5	22.1	MWh	16%
June	19021.3	634	26.4	MWh	19.1 %

Moreover, a 2019 January to June production average and Capacity factor are shown and data is plotted in power diagram in respect to wind turbine power curve.

**Table 4-4: 2019 January to June production average and Capacity factor
(Acciona Windpower, 2019)**

Month	Monthly Production	Daily Average	Hourly Average	Unit	Capacity Factor
January	6603.93	213.03	8.88	MWh	34%
February	5708.88	203.89	8.50	MWh	27%
March	5691.58	183.60	7.65	MWh	30%
April	5094.40	169.81	7.08	MWh	26%
May	4103.68	132.38	5.52	MWh	22%
June	4755.33	158.51	6.60	MWh	24%

The below Figure 4-10 to 4-15 shows a graphical representation of monthly average turbine power vs wind speed for month January to June in the year 2019.

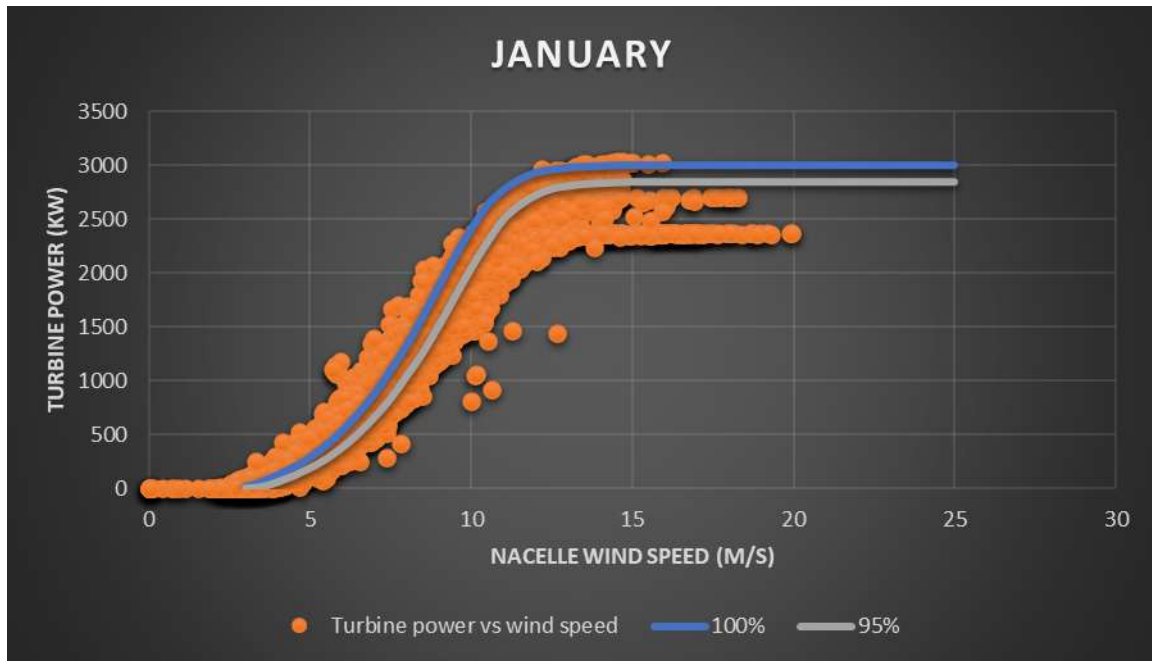


Figure 4-10: 2019 Wind speed in respect to turbine Power January (Acciona Windpower, 2019)

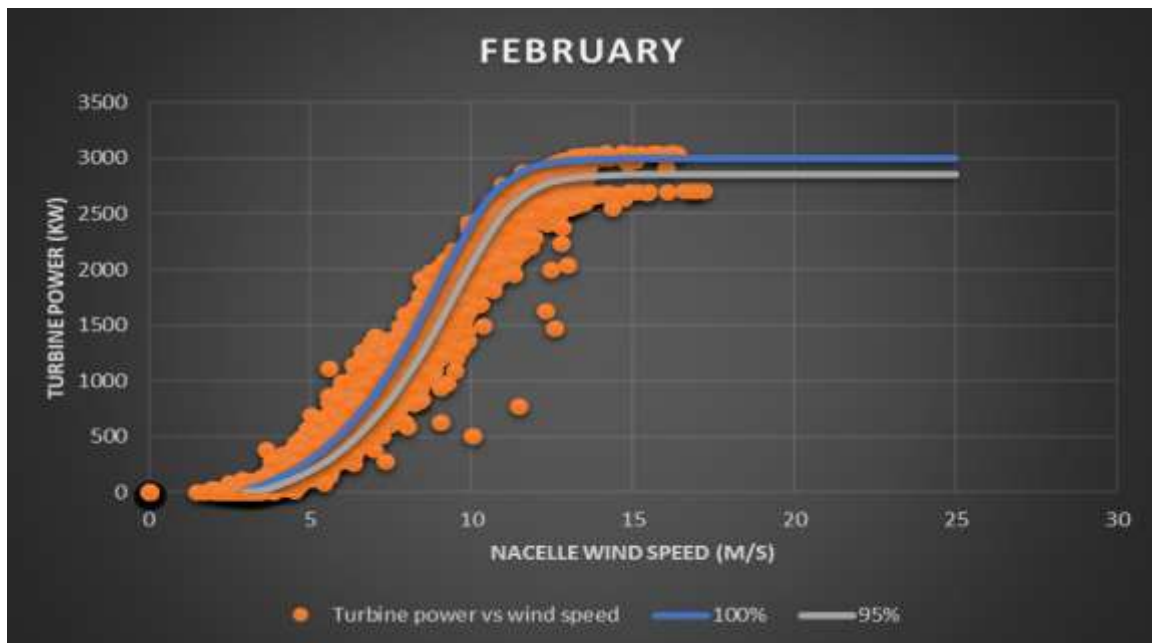


Figure 4-11: 2019 Wind speed in respect to turbine Power February (Acciona Windpower, 2019)

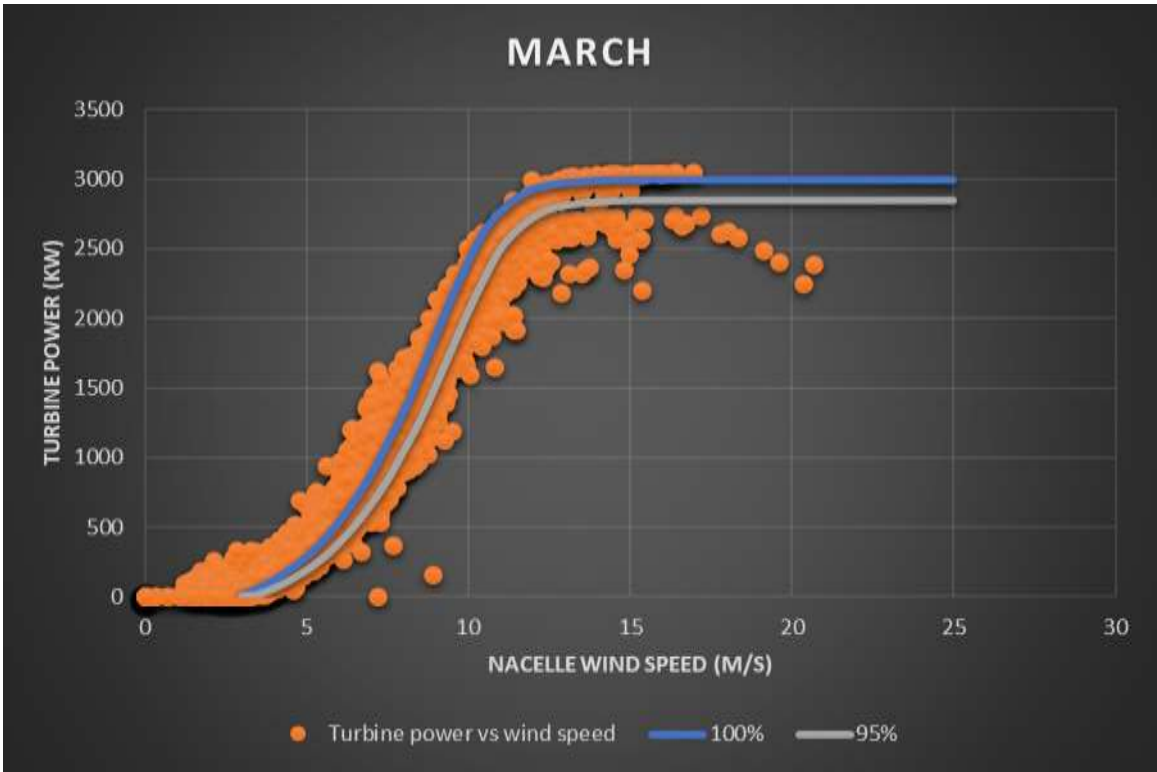


Figure 4-12: 2019 Wind speed in respect to turbine Power March (Acciona Windpower, 2019)

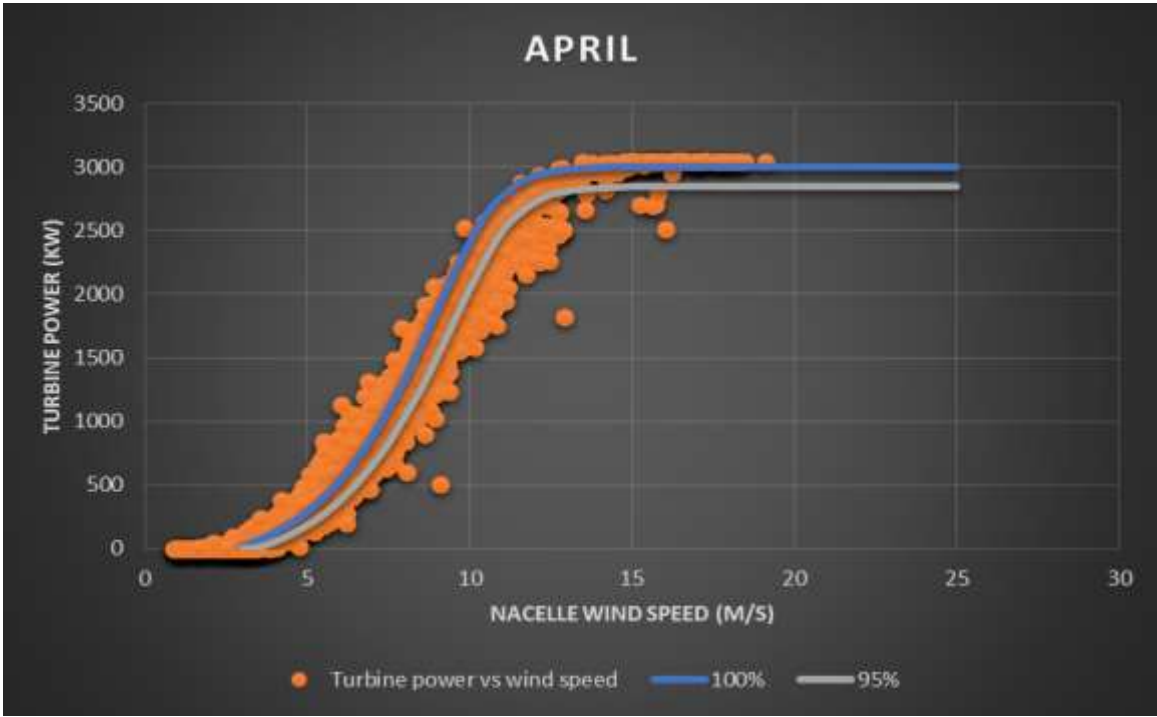


Figure 4-13: 2019 Wind speed in respect to turbine Power April (Acciona Windpower, 2019)

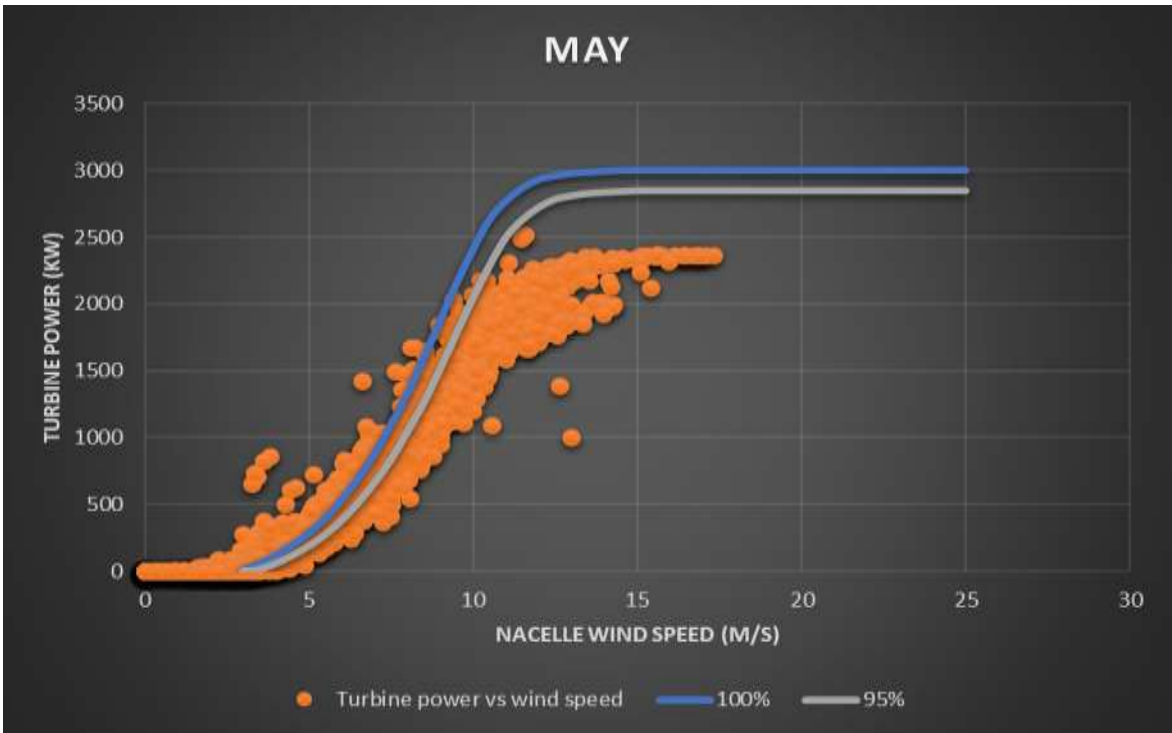


Figure 4-14: 2019 Wind speed in respect to turbine Power May (Acciona Windpower, 2019)

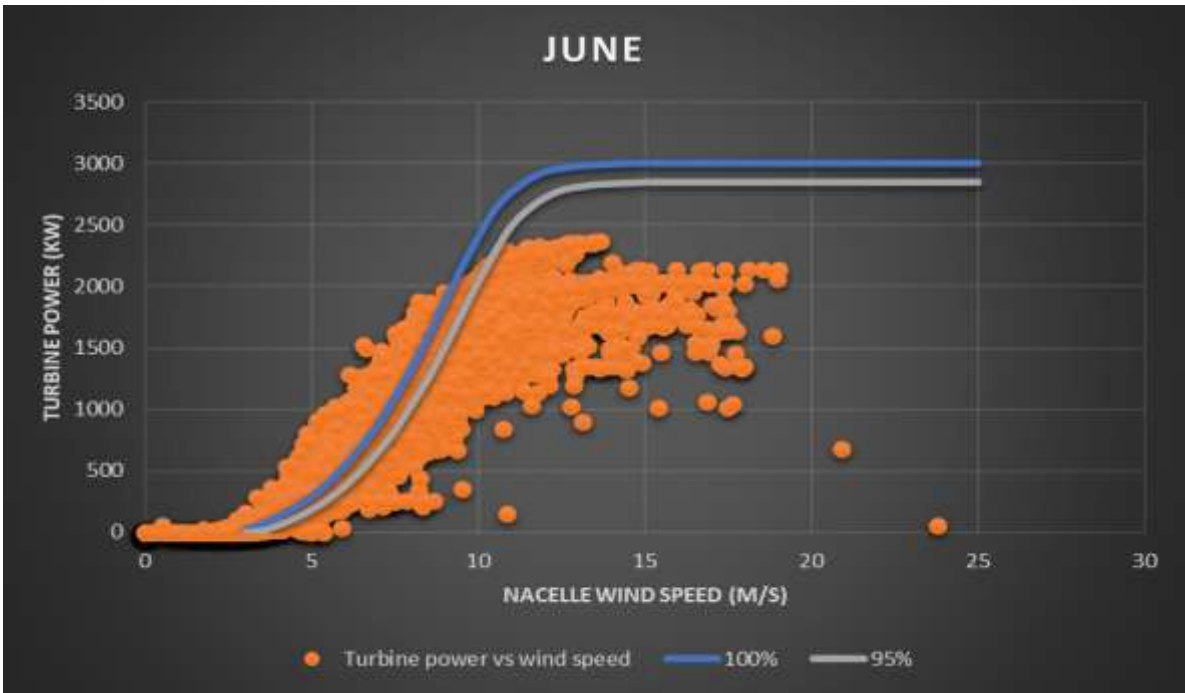


Figure 4-15: 2019 Wind speed in respect to turbine Power June (Acciona Windpower, 2019)

From the figure 4-10 to figure 4-15 illustrated above, it is observable that the months January to April were good months as compared to May, and June in terms of generation energy produced by wind turbines. The wind speed for June was very good but with low generation energy, this may be due to losses and outages.

4.6.3 Battery Selection Type

The battery used is 50 MW NAS (sodium sulfur), as a site's current largest device is 50MW, 300MWh (NGK Insulators, 2020). The data on the NAS battery is therefore obtained from the company NGK insulators. This battery is 1.2 MW and 8.64 MWh in terms of power capacity. A total of 42 batteries are considered to make up 50,4 MW and 362.88 MWh in terms of power capacity for this study. We use the following parameters for the battery model:

$$\alpha = 0.98, \beta = 0.95, \gamma = 1.05, M_d = 138 \text{ MW and } M_c = -50.4 \text{ MW}$$



Figure 4-16: Sodium-Sulfur (NAS) Package type unit (NGK Insulators, 2020)

Table 4-5: Simulated Constraints Parameters (NGK Insulators, 2020)

Parameter	Description	Total Units
Rated Output	1.2 MW and 8.64MWh	50,4 MW and 362.88 MWh
Configuration	40 NAS modules, each rated at 30kW and 216kWh.	40*42 = 1680 NAS Modules
Dimension	10.2W x 4.4D x 4.8H (m)	42 x 10.2W x 4.4D x 4.8H (m)
Weight	132 000 kg	132 000*42 = 5 544 000 kg

4.6.4 Detailed DigSILENT Simulation Model

DigSILENT offers an extensive library of models of power system components. The book contains models such as generators, engines, drivers, dynamic loads, and different network components (e.g. lines, transformers, static loads, and shunts). The grid model and the electrical components of the wind turbine model are also included in the latest work in the latest library as the standard components. DigSILENT 's dynamic modelling language is the wind speed models, physics, aerodynamics, and control systems for the turbines. The DSL enables users to build their own blocks as improvements in existing models or as new ones. These new models can be obtained from a database that can be further used for modelling wind farms on other wind turbines (A.D. Hansen et al., 2003).

The DIgSILENT programme, based on the comprehensive cooperation of DIgSILENT and the national laboratory Riso, was expanded and further optimized for wind energy applications. The two models in DIgSILENT are shown as follows (A.D. Hansen et al., 2003):

- i. Integrated versions that are already existing in the DIgSILENT library, standard electrical parts.
- ii. DSL models generated by the user in DSL simulation dynamics.

The integrated models are standard models for various electrical components that exist in DIgSILENT. These models are not explicitly available to the user in their internal data (e.g. equations, assumptions, and approaches) and can thus only be used as black boxes with predefined inputs and outputs.

Different built-in models, such as generators, electrical converters, transformers, and condensers, are used in the construction of the different wind turbine type in DIgSILENT. The results of the simulation are very much dependent on these integrated component models and are therefore defined briefly in accordance with DIgSILENT documentation. The detailed model of a wind farm in the Western Cape of South Africa is described in this section at the west of Malmesbury, at 35 km NE. This includes DIgSILENT modelling of its wind turbines, batteries, and grid connections.

4.6.4.1 Wind turbine Modelling

The integrated models are standard models for various electrical components that exist in DIgSILENT. These models are not explicitly available to the user in their internal data (e.g. equations, assumptions, and approaches) and can thus only be used as black boxes with predefined inputs and outputs.

Different built-in models, such as generators, electrical converters, transformers, and condensers, are used in the construction of the different wind turbine type in DlgSILENT. The results of the simulation are very much dependent on these integrated component models and are therefore defined briefly in accordance with DlgSILENT documentation (A.D. Hansen et al., 2003).

4.6.4.2 Electrical machinery

For both induction (asynchronous) machinery and synchronous machinery, DlgSILENT offers templates. The induction generators will be based in this article. Blank boxes with predefined inputs and outputs are the DlgSILENT computer types. Figure 4-17 shows the built-in blocks with the most important DFIG input and output signals.

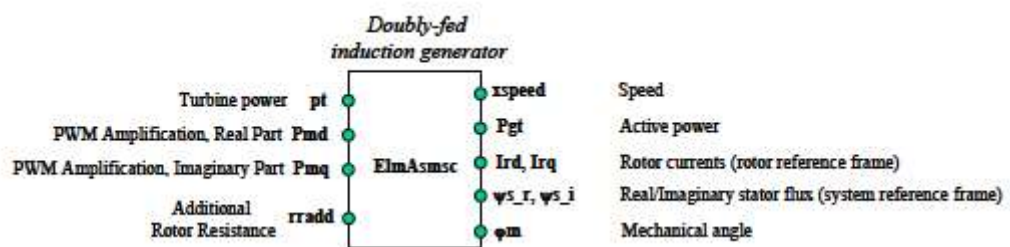


Figure 4-17: Blocks of the DFIG induction generator (A.D. Hansen et al., 2003)

Double-fed induction generator model – with the mechanical input strength of the wind turbine, pulse width modulation factor Pmd, Pmq input, as well as the extra rotor resistance – has Elmsc slip asynchronous system block model. The rotor currents, the stator flux and the mechanical angle of the rotor can be supplied as outputs, as well as the speed and the activated power. The active power, the response power and the slip must be defined for the load flow calculation.

Internally, the corresponding element of modulation of the converter is determined and the power balance between the converter side of the AC and DC is obtained, the DC voltage and DC current (A.D. Hansen et al., 2003).

a) Doubly fed induction generator (DFIG)

In DlgSILENT, a model of the DFIG (Figure 4-18), the typical induction generator is extended to the Z_{rot} rotor impedance by means of an induction rotor side converter sequence (DlgSILENT GmbH, 2002).

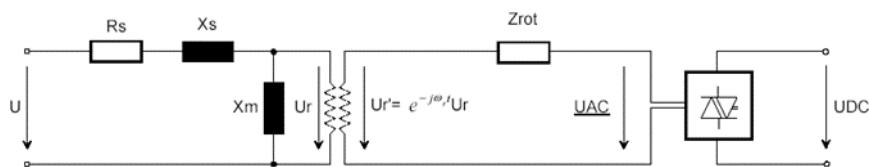


Figure 4-18: Double-fed induction machine with rotor side converter induction unit (DlgSILENT GmbH, 2010)

The PWM converter built into the rotor circuit allows the system to be flexibly and easily operated by changing the size and phase angle of the AC voltage U_{AC} generator on the rotor side. The modulation factor PWM is changed. The DC voltage and the DC current can be determined based on the power balance between the AC and DC side of the converter.

b) Power Converters

For various power converters such as: rectifiers / inverters, PWM converters and soft starters, DlgSILENT offers models. The following are briefly illustrated.

i. Rectifiers/Inverters

For DC control connections or for built-in control electrical devices like variable speed drives, the corrective / inverter model is used. Modeling of various frequency converters can be achieved by rectifier and inverter. For example, in the doubly fed induction generator concept,

the rotor circuit is connected to the grid through two PWM converters working back-to-back (DIgSILENT GmbH, 2010).

ii. Converter for PWM

In general, self-determined pulse-width modulated circuits are used for converters used in wind turbines (see Figure 4-19).

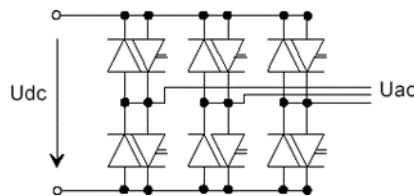


Figure 4-19: Generic PWM converter model (DIgSILENT GmbH, 2010)

Six valves with turning capacity are installed in these circuits and six diodes are constructed in parallel. The valves are usually made by IGBTs since they allow for higher frequency of switching than classical GTOs.

Figure 4-20 demonstrates the general model for the PWM converter, which generally acts as a converter of the volt-age source.

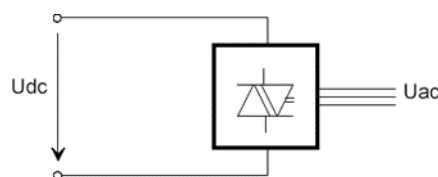


Figure 4-20: PWM converter model (DIgSILENT GmbH, 2010)

DlgSILENT gives multiple converter control modes, such as (Sørensen, 2001):

- U_{dc-Q} mode: dc voltage and reactive capacity control. This mode is typical of a double feed induction machine's grid-side converter.
- $U_{ac-\phi}$ mode controls the magnitude and corner on the DC side of the ac-voltage. This mode is popular when a converter drives an induction machine at AC side for variable speed-driving applications.
- P-Q mode: active and reactive power management

iii. Soft Starter.

The soft starter is a basic, inexpensive electrical power component used in a wind turbine at fixed speeds when the power generator is attached or disconnected. The role of the soft-starter is to reduce the in-start current and restrict storms to the grid.

The input current can be up to 7-8 times the rated current without a soft starter, which could result in extreme voltage rupture in the grid. As switching devices in each step, the soft starter contains two thyristor systems. In anti-parallel, they are linked to each point. During predefined grid cycles, the smooth connection of the generator to the grid is accomplished by changing the firing angle (α) of the thyristors. There is a clear non-linear connection between the firing angle (α), and the resulting amplification of the soft starter and the power factor of the connected element is also dependent upon it. The thyristors are circumvented after in-rush to eliminate losses in the whole device. The DlgSILENT soft start model is a dqo model that takes a stage and an RL source into account. There are several soft starter configurations, which supply a machine, such as (Sørensen, 2001):

- link to the star
- connection to the Delta and

- link between branch and delta.

Mostly, the Delta relation for the induction machine is used in wind turbine applications since the current rating of stator currents can be decreased and, in this case, the third harmonic in line currents is omitted. The soft starter does not come in series on the induction generator lines in delta branch attachment but is installed in the generator delta and thus reduces the power rating for the thyristor.

As in DIgSILENT, two separate components are the soft starters and the generator block, the soft starter generator cannot directly be modelled with a delta branch. The delta branch relation can be equal with an ideal delta / star transformer with the soft starter and a star-connected induction generator in sequence (Sørensen, 2001).

i. Capacitor bank

The condensing unit provides reactive power to an electrical part (e.g. to the induction generators or the grid). This lowers the reactive power that the grid generator consumes. A series relation of a condenser (C), a L reactor, and a resistance (R) models the general compensatory instrument in DIgSILENT. The user can choose different types of shunt, e.g. C, R-L, R-L. The condenser can be connected in a star or delta configuration. A parallel link of condensers must be connected by several compensators parallel to the same busbar, as shown in Figure 4-21.(A.D. Hansen et al., 2003).

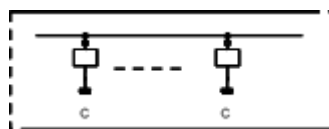


Figure 4-21: Capacitor bank in DIgSILENT (A.D. Hansen et al., 2003)

In response to changes in demand from reactive electricity, the condenser bank system is a combination of shunt condensers which can be turned on and off individually.

c) Transformers

In both 2-winding transformers as well as 3-winding transformers, DlgSILENT offers model blocks. The 2/3 winding transformer is a 2/3-port feature that links the power system with 2/3 cubicles. Both transformers have voltage, electricity and reactive power control manual and automatic tap changers. The following shows briefly the model of the 3-wind transformer. The diagram of the positive sequence is shown in Figure 4-22 with a simplified form of tap changer (A.D. Hansen et al., 2003).

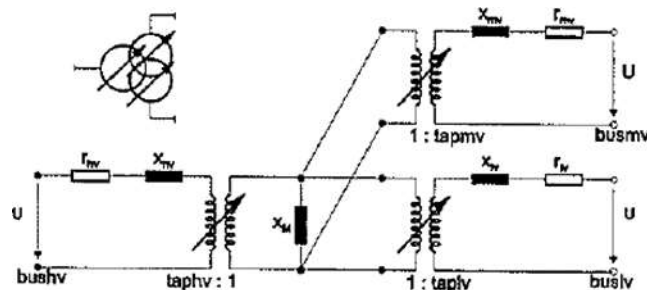


Figure 4-22: Positive sequence : three windings transformer equivalent model (A.D. Hansen et al., 2003)

A linear or piecewise linear magnetization current may be chosen which is described by a current knee, a linear current and a saturated current. Figure 4-23 to Figure 4-25 show the zero sequence equivalents of 3 common winding links.

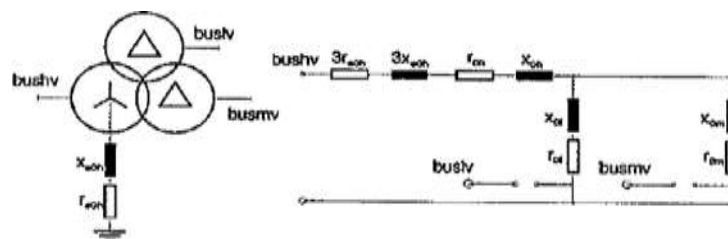


Figure 4-23: Zero sequence - grounded star/delta/delta connection (A.D. Hansen et al., 2003)

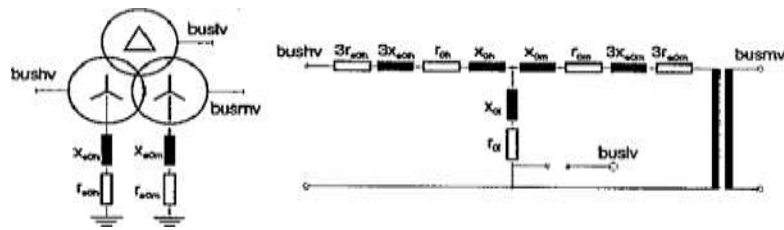


Figure 4-24: Zero sequence - grounded star/grounded star/delta connection (A.D. Hansen et al., 2003)

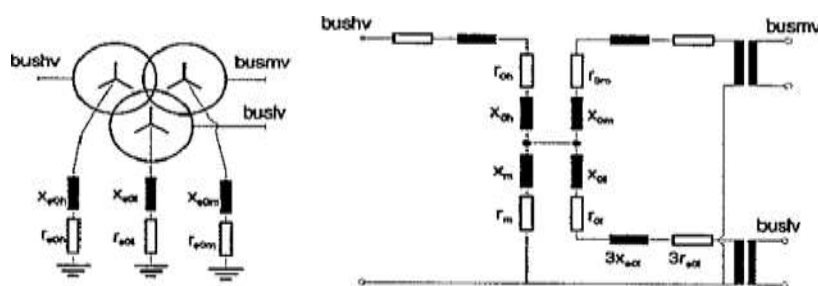


Figure 4-25: Zero sequence - grounded star/grounded star/ grounded star connection (A.D. Hansen et al., 2003)

4.6.4.3 DSL models of wind turbine in DigSILENT

As already mentioned in DigSILENT, models of the electrical components often include wind speed, aerodynamic, mechanical systems, and control systems in addition to models of electrical components (A.D. Hansen et al., 2003). The Dynamic Simulation Language (DSL) is an important feature of DigSILENT. It allows for the complex simulation of linear and non-linear systems.

DSL is used for designing and implementing many kinds of controls including condensers (RPCs), dual-powered DFIG generator controllers, active stall controllers, variable wind to pitch controls, and models of non-electrical wind turbines. DSL can be used for the design and implementation of different styles of controllers. DSL is also used to design and implement different controller types (Anca D. Hansen et al., 2002b).

Instead of the built-in electrical models with initialization methods based on the load flow calculation, the user needs to initiate DSL models carefully. This initialization is very useful to evaluate the system during normal operation or transitional failures (the wind turbine connected to a grid). The wind turbine and the electric energy system must be seen as one system despite their formal separation of initialization (Anca D. Hansen et al., 2002a).

A wind turbine, which is directly connected to the grid, is used for example. The complete structure of such a model of wind turbine connected to the grid is shown in Figure 4-26. It requires:

1. The model wind speed,
2. Mechanical and aerodynamic model, generator, and grid,
3. Models of control systems (e.g. models for control blades, models for condenser banks).

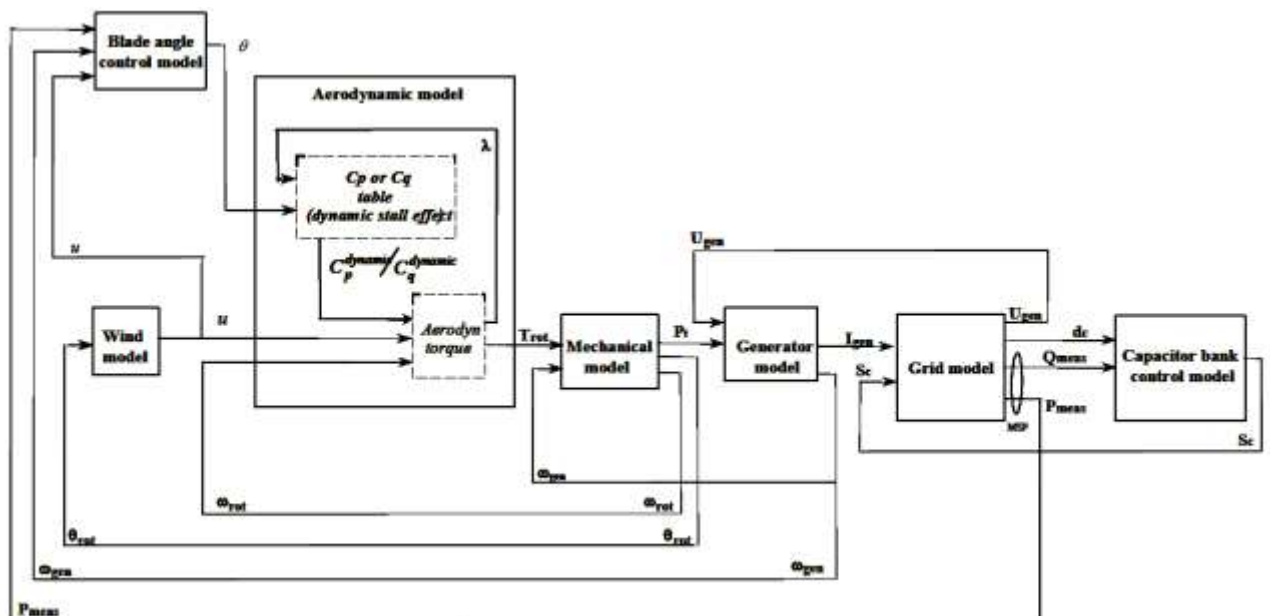


Figure 4-26: Example of grid-connected wind turbine model (A.D. Hansen et al., 2003)

The equivalent wind speed, extending to the stationary dynamic effect, oscillate the rotor speed to the system and the bladed angle to the control model is supplied for the aerodynamics model. The mechanical model determines the dynamics of the drive train and transmits the mechanical P_t turbine to the generator model. Besides the mechanical turbine P_t , the input voltage U_{gen} from the grid model is given. It provides the current I_{gen} as outputs for the rotational speed as a ω_{gen} . The control consists of the control of the blade angle and the control mechanism for the condenser banks.

The generator speed ω_{gen} and wind speed u of the blades control model supply the angle alloy of the blade to the aerodynamic model with details about the P_{meas} measured active power. The condenser bench control model produces SC-to-grid control signal based on information on reactive power measured by Q_{meas} and condenser status signals dc. Active and reactive power P_{meas} and Q_{meas} are calculated at the main MSP Switching Step of the wind turbine (A.D. Hansen et al., 2003).

4.6.4.4 Battery Modelling

DSL (Figure 4-27) is used to implement the battery model. As an input signal of the model, only the DC-current is required. The model includes the exterior DC-voltage, the SOC and the DC-cell tension that can be used to regulate a loading unit (DlG SILENT GmbH, 2010).

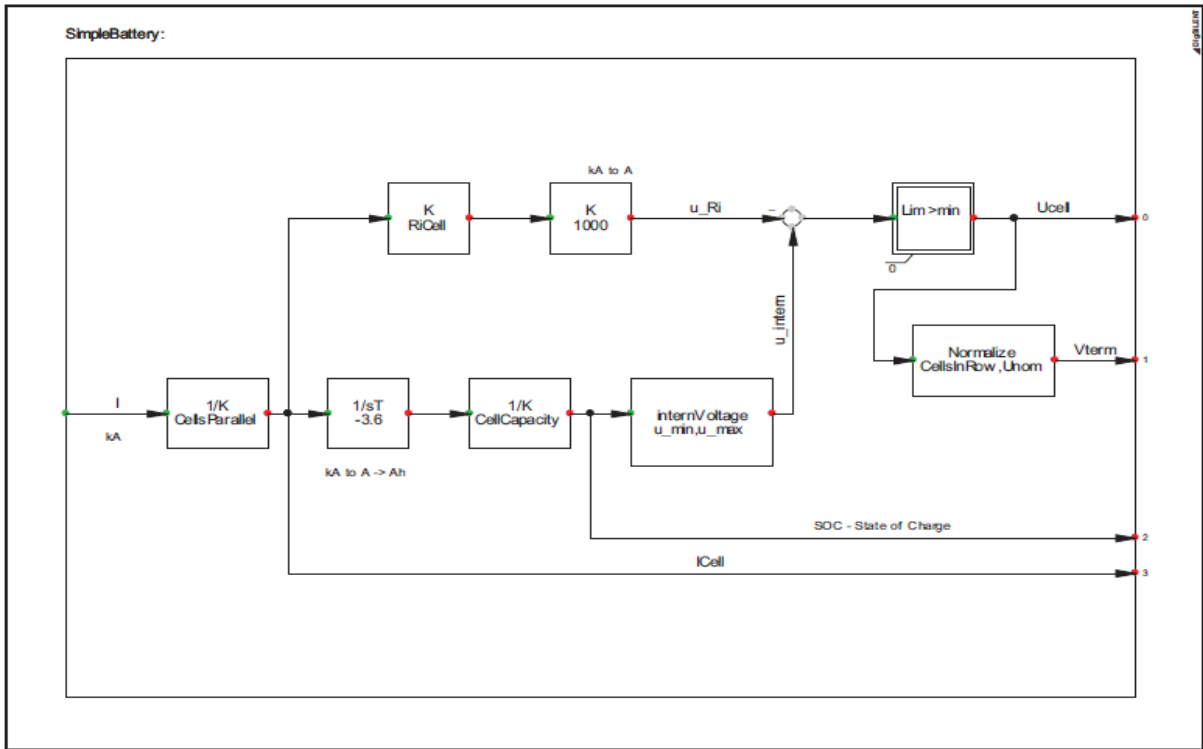


Figure 4-27: Simplified Battery Model in DSL (DlGSiLENT GmbH, 2010)

An initial condition (SOC0) is needed for the integrator ($1 / sT$) that counts current battery input and output. This is part of the parameters of the model. The battery is not charged or discharged during the initialization process. The active BESS power exchange for the load flow is thus zero. In the single line diagram, the battery is a DC-tension source in PowerFactory. A DSL-frame (Figure 4-28) is necessary for the application of the battery model voltage output to the DC-voltage source (DlGSiLENT GmbH, 2010).

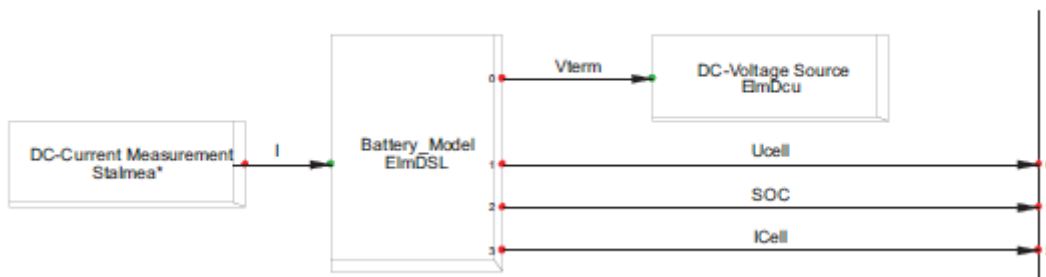


Figure 4-28: Frame for the Battery Model in DSL

Below Table 3-6 show Battery Model in DSL parameter (DIgSILENT GmbH, 2010):

Table 4-6: Battery Model in DSL parameter (DIgSILENT GmbH, 2010)

Variable	Unit	Description
U_min	V	Cell voltage of discharged cell.
U_max	V	Cell voltage of fully loaded cell.
Cell Capacity	Ah	Capacity of one cell for the used discharge current (see Peukert's law)
Cells Parallel	Int	Amount of parallel connected cells (increases the total capacity).
Cells in Row	Int	Amount of serial connected cells (increases the output voltage).
Ri Cell	Ohm	Internal resistance per cell (average value).
Unom	kV	Voltage rating of the connected DC-busbar.
SOC0	Int	State of Charge at the beginning of the Simulation.

a) Voltage Sourced Converter (VSC)

By switching IGBT valves easily, the VSC converts the DC voltage from the battery into AC voltage.

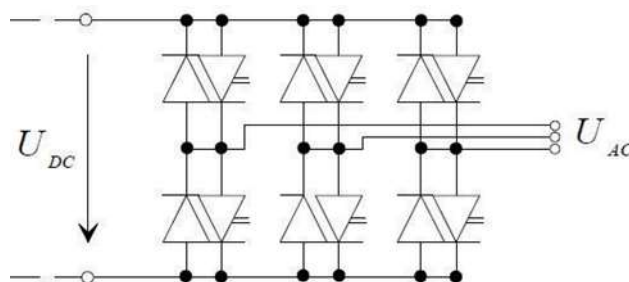


Figure 4-29: Equivalent Circuit of a PWM Converter (DIgSILENT GmbH, 2010)

The Switching Signal, also known as the VSC control system as the amplification factor (Pm). Figure 4-30 may also explain this.

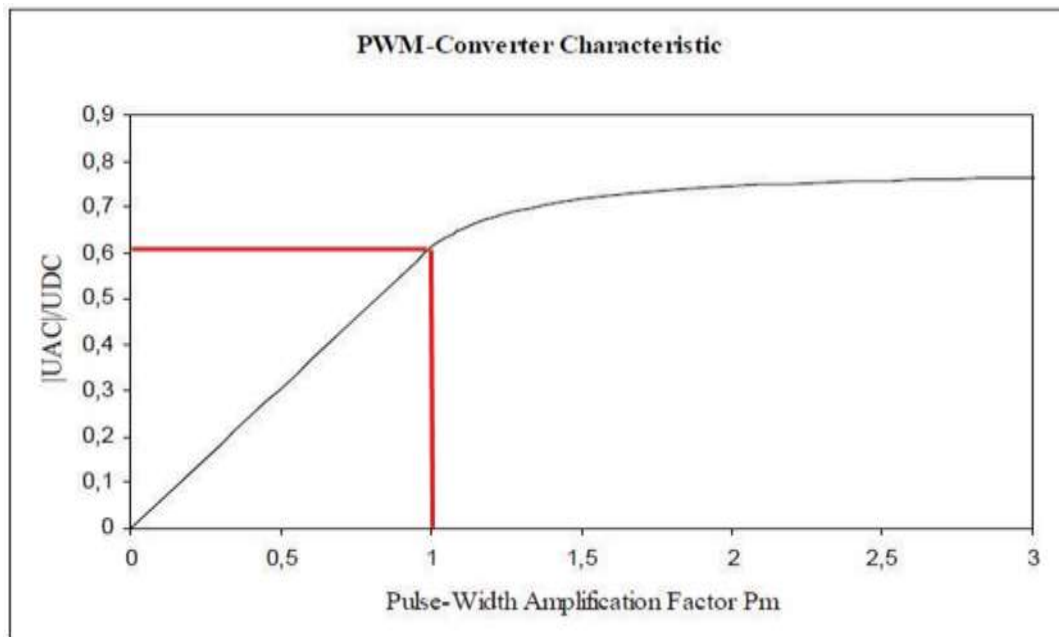


Figure 4-30: Saturation of a VSC with Sinusoidal PWM (DIgSILENT GmbH, 2010)

The PowerFactory PWM-converter model has many potential input combinations. In that case, the input "id_ref" and "iq_ref" are used. This is the new PWM-converter phasor converted into a dq-reference frame. The benefit of the transformation is that "id_ref" equals the active power output of the converter and "iq_ref" equals the reactive power of the PWM converter. So, the BESS controller is simple to implement. The PWM model uses an internal current controller to produce the actual signal for the modulation factor (DIgSILENT GmbH, 2010).

b) Short Circuit Calculation

Short circuit calculation according to IEC60909 / VDE0102 is not possible with BESS since devices with power electronics such as the PWM-converter do not comply with the standard. But PowerFactory also offers the possibility to measure a short circuit according to the so-called complete process.

The complete method also takes account of the load movement. In addition, the PWM-converter model can be configured for the complete short circuit process. Both choices are constant current or constant voltage. It will be "constant I" for an IGBT-based converter. The right option, since the converter valves are configured for a certain maximum current only. (DIgSILENT GmbH, 2010). To obtain the maximum current with the complete short circuit method the PWM-converter must be configured to full active power on the load flow page.

c) The BESS Controller

The BESS controller is divided into three parts:

- i. Frequency controller (Frequency Control)
- ii. Active/reactive power controller (PQ-Control)
- iii. Charging controller (Charge Control)

Together with the necessary measuring instruments, the structure is shown in Figure 4-31. This arrangement is called a PowerFactory frame. A frame and a DSL model (like the battery model shown in Figure 4-31 and 4-32 are just the description (*. BlkDef) of a line type or a transformer. The frame is a composite type (*. ElmComp). The DSL model is a standard model (*.ElmDsl) (DIgSILENT GmbH, 2010).

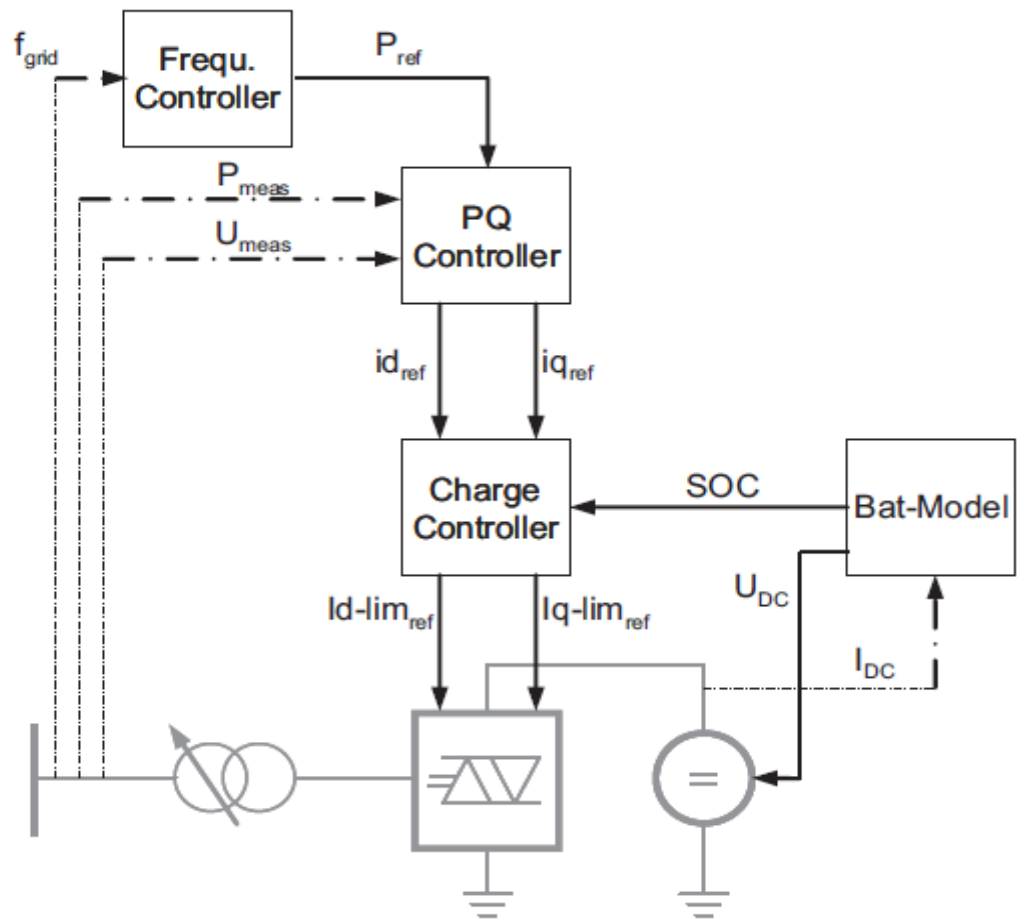


Figure 4-31: Structure of the BESS

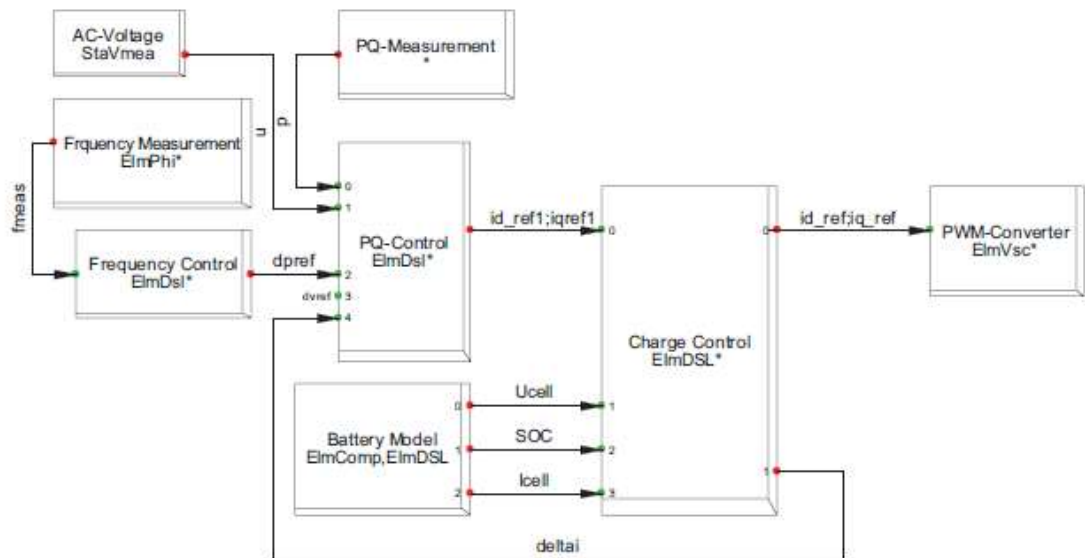


Figure 4-32: Frame for the BESS-Controller (*.BlkDef) (DIgSILENT GmbH, 2010)

The Frequency Controller is a basic proportional controller with a tiny dead band. It is critical that there is only one integrator in a real power system that controls the frequency. Otherwise there may be issues with oscillations. The frequency controller model is shown below. The decrease determines how much active power is triggered in the event of a frequency deviation. If $K = 0.04$ is granted, the full active power of the BESS is activated if the frequency deviation is equal to or greater than 2 Hz (in the 50 Hz system). All values are per unit value. In an application scenario, the drop should be organized to satisfy the specifications of the grid code (DIgSILENT GmbH, 2010).

The command variable is $f(0)$, this value will be set to frq (usually 1) with the command $inc(f0) = frq$ during the initialization process. The "offset" block with the output "p0" is used to compensate "dpref" if the value is not equal to zero after the load flow (because "p order frequ" is always zero after initialization) (DIgSILENT GmbH, 2010).

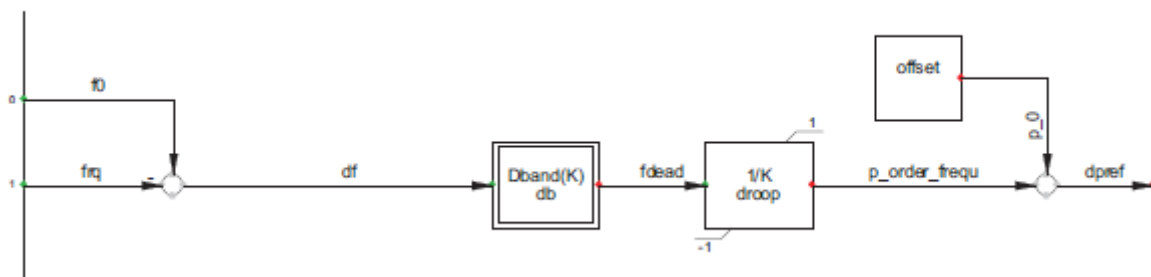


Figure 4-33: Model of the Frequency Controller (*.BlkDef)

The controller for active and reactive power is a little more complex. It is shown in Figure 4-33. The control deviation is filtered using the PT1 element. The signals are then used as input to the PI-controller. The "delta I" signal is added to the active route. Figure 4-32 indicates that "delta I" comes from the charge controller. The voltage (or Q) controller is fitted with a very slow I-controller for fixed point monitoring and a slope with a dead band for proportional voltage support (DIgSILENT GmbH, 2010).

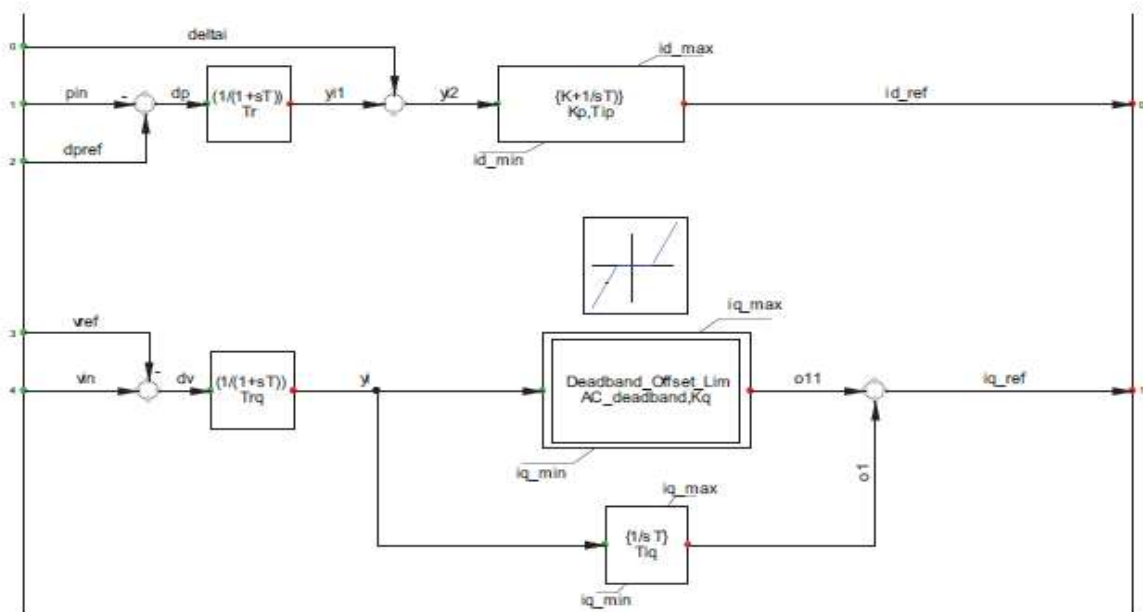


Figure 4-34: Model of the PQ-Controller (._BikDef) (DIgSILENT GmbH, 2010)

Two sections (Figure 4-34) are included in the load control. A charge-logic to meet the specified limits and a block to limit the absolute value of the current order.

There is still more emphasis on active current (d-axis) than on reactive current (Q-axis). It needs only four parameters. Present charging, SOC (min SOC), SOC (maxSOC) maximum and total present (maxAbsCur) are the minimum charging currents. The 'delta-I' signal is the difference between the PQ Controller's reference d-current and the modified d-current of the loading logic. It cannot be disabled by the signal's input into the PQ controller (DIgSILENT GmbH, 2010).

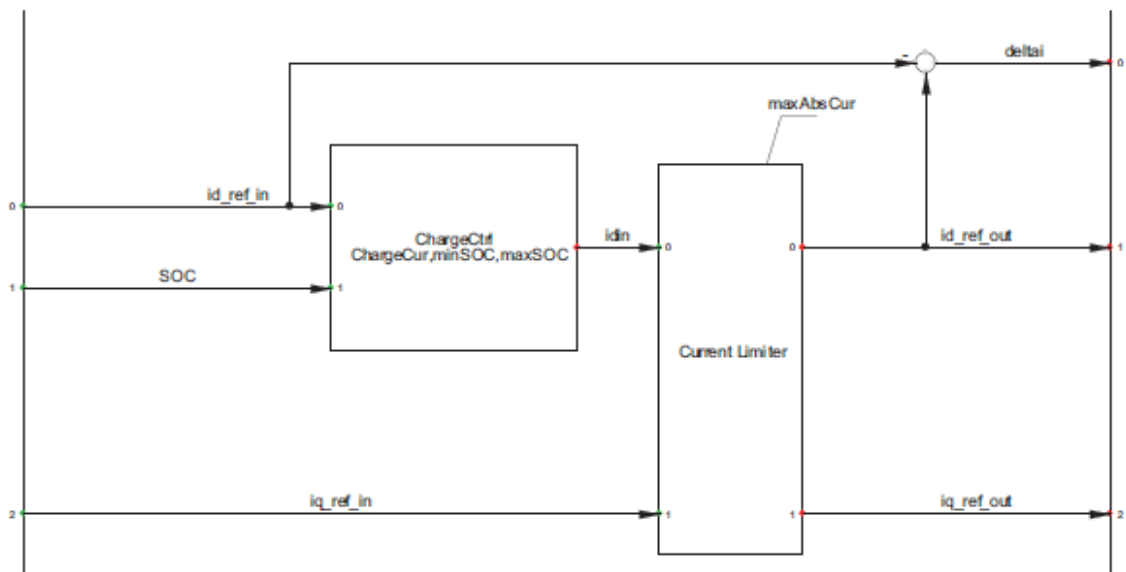


Figure 4-35: Model of the Charge Controller (*.BikDef) (DIgSILENT GmbH, 2010)

It is necessary to use the right names for the signals in the frame description to get a working model for the controller in PowerFactory. Only the signals with the same names in the frame and the model placed in the frame are related. It is also important to understand how the initialization process works. The initialization is the first step of the simulation. PowerFactory uses a load flow for this reason. If the load flow converges, the results will be used within the DSL models to set all integrator outputs. A balanced state should always be the starting point for a simulation. So, all derivatives must be zero, i.e. all integrator inputs must also be zero. The inputs known from the load flow results are in the composite controller model (Figure 4-35) (DIgSILENT GmbH, 2010):

- id ref/iq ref - (the currents in the dq-frame in pu) known from the PWM-converter
- fmeas - (the frequency in pu) known from a PLL measurement device
- u - (the absolute AC-voltage in pu) known from a voltage measurement device
- p - (the active power in pu) known from a power measurement device

The "Battery Model" slot is filled with a composite battery model (Figure 4-28). From there, the current is also known after the initialization load flow. After the design of the frames and the models (i.e. the types) the composite and common models could be made. There are two composite versions, one for the battery (Figure 4.36) and the other for the BESS controller (Figure 4.37). The slots are filled with the required DSL model entities. Measuring instruments must be correctly constructed and connected. Only the correct bus must be connected to the voltage measurement unit. But it is also important to pick the correct cubicle on the bus for a current or power measurement unit. Otherwise, the prefix of the calculated signal could be incorrect, so the whole control strategy could be incorrect (DIgSILENT GmbH, 2010).

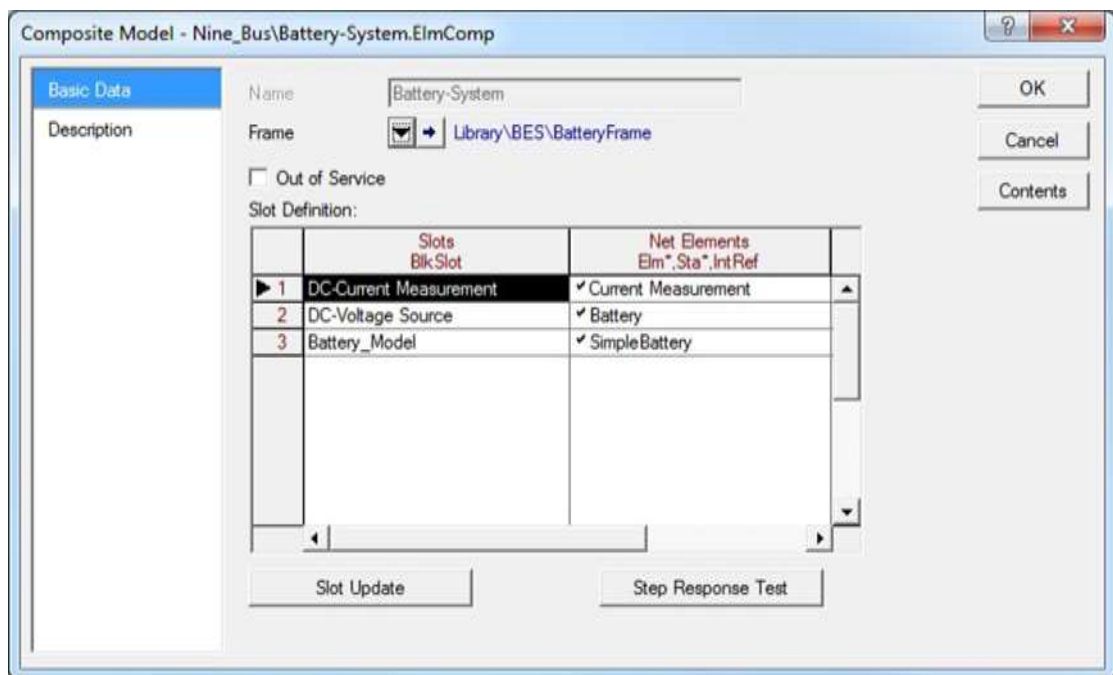


Figure 4-36: Composite Model of the Battery (*.ElmComp) (DIgSILENT GmbH, 2010)

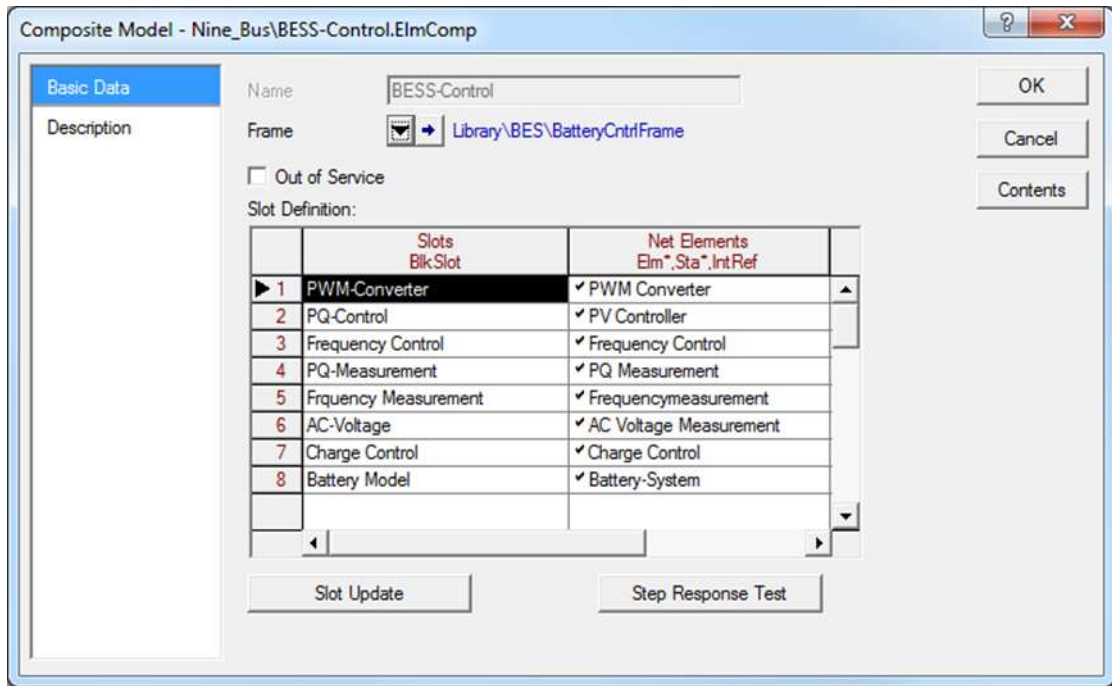


Figure 4-37: Composite Model of the BESS Controller (*.ElmComp) (DIgSILENT GmbH, 2010)

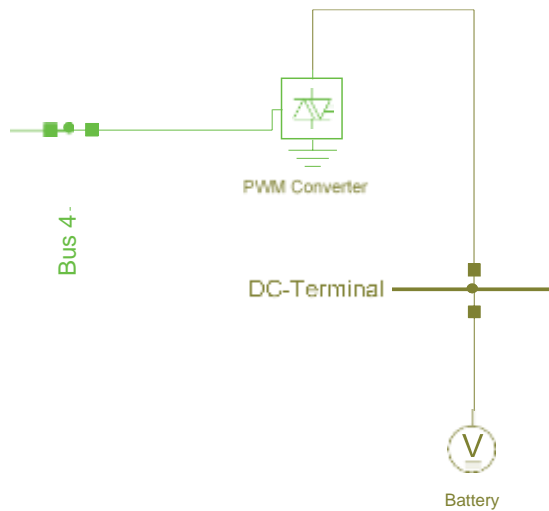


Figure 4-38: The BESS in the Single Line Diagram (DIgSILENT GmbH, 2010)

The BESS model is now complete (Figure 4-38); only the parameters and configuration of the elements in the single line diagram are missing. All the elements in the single line diagram have different basic data tabs, load flow, etc. Only the basic data must be configured for the DC-voltage source. Only the nominal voltage (U_{nom}) value is of interest. The value in the monitor is 0.8 kV (DIgSILENT GmbH, 2010).

The data for the battery model should be selected in such a way that the equation is met for all charging states. Otherwise, the PWM converter would saturate and the power of the entire BESS will not work properly. The PWM-converter must also be configured. The AC-and DC-voltage (U_{nom} / U_{ndomdc}) and the rated power (S_{nom}) must be inserted on the basic data tab. The data on the load flow page is critical for the load flow of the initialization. As already stated, one control condition should be $P = 0$ (this is the condition for the d-axis). The other condition may be a certain value for the reactive power or the AC-voltage of the selected node (q-axis). The data on the RMS-Simulation tab is also essential for the PWM-converter. The "Use Integrated Current Controller" should be activated. The gain is 1 for both axes; the time constants for the integrator are both 1ms, a very fast internal control loop for the current (DIgSILENT GmbH, 2010).

The frequency, PQ and load controller parameters depend on the application case requirements. The parameters of the battery depend on the battery selected and, on the model, used. It is important to consider the limitations of the battery and the PWM-converter during operation. For that the single controllers are equipped with limiters. For realistic simulation results these limits should be set right. Some batteries could be discharged with a higher current than they could be charged. For that case, the PQ-controller needs other limits for the positive d-current than for the negative d-current. In some cases, it may be also high active negative control power needed. In that case a copper inside the DC circuit could consume that power. But usually a BESS is required to prevent a frequency under-run. Then a copper is not required (DIgSILENT GmbH, 2010).

4.6.4.5 The Grid Modelling

The grid side converter control in DlgSILENT indicates the inputs and outputs (see Figure 4-39). The following blocks compose the scheme:

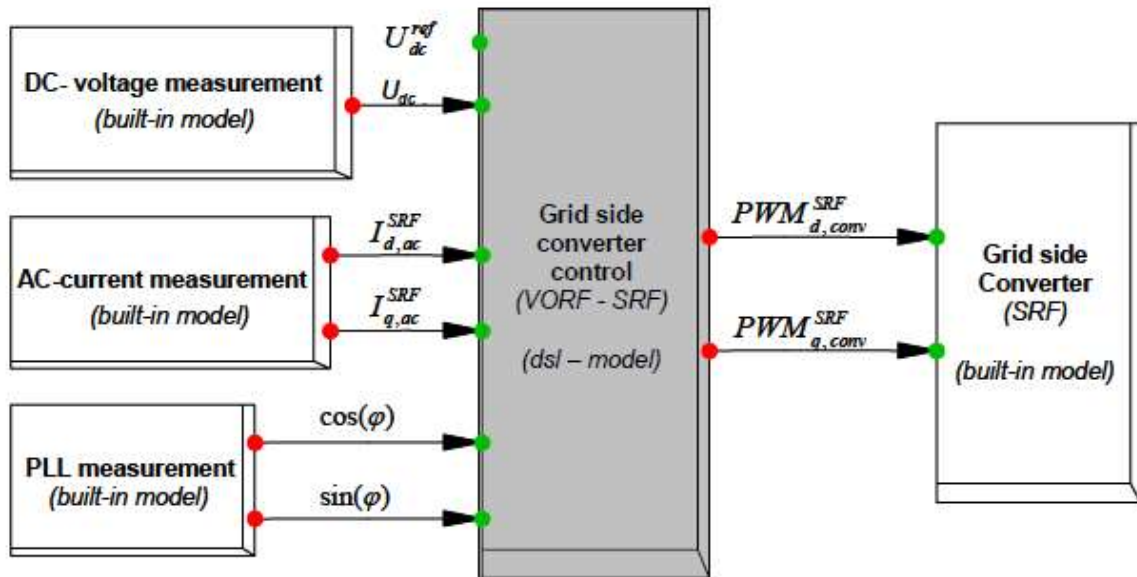


Figure 4-39: Grid side converter control (A.D. Hansen et al., 2003)

PLL (built-in model) measurements – tests the phase Angle of a grid side converter AC-voltage. To synchronize the voltage of the AC-converter to AC-grid voltage, the voltage phase angle is determined. Built-In (built-in) Grid side converter block is an independent DlgSILENT library IGBT converter part. DlgSILENT offers various control modes for the control of converters, as already stated. The normal Udc-Q mode for the DFIG grid side converter is its feature since the dc-voltage and reagent power are changed. The grid-side converter control pad (dsl model), shown in Figure 4-40, is a grid-side converter control. Likewise, the grid side converter is currently controlled for the rotor side converter. By regulating grid side converters present, the dc-tension and reactive power are regulated indirectly (A.D. Hansen et al., 2003).

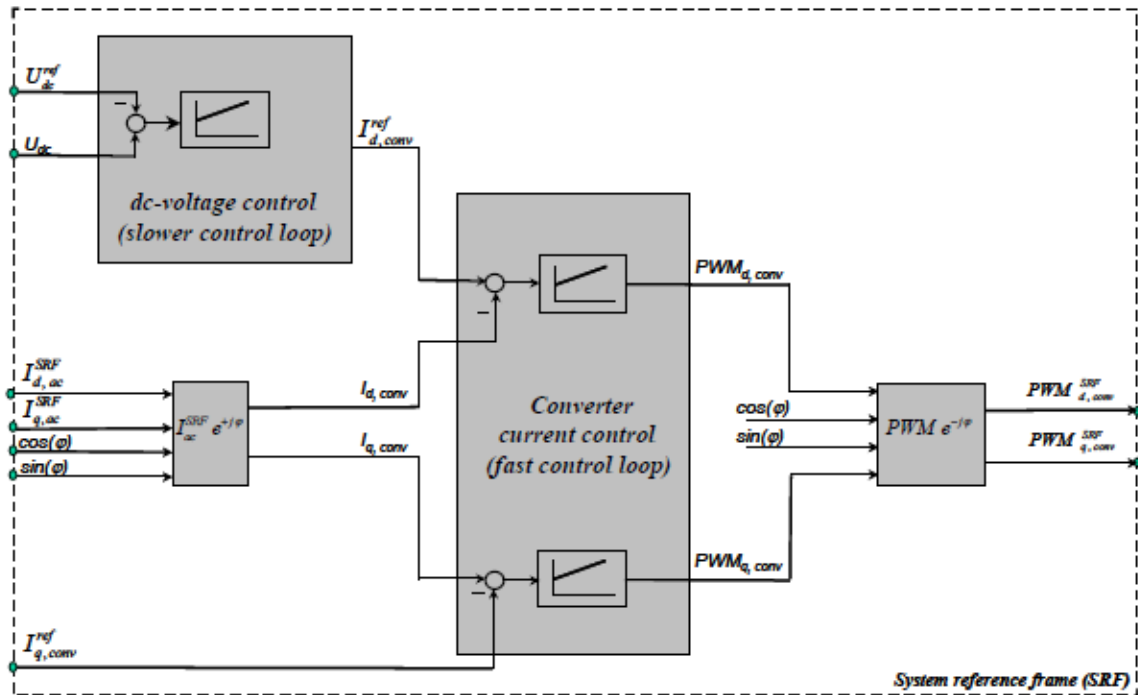


Figure 4-40: Grid side converter control in DIgSILENT (A.D. Hansen et al., 2003)

Two PI control loops in cascade are provided for grid side converter control:

- DC-voltage loop slower (outer)
- Present power of a very fast (inner) converter.

The DC- voltage control loop adjusts the DC-link-voltage to a value U_{def}^{ref} , while, while the extremely fast current control loop controls the currency converter to a slower dc-voltage controller (A.D. Hansen et al., 2003).

The outputs of the Grid side converter controls decide the size and phase angle of the AC-voltage terminal of the converter. The current control works in GCVRF in the GCVRF reference frame. The transducer current is divided into a parallel orthogonal portion on the grid-side converter voltage (A.D. Hansen et al., 2003). In that reference framework, the d-Axis is equal to the active ingredient, while the q-Axis is equal to the reactive ingredient. The converter 's energy portion is used to regulate the dc voltage (active power) along with the Id, Conv voltage converter (direct phase).

The reactive power is regulated from the IQ to the converter Voltage (Quadrature) (A.D. Hansen et al., 2003) with the orthogonal portion. The d-converter current portion regulates the DC-link voltage in the outer slow control loop to its value value U_{def}^{ref} by The directory step component reference of the current $I_{d,conv}^{ref}$. converter is created. The quadrature part of the $I_{d,conv}^{ref}$. converter current is constant, nearly proportional to reactive power. To run the unit factor conversion system ($Q_{conv} = 0$) a zero q- $I_{d,conv}^{ref}$. relation is 0(A.D. Hansen et al., 2003).

The PWMd Direct PWMd, Conv and PWMq Orthogonal is a pulse-width modulation factor converter for GCVRF, created with a current control transformer loop. These components are then transformed into an SRF reference system because SRF power is needed for the grid converter (A.D. Hansen et al., 2003).

4.6.5 Simulation Results and Discussion

The simulation of both sections consists of the dynamic control of an integrated wind farm energy storage device linked to the grid. Second, monitor the storage component in an electrochemical process which can store / restore energy. The second is a remedy / inverter, which can convert the DC voltage from the storage component into the AC voltage required for the grid. Normally the rectifier / inverter is based on a pulse width modulation (PWM), voltage-sourced converter (VSC). This is well-known in PowerFactory and is available. The storage component of a rechargeable battery in this case is an element depending on the application. The battery issue is the broad variety of technologies inside a battery. So, for all batteries, there is no clear precise model (Taghi & Fard, 2017). The following parts include network modelling, simulation, and case study.

4.6.5.1 Network Model

The wind farm network consists of 46 wind turbines, 12kV with an output power of 3MW and a total capacity of 138MW. The 46, 12kV wind turbines are parallel to the three, 50MVA 132/12 kV step-up transformers. The BESS of NAS with 42 kit enclosures and battery modules, consisting of 1 680 NAS modules, each rated at 30kW and 216kWh, with a rated performance of 50.4 MW and 201.6 MWh. The grid model consists of a 132 kV, 50 Hz, 40 KVA grid supply stage.

With PowerFactory, it is easy to get a full report of all the active or reactive power installed, the installed energy, and the spinning reserve installed in the model. The cumulative load is assumed to be 300 MW. The minimum load case shall be 150MW of the full load. Service Scenarios are used in PowerFactory for various load scenarios. The overall structure of the integrated Wind Farm Battery Energy Storage System (BESS) is illustrated in Figure 4-41.

The system consists of a wind farm, a BESS, a converter, a Power Management Unit (PMU) and the transmission line connects the system to the main grid. Often the PCC coincides with the POC (European Wind Energy Association, 2021). Also, this study PCC and POC coincides. At PCC, the BESS is linked to the grid and charges/discharges power through the converter to smooth the wind power injected into the grid. $P_G(t)$: Grid-connected power at time t , $P_W(t)$: Wind farm output power at t , $P_B(t)$: Output power of energy storage battery, SOE: state of the energy and PMU: Power management unit. A key component of the design of the wind storage system is the BESS PMU used for smoothing the wind power grid (Yun et al., 2018).

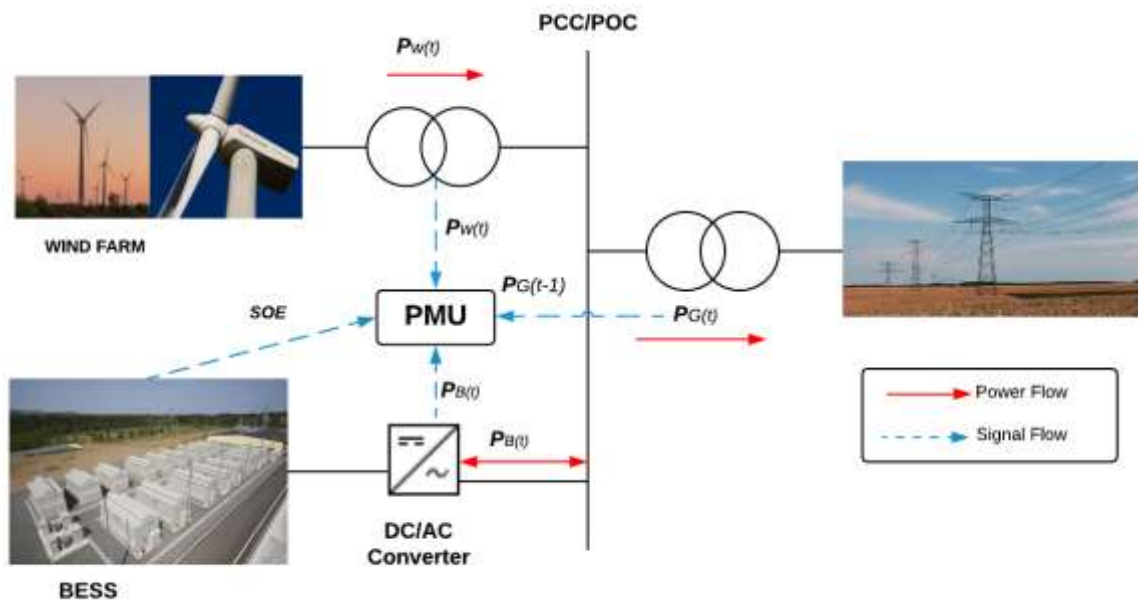



Figure 4-41: Network Modelling on DIgSILENT

For a steady state load flow analysis (), there are no further dynamic models of the power plants needed. Only the generator types of the wind farm and the information on the load flow page must be configured. In that information is also the capability limit curve for reactive power included. It is important to have one reference machine in the grid. The generator from the wind farm is the reference in the sample grid. The other generators are configured as Power and Voltage (PV) nodes, they control their active power output and the local voltage (DIgSILENT GmbH, 2010).

If the load flow is determined with the option "Active Power Control according to Secondary Control" then the involvement of the plant can be configured to compensate for the shift in load with the variable "Main Frequency Bias" (Kpf). For example, a generator shutdown is a very large shift in the network load. It is possible to establish the maximum frequency deviation with the configuration of Kpf.

If the shutdown of the wind farm is to be compensated from the grid and the storage of the battery within a frequency deviation of 1,5 Hz, the Kpf-factor must be 20 MW / Hz (= 60 MW/2/5 Hz) (DIgSILENT GmbH, 2010).

Transformers are fitted with automatic tap changers to control the voltage on the high voltage side. To ensure that tap changers operate automatically and that generators are within their reactive capacity, the options "Automatic Tap Adjusting Transformers" and "Consider Reactive Power Limits" must be triggered in the load flow measurement dialog (DIgSILENT GmbH, 2010).

It is critical that the original grid is configured correctly. Otherwise, it is more difficult to locate faults or problems later along with the BESS. The first step should therefore be the verification of data). If there are no errors or alarms, a load flow with the original setup is suggested as a next step. If the "Display Verification Report" option on the "Output" tab of the load flow command is checked, only overloaded (more than 80 percent loading) elements are printed in the output window. It is also critical that after the load flow, there are no warnings in the output window.

It is advised to use the variations in PowerFactory for the expected expansion of the grid, as in this case with the BESS. As a result, the original grid could be easily restored and quick switching between various expansion stages is possible. Various research cases are used to model various cases (wind farm outage, load shifts, short circuits, etc.) in the time domain (DIgSILENT GmbH, 2010).

Thus, each case could be viewed separately with a different set of simulation events, outcome charts, active operating scenarios and variations. It is usually recommended to deal with research situations, operating scenarios, and variations. Service scenarios are used to model various operating points of the same grid layout.

Thus, the original configuration is not updated because all parameters are stored in the required scenario. Variations are used to handle changes in the grid configuration. Variations could result in various expansion stages of the original grid being controlled without a change to the original grid. In PowerFactory, the variations are linked to a certain (user-defined) date and time. Each study case also has its own time set by the consumer. With the case study period, various stages of expansion of one variety could be treated. Up to that point, only a static load flow has been considered. However, more detailed models of power plants are required for the RMS simulation in the time domain. The models are implemented in the DSL (DigSILENT Simulation Language) edition (DIgSILENT GmbH, 2010).

Predefined and standardized models are used for the various power plants. Average voltage controller (vcolIEEE1), turbine controller (pcuIEEE1) and. In this case, no power system stabilizer (PSS) is used; thus, the pss-slot is empty. The turbine governor controls the speed of the turbine and the electrical frequency of the turbine is controlled by the synchronous machine. In the event of a sudden shift in load, such as a power plant shutdown, the frequency decreases rapidly due to lack of active power in the grid. To prevent the device from slowing down, the turbine governor must trigger more power. This is called the primary frequency control or the spinning reserve, the activation must be instantaneous (DIgSILENT GmbH, 2010).

This means that the grid has a lack of energy all the time due to the permanent shock of the turbine valve. It would be more economical, therefore, if another system could deliver primary control energy before the grid has increased the active capacity. This is called secondary frequency control; it must be triggered within 15 minutes of the frequency deviation. The solution may be a battery energy storage device (BESS) to fill this void (DIgSILENT GmbH, 2010).

4.6.5.2 Case Study

The case study consists of four parts. The first part is a simulated wind farm load flow and fault analysis. The second element is a battery load flow and fault analysis. The third component is load shift for which two experiments are used in the PowerFactory project: one with and one without BESS. The fourth element is a simulated 20 % wind farm outage of wind turbines. Primary control energy is required in the grid to control the frequency within a very limited distance between the upper and lower frequency limits. In South Africa, the Grid Code for Renewable Power Plants is only 47-52 Hz with a minimum accuracy of 10mHz in positive and negative direction (NERSA, 2014).

The grid already mentioned is used for the following investigation. The PWM converter has a rated capacity of 30 MVA. This corresponds to the frequency control bias already stated with a frequency bias of $30 \text{ MW}/0.2 \text{ Hz} = 150 \text{ MW} / \text{Hz}$. A sudden change in load in 30 MW of active power (simple connection of additional load) is simulated to test the BESS. The dispatch command is set to PowerFactory via an event parameter. To obtain a slope with a certain gradient and not a phase, the governor model was extended with a gradient limit block (see Figure 4-42).

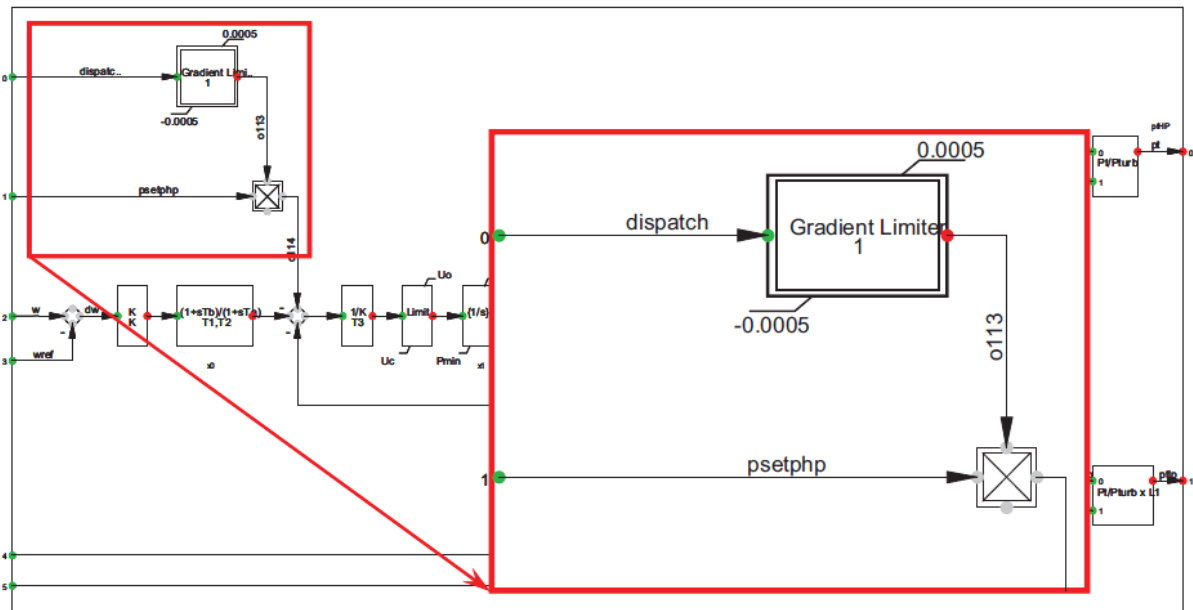


Figure 4-42: Edited Governor Controller for Dispatch Command (DlG SILENT GmbH, 2010)

With PowerFactory it is possible to display results from different simulations within one plot. For that are different result files used. But it is also possible to use several result files within one study case. The advantage of one study case/variation per result file is that the results and the used parameters for the simulation match together.

4.6.5.2.1 Simulation Results and Discussion (Wind Farm Load Flow and Fault Analysis)

i. Wind Farm Load Flow

A range of load flow calculation methods are offered by DlgSILENT PowerFactory, including a complete AC Newton-Raphson technique (balanced and unbalanced) and a linear DC method. Typically, the improved non-decoupled Newton-Raphson solution technique with current or power mismatch iterations yields round-off errors for all buses below 1 kVA.

The algorithms implemented exhibit excellent stability and convergence. Under all conditions, several iteration levels guarantee convergence, with optional automatic relaxation and constraint modification (DIgSILENT, 2021). Below load flow simulation results from collector bus and at the point of connection (POC) were performed and collected in DIgSILENT. Voltage and frequency plots are shown below for POC bus and Grid bus.

At POC bus: load flow result below Figure 4-43 shows the voltage magnitude of the system on the POC bus is at 1p.u and the system frequency is at 50Hz as shown in Figure 4-44, so the system network on the DigSilent simulation can be trusted to work well under no fault condition.

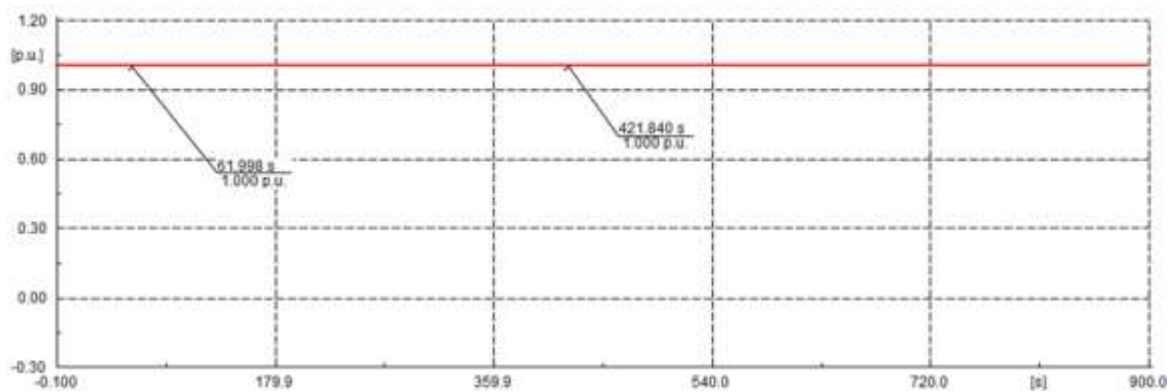


Figure 4-43: Simulation results of Voltage Magnitude at POC

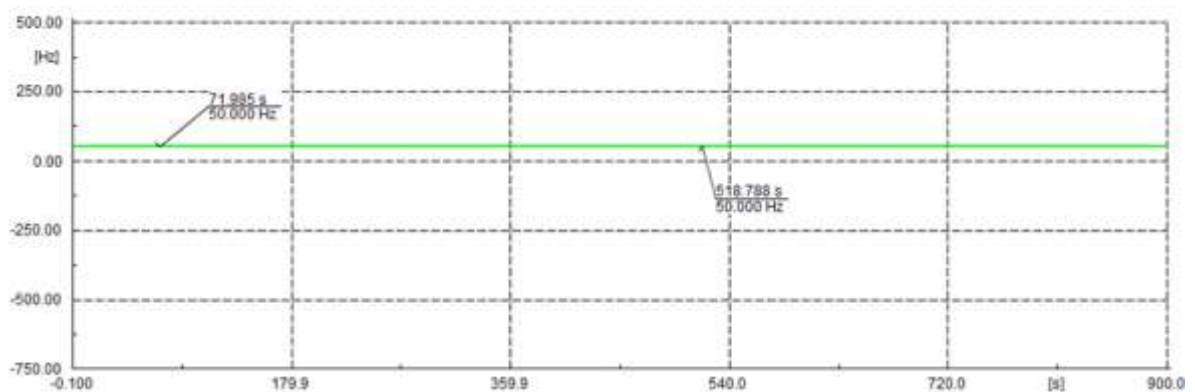


Figure 4-44: Simulation Results of frequency magnitude at POC

At Grid Bus: Figure 4-45 shows the voltage magnitude at 1p.u with respect to time. Figure 4-46 shows the frequency of the grid bus at 50-Hz with respect to time. The system frequency also remained stable under normal operating conditions. Therefore, the system network does not work well under any fault condition.

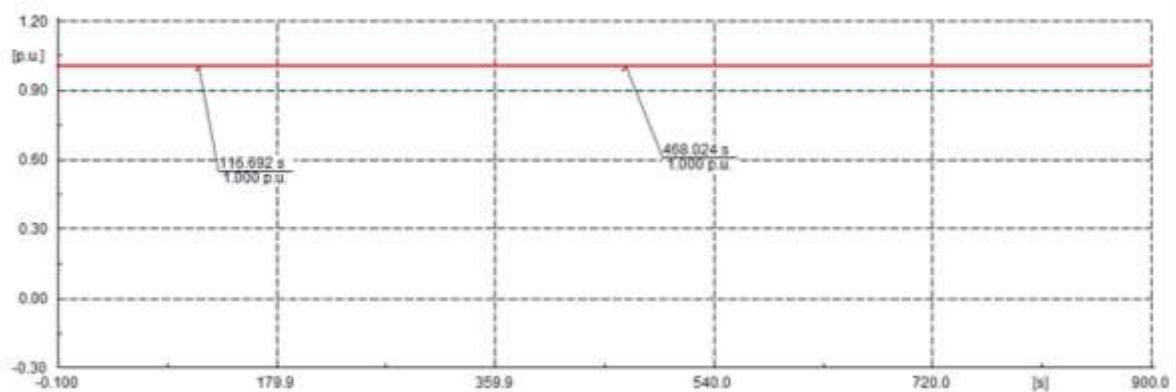


Figure 4-45: Voltage Magnitude of voltage at Grid bus

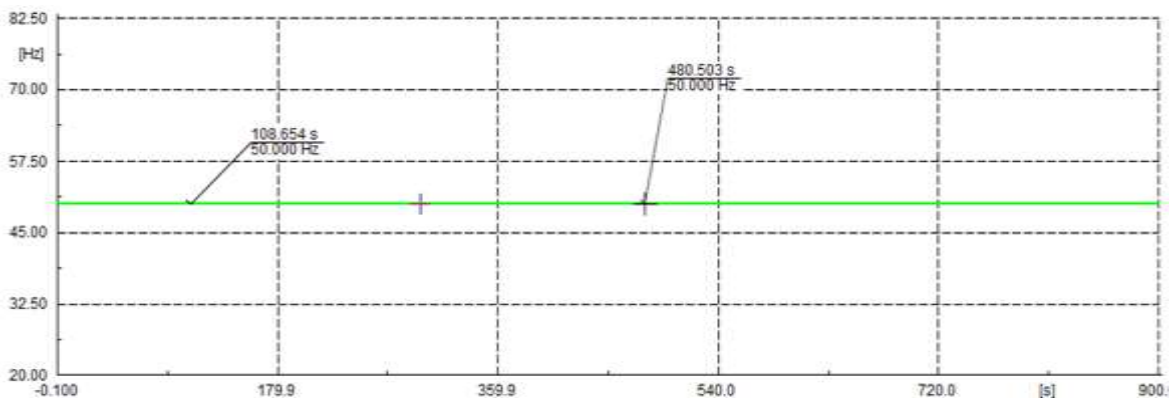


Figure 4-46: Simulation Results of frequency magnitude at Grid bus

ii. Wind Farm Fault Analysis

DlgSILENT PowerFactory offers short-circuit calculations, together with several reporting options, for single and multiple faults. Since short-circuit calculations are required for a variety of purposes, PowerFactory short-circuit calculation supports various representations and methods of calculation based on a range of international standards, as well as the superposition method (also known as the Complete Method).

This is based on a particular operating point of the network and provides the algorithms and accuracy required to determine the "true" or "operational" short-circuit currents without taking into account the simplifications or assumptions typically made in standard fault analysis (DIgSILENT, 2021).

At POC bus: Below figure 4-47 and figure 4-48 illustrates when the a single phase earth fault occurs at POC busbar, it immediately created a voltage dip to 0pu as shown in figure 4-47, the system voltage gets restored after the fault is clear. Figure 4-48 shows frequency deviating between 342 Hz to -268Hz once the fault occurs and get stabilized to 50Hz once the fault is cleared.

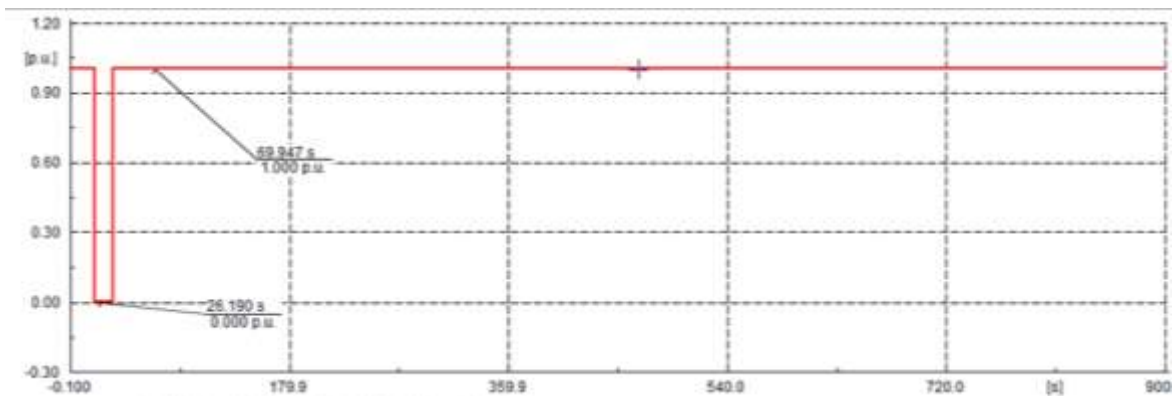


Figure 4-47: Simulation results of Voltage Magnitude at POC bus results

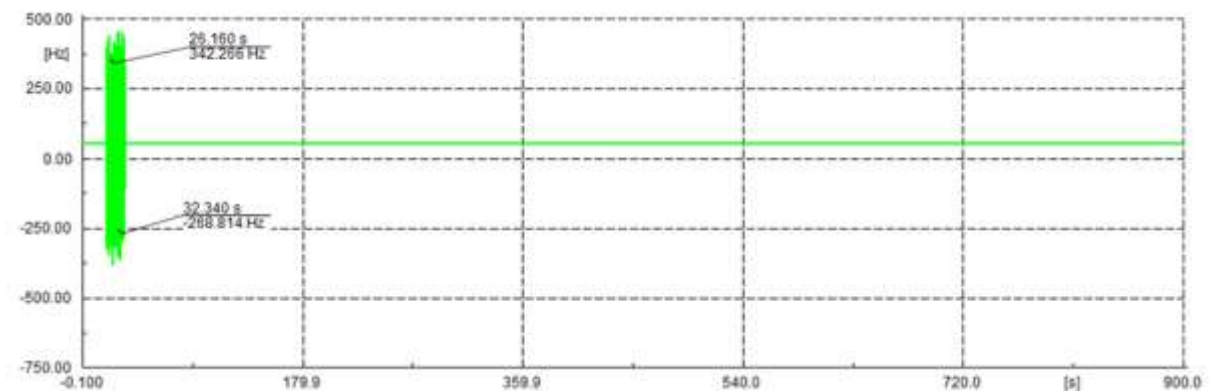


Figure 4-48: Simulation results of Voltage Magnitude at POC bus results

At Grid bus: When an external grid fault occurs, the frequency deviates above the maximum and minimum operating limits but is cleared again after 5 seconds.

This means that the systems continue to operate under normal operating conditions within acceptable frequency and voltage limits. Figure 4-49 below shows the voltage dip that occurs at the system busbar to 0pu when the fault is cleared after 5 seconds, and the system voltage is restored back to 1pu.

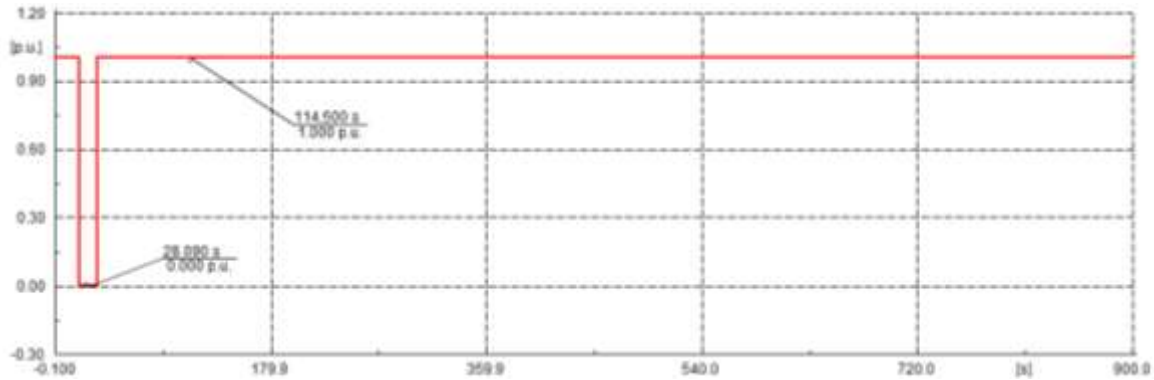


Figure 4-49: Simulation results of Voltage Magnitude at Grid bus results

Frequency deviating between 65Hz and 33 when the fault occurs, system Frequency is restored back to 50Hz after the fault is cleared as shown in below figure 4-50.

Simulation results of Voltage Magnitude at Grid bus results

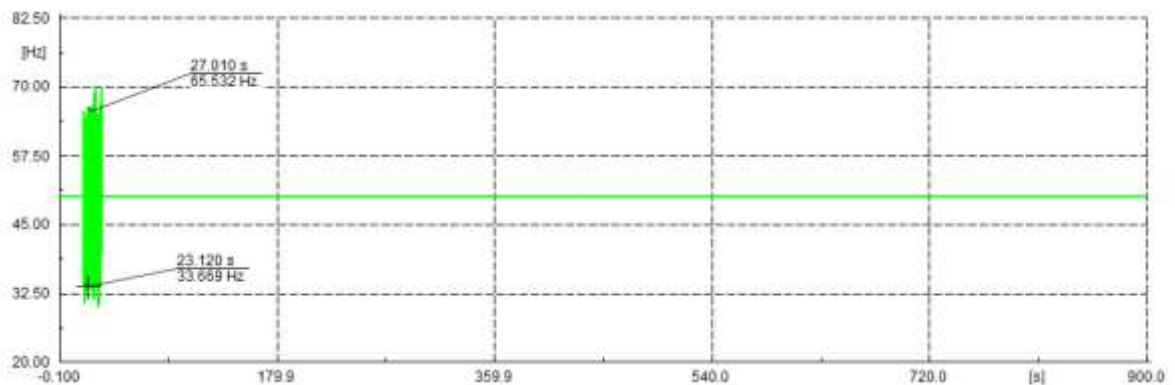


Figure 4-50: Simulation results of Voltage Magnitude at Grid busbar results

4.6.5.2.2 Simulation Results and Discussion (Battery Load Flow and Fault Analysis)

i. Battery Load Flow

Figure 4-51 below shows the Charge State (SOC) graph. The initial SOC is set to 0; the SOC is determined to be 0 at 10.103 seconds of simulation time, slowly increasing with time, at 733.032 seconds of simulation time, the SOC is determined to be 0.44 at 1578 seconds of simulation time, the SOC estimated to be 0.997, and then it can be concluded that the BESS charge is approximately 15580 seconds of simulation time. The external demand for energy is expected to be poor during the periods highlighted.

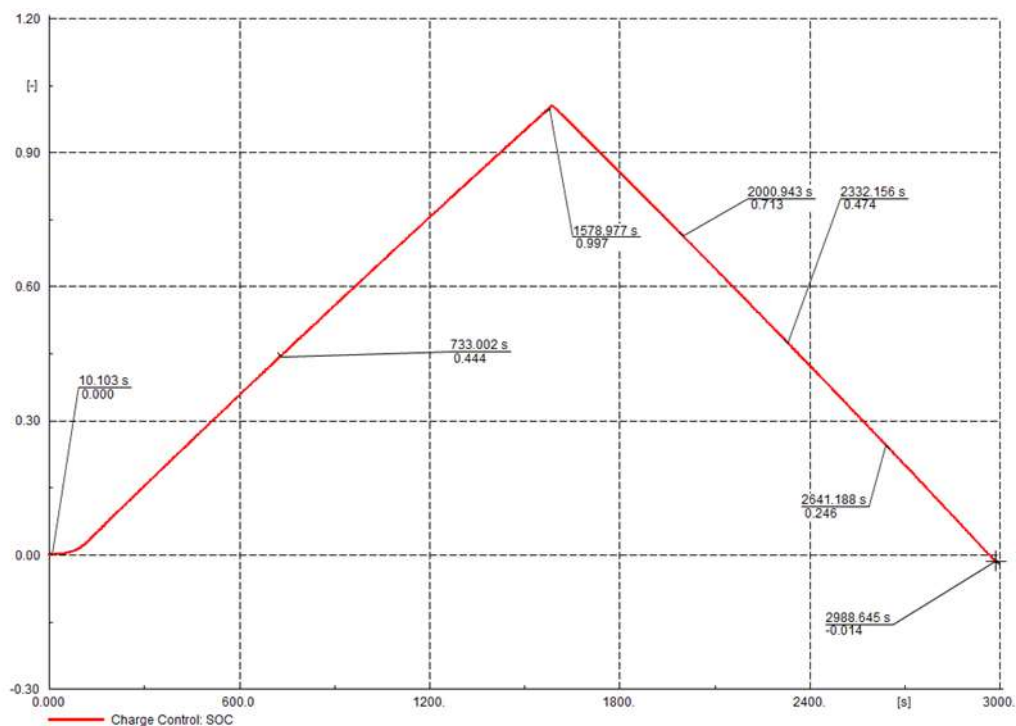


Figure 4-51: State of Charge (SOC)

Once the BESS is fully charged, the SOC shall be equal to 1 and shall be ready for loading energy as per demand requirements. As can be seen from the above example, the charge status is progressively reduced to zero, which means that the power is sent to the load.

At 2000 seconds, the SOC is estimated to be 0.713 out of 1 and decreases as time passes before the demand for the load or the battery is completely discharged. As estimated at 2988 seconds, the SOC is 0.014, which means that the BESS is totally discharged. Figure 4-52 below shows the voltage charge of the battery rising in relation to the SOC as shown in Figure 4-51. At 1572 seconds, the voltage set-point is 1.023, which is while the battery is fully charged and SOC=1. Voltage set point steadily decreases in proportion to the discharge time of the battery but does not exceed 0.p.u since the discharge depth is set to 80 %.

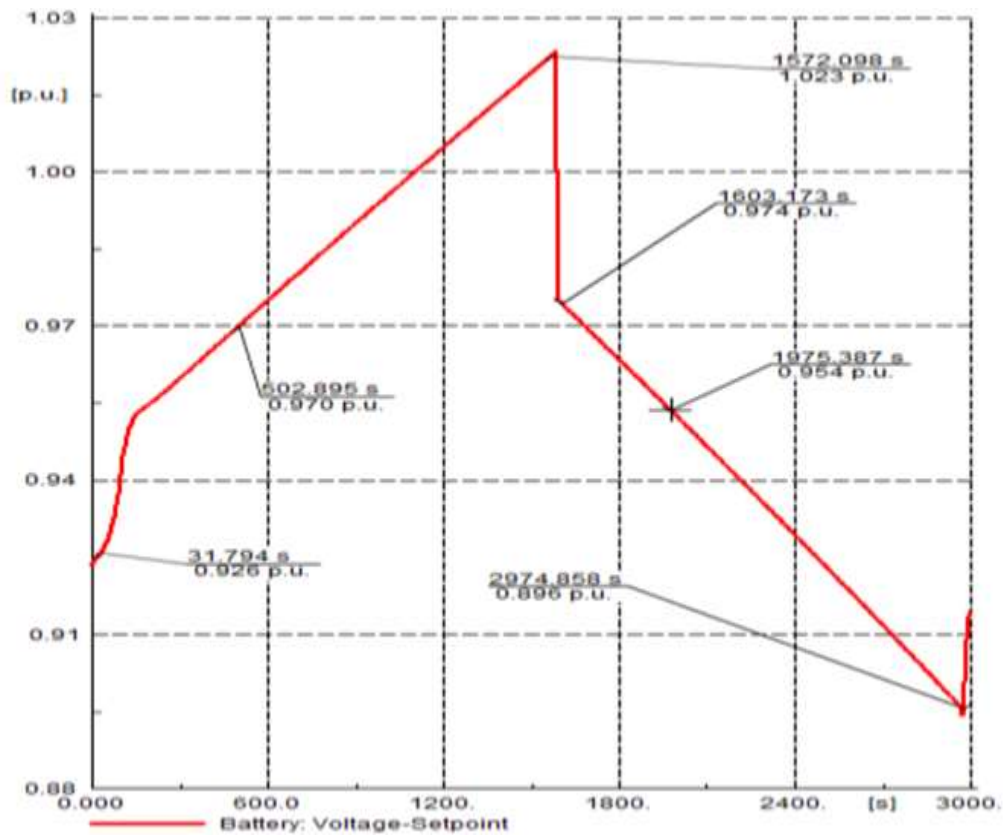


Figure 4-52: Battery Voltage

Figure 4-53 below illustrate the power of the battery. Before the simulation began, the active power of the battery was zero but gradually increased with the charging status.

Negative active power depicts the energy consumed by the battery when it is dispatched when the charging state is reached to 1. Positive active power is an example of the power delivered to the external load.

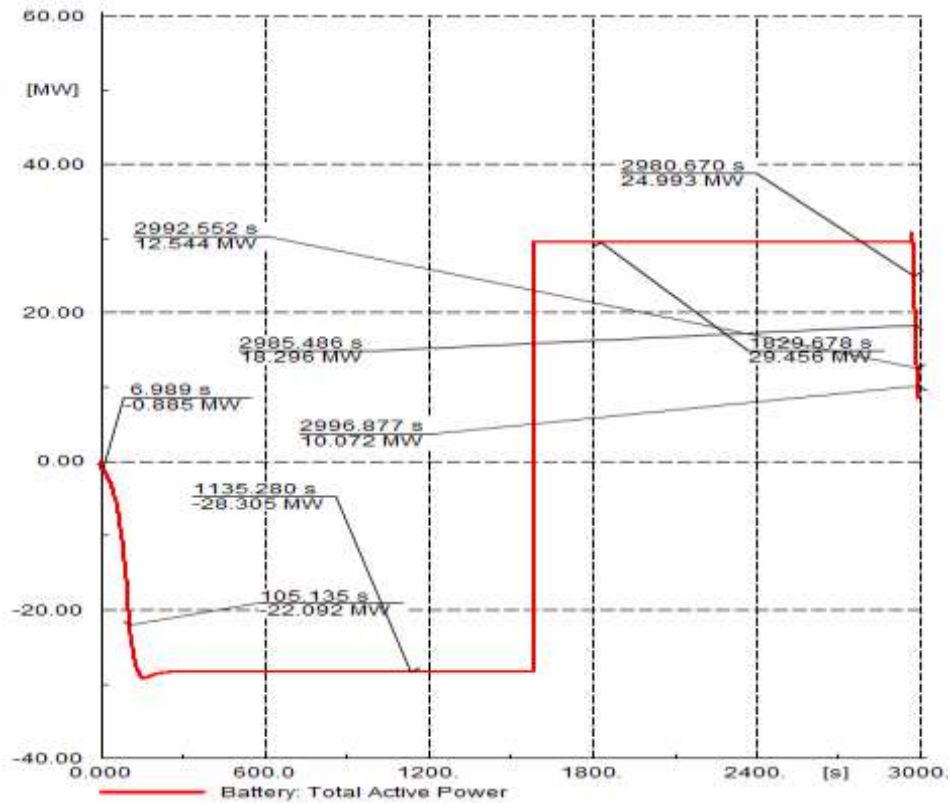


Figure 4-53: Battery Total active Power in MW

Battery therefore seemed to be operating and performing as planned under normal operating conditions. During peak demands, the BESS re-supplies the load once the charging status has been reached, which means that the energy reserve was efficient based on the above-mentioned figures (Figure 4-51, Figure 4-52, Figure 4-53).

ii. Battery Fault Analysis

The charging status of the battery is presumed to be 1, which means that the battery will be fully charged prior to the simulation phase. The single-phase earth fault was generated at the coupling point for 5 seconds, the fault begins at 30 seconds of simulation time and is cleared at 35 seconds of simulation time.

Below the figure indicates the voltage dips and the frequency deviation. From the above, it can be seen from Figure 4-54 that the presence of BESS in the device network plays an important role in stabilizing the voltage magnitude in the POC busbar to 0.332 pu compared to 0 pu without BESS.

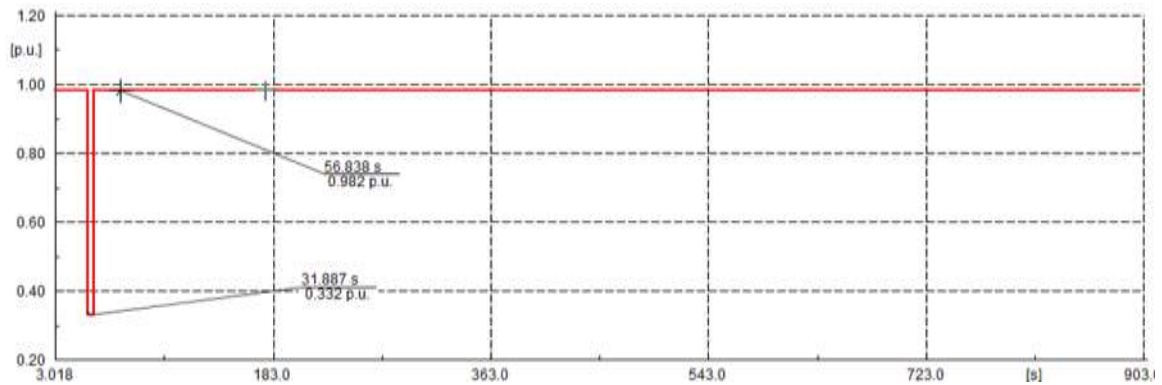


Figure 4-54: Voltage magnitude at POC busbar (bus)

This means that the BESS is injecting reactive current into the grid to regulate the voltage while the device frequency is stabilizing to the minimum and maximum operating limits as shown in Figure 4-55.

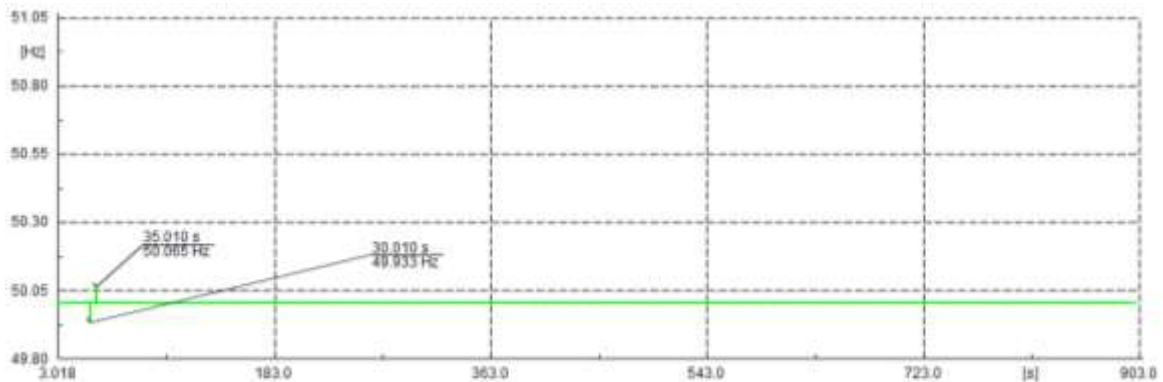


Figure 4-55: Frequency at POC bus

At Grid bus: From the following figures 4-56 and 4-57, it can be seen from Figure 4-56 that, with the presence of BESS, the voltage magnitude at grid is stabilized at 0.332 p.u., compared to 0 p.u., without BESS.

This means that the BESS injects reactive current into the grid to stabilize the voltage while the device frequency is stabilized to the minimum and maximum operating limits as shown in Figure 4-57.

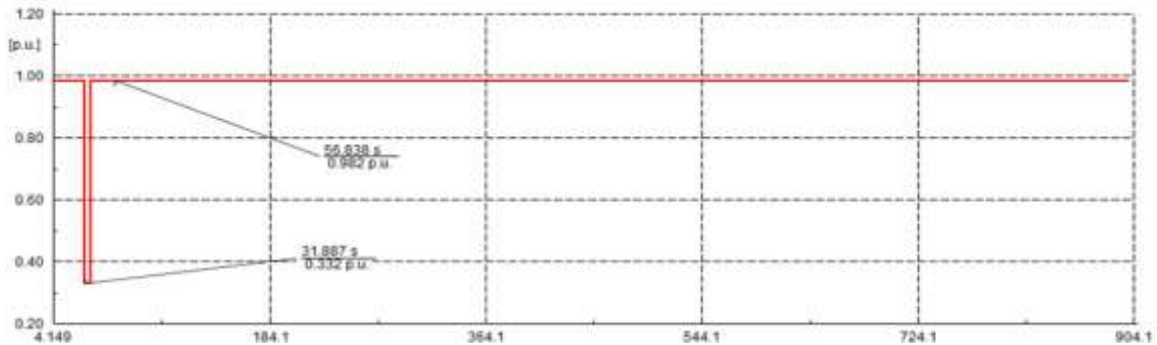


Figure 4-56: Voltage Magnitude at Grid bus

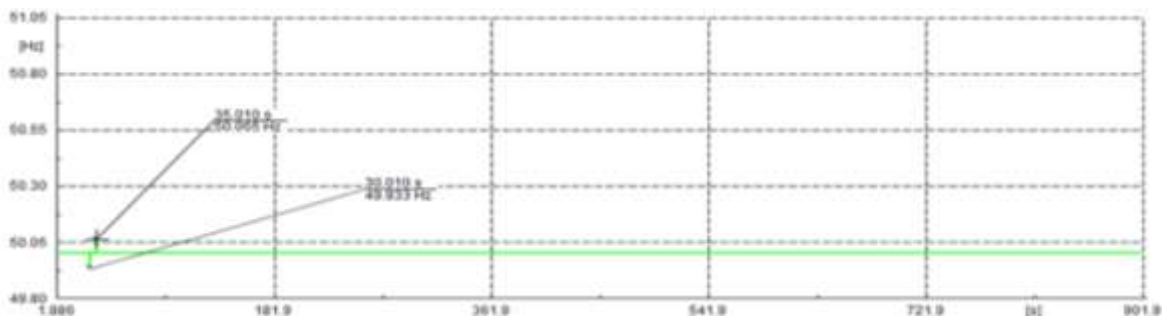


Figure 4-57: Frequency at Grid bus

4.6.5.2.3 Simulation Results and Discussion (Load Change)

During the simulation without the BESS (study case: load without BESS) all governor controllers are tuned with standard values. It is obvious, that a load change of nearly 10% of the total grid load causes a big frequency under-run (red curves in Figure 4-58 up to Figure 4-65). The compensation is important for the grid because it could increase the active power output much faster than the wind farm. A under frequency of nearly 49 Hz would lead in the grid to severe action. The BESS replaces the primary control power of the wind farm in the second simulation (study case: "load with BESS"). The turbine control of the wind turbine is modified for this purpose.

The benefit for the controller is reduced from the normal value ($K = 25$) to $K = 1$. The participation of the wind farm in primary control is now reduced to almost zero. With the fast BESS, the underrun frequency is stopped and stabilized within a 200 mHz radius. The following section discusses 150 MW, Load Step down (- 30MW) and 30 MW Load Step up (+ 30 MW minimum) respectively.

A. Load Step down (-30 MW)

i. Wind Farm

Figure 4-58 shows the wind farm with and without battery storage facility. It can be noticed that variations from 60 to 70 seconds without a battery storage device are severe. With the implementation of BESS, fluctuations are mitigated, and the output power control system has been improved.

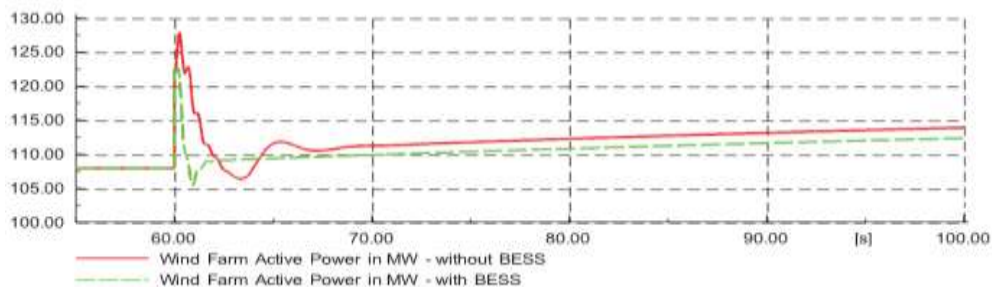


Figure 4-58: Wind Farm Active Power with and without BESS

Figure 4-59 indicates a 50 percent wind farm with and without battery storage facility. Similarly, when the Wind Farm runs at maximum capacity, variations from 60 to 70 seconds without a battery storage system are serious. The difference, however, is that with the BESS implementation, fluctuations are minimized much more rapidly.

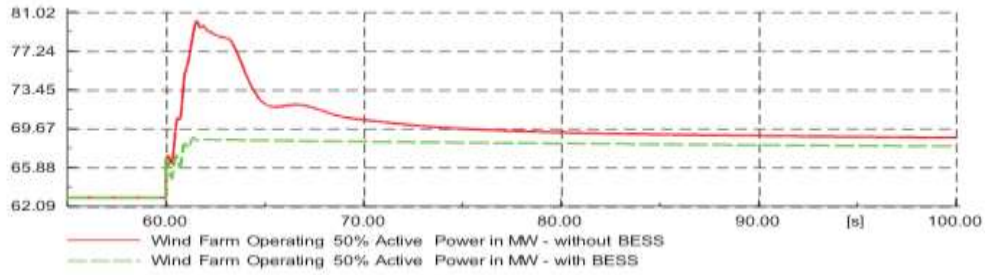


Figure 4-59: Wind Farm Operating 50% Active Power with and without

Figure 4-60 below shows the response of the wind farm to the period when the load was a phase. It can be deduced that without BESS it will take longer to stabilize because of the loss of control. Introduction of BESS reduces this time and enhances the weakness of the wind turbine control system to generate reliable power during load changes.

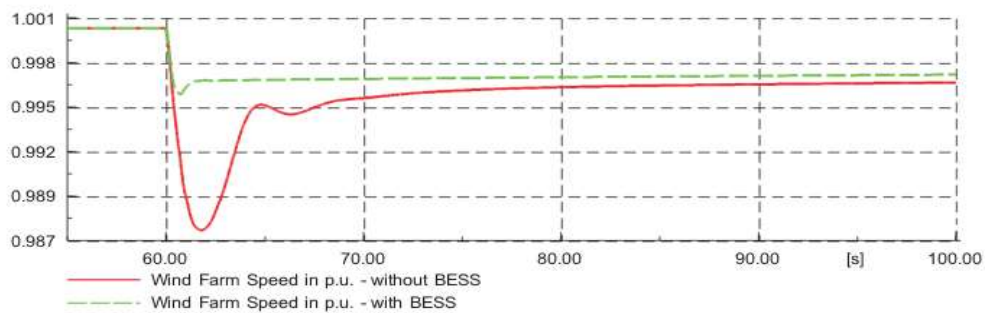


Figure 4-60: Wind Farm Speed in pu with and without BESS

ii. Grid

The grid response in Figure 4-61 when step load is provided creates severe output power fluctuations while not supported by BESS. The implementation of BESS mitigates these variations and ensures the reliability output power supply for the load.

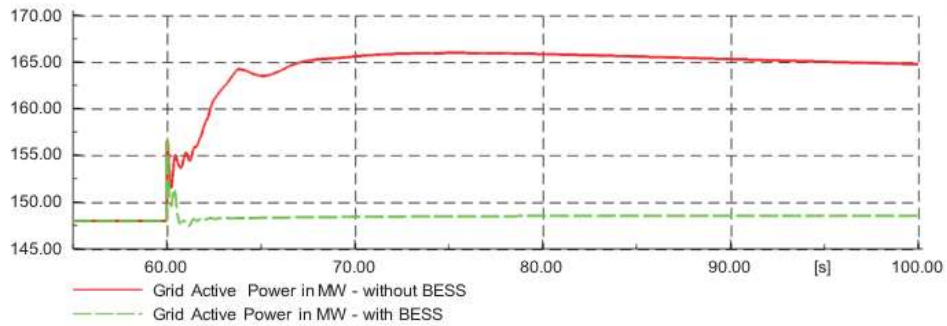


Figure 4-61: Grid: Active Power with and without BESS

B. Load Step up (+30MW)

i. Wind Farm

For both Figure 4-62 and 4-63 seven minutes after the loading step, the active power of the wind farm power plant is increased by the order of dispatch. Power rose from 105 MW to 125 MW and 63MW to 78MW in five minutes, respectively. This is equal to a gradient of just 2.6 percent / min. The BESS wind farm is unburdened by quick load changes.

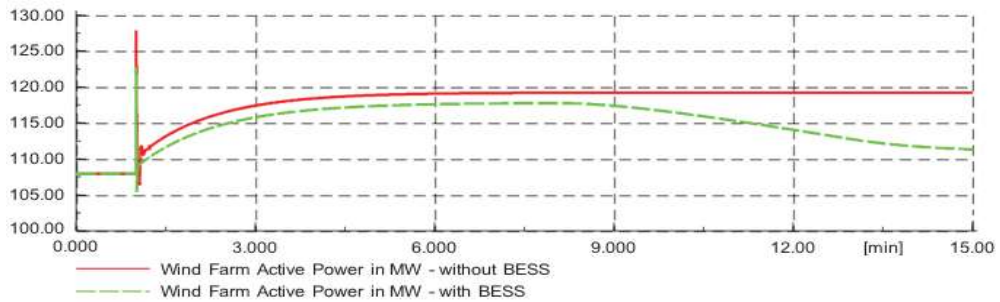


Figure 4-62: Wind Farm: Active Power with and without BESS

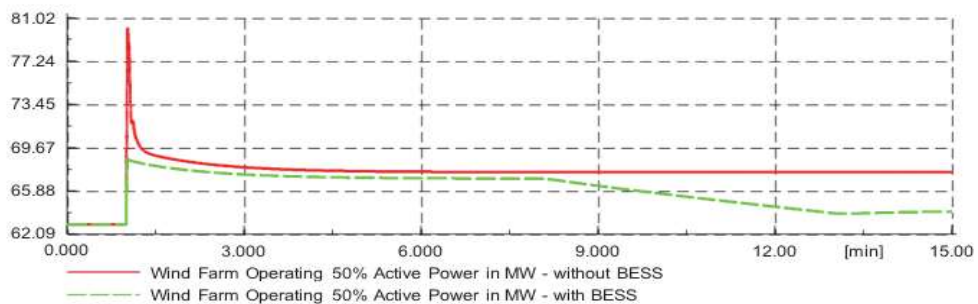


Figure 4-63: Wind Farm: Active Power with and without BESS

Figure 4-56 below shows the response of the wind farm to the time when the load was phased. Seven minutes after the loading phase, the order of dispatch increases the wind speed of the wind farm power plant. It can be deduced that it takes roughly the same time with and without BESS to stabilize since the load being supplied is larger than full capacity. Therefore, the introduction of BESS reduces this time by marginally improving the control system of the wind turbine to produce reliable power during load changes.

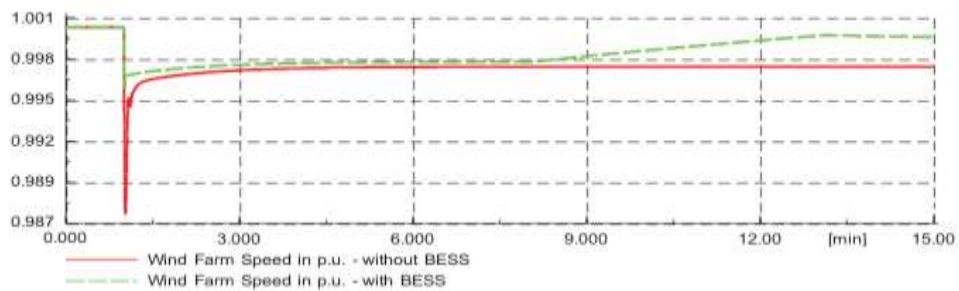


Figure 4-64: Wind Farm: Speed in pu with and without BESS

ii. Grid

It can be deduced in Figure 4-65, during full load Grid variation is large and the introduction of the BESS power was stable from 150 MW then after some time rose to 170MW. The implementation of BESS stabilizes the grid and mitigates these variations and ensures the reliability output power supply for the load.

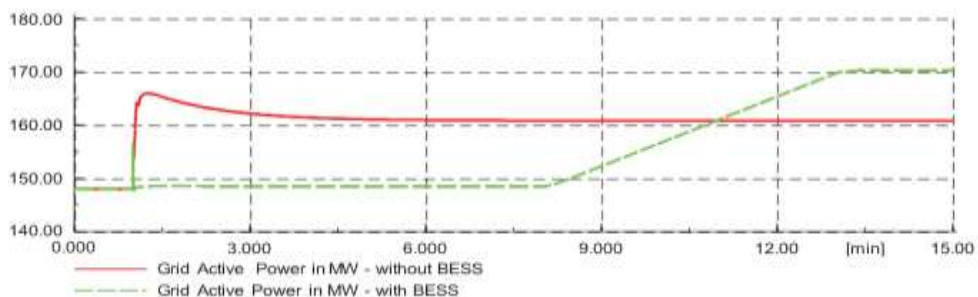


Figure 4-65: Grid Active Power with and without BESS

4.6.5.2.4 Simulation Results and Discussion (Outage)

The case of a wind farm 20% outage (111MW = 9 wind turbines are switched off 27 MW) in a small showcase grid is an outage of the wind turbine. Without this fast-controlling plant, it would be much harder to control the frequency of a disturbance. To research the outage with more practical performance, only 80 percent of the original loads are believed to have a low load scenario (Loads= $150 \times 0.8 = 120\text{MW}$). This is the operating scenario used in PowerFactory. For an operating situation, it is possible to adjust and store operating data in various situations, such as a low load and a high load event, without the need for additional variance. The shutdown of the wind farm with the wind turbine and grid is simply simulated by opening the switch on the HV side of the main transformer.

The following frequency under-run is more distinct from the load shift chase without the BESS. This is due to the lack of a fast-controllable power plant. Again, the BESS is used to improve the behaviour of the grid performance and to replace the primary control power of the grid. Below are results from DIgSILENT obtained and clearly explained.

A. Wind Farm 20% Outage Load Step down (-30 MW)

i. Wind Farm

In Figure 4-66, the wind farm can be deduced from the fact that the wind farm takes approximately 18s to monitor the fluctuation of the power output. With the implementation of BESS, the active power output could be regulated within 7 seconds which is much faster than the power plant because there is no mechanical inertia and delays. The frequency deviation is also lower.

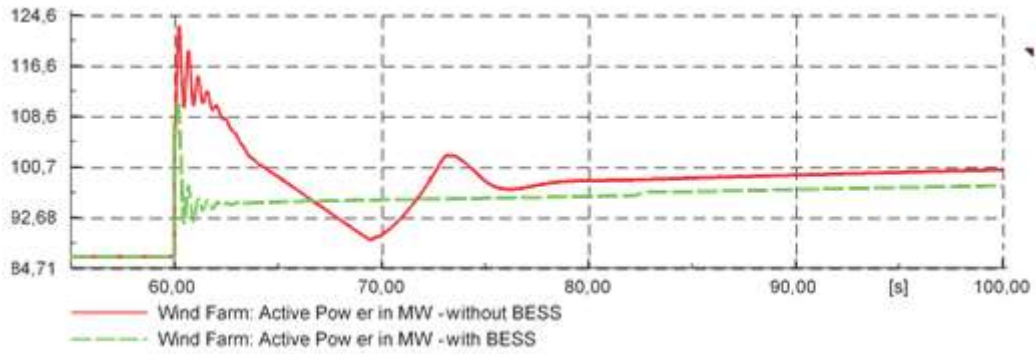


Figure 4-66: Wind farm Active Power with and without BESS

Figure 4-67 below shows the response of the wind farm to the time when the outage and load was phased. It takes for both with and without BESS approximately 15s to control the wind turbine speed minutes after the loading phase, however in terms of speed there's difference of 0.029pu. Therefore, the introduction of BESS improves the wind turbine output power control during the outage and load change.

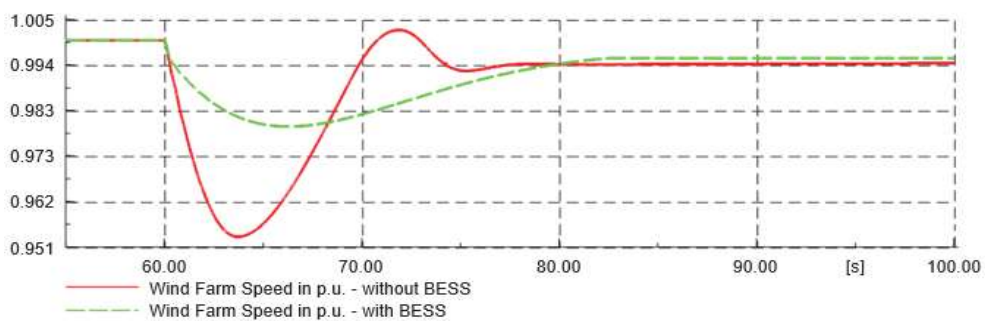


Figure 4-67 Wind Farm Speed in pu with and without BESS

ii. Grid

The grid response in Figure 4-68 active power with and without BESS is provided. The response of grid is like previous load step down (4.6.5.2.2), where it creates severe output power fluctuations while not supported by BESS. The implementation of BESS mitigates these variations and ensures the reliability output power supply for the load.

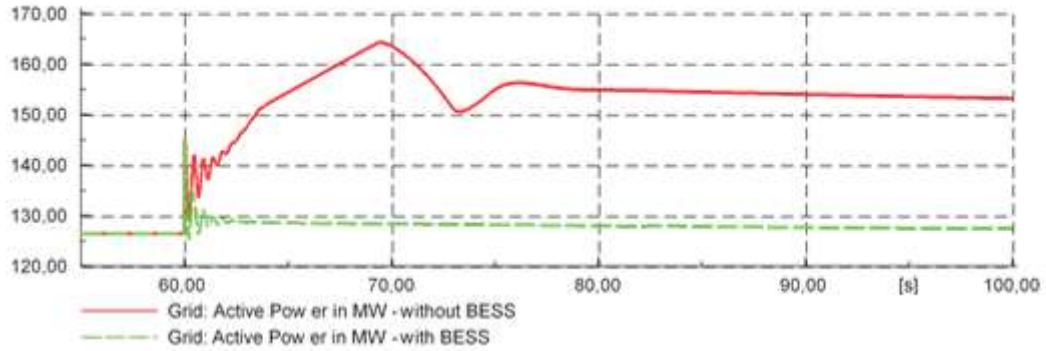


Figure 4-68: Grid Active Power with and without BESS

B. Wind Farm 20% Outage Load Step Up (+30 MW)

i. Wind Farm

The wind farm active power with and without BESS is provided in Figure 4-69.

With BESS, the active power output could be controlled within a minute that is much faster than the power plant since there is no mechanical inertia and delays. The frequency deviation is smaller, too. It should be noted with time that the power supplied by the wind farm and the batteries steadily decreases since the power of the battery decays with time.

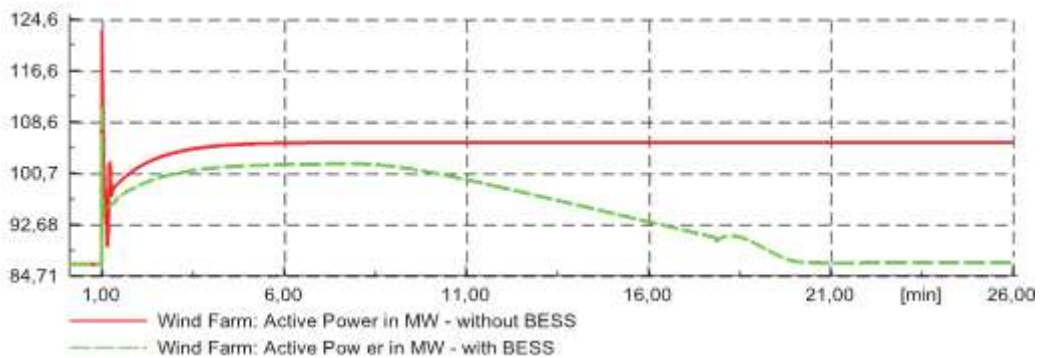


Figure 4-69: Wind farm : Active Power with and without BESS

Figure 4-70 below shows the reaction of the wind farm to the time the outage and load was phased out.

It takes about a minute to monitor the wind turbine speed, both with and without BESS, minutes after the loading process, but in terms of speed the wind farm speed fluctuates between 16 and 21 minutes. With the implementation of BESS, the speed remains constant, which increases the power output control of the wind turbine during outage and load change.

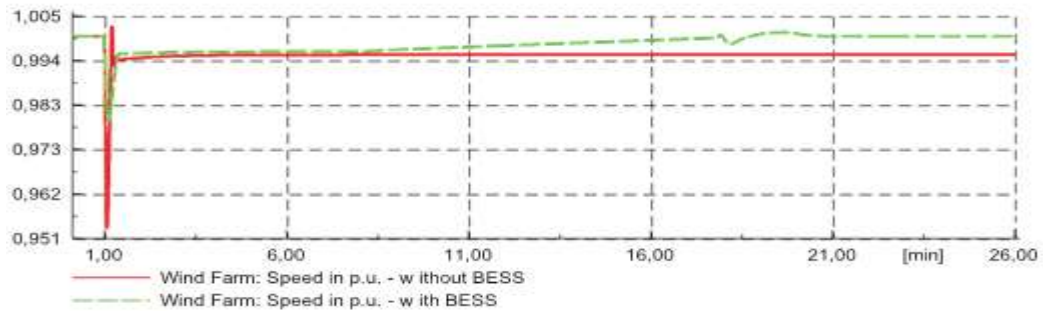


Figure 4-70: Wind Farm Speed in pu with and without BESS

ii. Grid

The grid response in Figure 4-71 active power with and without BESS is provided. The response of the grid without BESS it takes approximately 3 minutes to control fluctuations and remain constant and not meet the load demand. The implementation of BESS mitigates with a minute these variations and increase output power to ensure it meet the load demand.

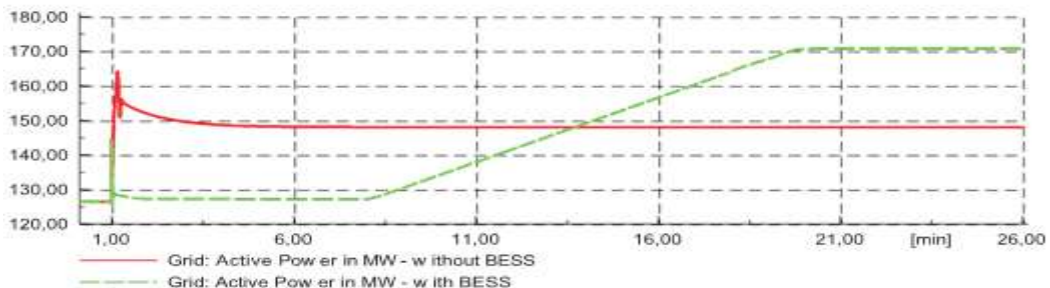


Figure 4-71: Grid Active Power with and without BESS

4.6.5.2.5 Results Discussion

Fault analysis according to IEC60909 / VDE0102 is not possible with a BESS because devices with power electronics like the pulse width modulation (PWM) converter are not considered by the norm. But DSL also offers the possibility to calculate a short circuit according to the so-called complete method. The complete method also takes the load flow into account. Furthermore, it is possible to configure the PWM-converter model for the complete short circuit method. The two options are constant current or constant voltage. For an IGBT-based converter “constant I” current would be the right choice because the valves of the converter are only designed for a certain maximum current. To obtain the maximum current with the complete fault analysis the PWM-converter must be configured to full active power on the load flow dashboard.

The fault results were achieved on this study by configuring the PWM-converter to full active power. The BESS could only consume active power if the battery is not fully loaded ($SOC < 1$). The BESS could only supply active power if the battery is not discharged ($SOC > 0$). The battery should be recharged if the SOC is below a certain level. Therefore, the BESS can control the active power in both ways. The total output of active and reactive power should together not be bigger than the apparent rated power. Hence a priority for the active or reactive power is needed. All the conditions were fulfilled from a charge controller. For the results it was assumed, that the SOC is available as a signal. Also, the SOC can be calculated from the battery current and voltage. All tasks and conditions for the controller were known and the design in DlgSILENT was activated. In (A.D. Hansen et al., 2003; Luta, 2014), a better overview it is recommended to divide the whole controller in smaller parts:

- Frequency controller (Frequency Control)

- Active/reactive power controller (PQ-Control)
- Charging controller (Charge Control)

The frequency controller is a simple proportional controller with a small dead band. In this case study, power system, it was important that there is only one integrator that controls the frequency, otherwise we could have experience problems with oscillations. The frequency control determined how much active power is activated in a case of a frequency deviation. Granted that $K = 0.04$ then the full active power of the BESS is activated if the frequency deviation is equal or greater than 2 Hz. The results values were in per unit values. The frequency control was coordinated to fulfil grid code requirements in a certain application case. In Figure 9, the command variable is f_0 , during the initialization process this value will be fixed to frq (normally 1) with the command including $(f_0) = frq$.

The block "offset" with the output "p 0" is used to compensate "dpref" if that value is not equal to zero after the load flow (because "p_order frequ" is always zero after the initialization). For a steady state load flow analysis, there are no further dynamic models of the wind farm BESS needed. Only the generator types of the power plants and the information on the load flow page is configured. In that information is also the capability limit curve for reactive power included. It is important to have one reference machine in the grid. The generator from the wind farm is the reference in the sample grid. The BESS control the active power output and the local voltage. If the load flow is calculated with the option "Active Power Control according Secondary Control" then it is possible to configure the participation of the plant on the compensation of a load change with the variable "Primary Frequency Bias" (K_{pf}). The turbine governor controls the speed of the turbine and so, via the synchronous machine the electric frequency.

In (Abhinav & Pindoriya, 2016; Sheng et al., 2005) case of a fast load change, the frequency rapidly drops due to the lack of active power in the grid. To prevent a slowdown of the whole system the turbine governor must activate more power. This is called primary frequency control or also spinning reserve, activation must be instantaneous. This means that a grid has all the time a loss of energy due to the permanent choking on the turbine valve. So, it would be more economic if another device could deliver the primary control energy until the wind farm has increased the active power. This is called secondary frequency control; activation must occur within 15 minutes after the frequency deviation. To fill that gap a BESS has been used as a solution on this study.

The simulation results on load changes confirm the BESS fill the gap. The study simulated different outages in the time domain, a 20% outage during step up and down respectively. During an outage primary control energy is needed in a grid to control the frequency within a very small gap between an upper and a lower frequency limit. The compensation must be activated within 30 seconds and the power must be continued for at least 15 minutes. But there are a lot of power plants who do that primary control, so the control power of each plant is not so big.

In (Y. Liu et al., 2014; Yang et al., 2016), demand from the grid is that each grid operator must deliver 2% of his actual produced active power as primary control power, the primary control power could also come from a BESS and the outage of a generator is a very big load change in the network. Therefore, due to the configuration of K_{pf} it is possible to define a maximum frequency deviation. An outage of the wind farm (60 MW) should be compensated from the BESS within a frequency deviation of 1,5 Hz, then the K_{pf}-factor must be 20 MW/Hz (=60 MW / 2 / 1,5 Hz). The transformers have automatic tap changers to control the voltage on the high voltage side. To make sure

that the tap changers work automatically and that the generators are inside their reactive power limits the options are Automatic Tap Adjust of Transformers and Consider Reactive.

4.7 Conclusion

In the power system simulation tool DlgSILENT, the complete wind farm battery dynamic control model was modelled and simulated, which included the key effects that lead to the power fluctuation from the wind farm. It consists of the wind farm, the battery storage system, the wind data, and the grid.

Secondly, all modelling and parameters that need to be considered when establishing the DlgSILENT model are outlined in the network model theoretical framework. Finally, a wind farm and battery load and fault analysis respectively, load change and outage were simulated, and the results discussed. The conclusion and potential recommendations are discussed in the following sections. The next chapter presents the conclusion and findings of the research study, research contribution to the body of knowledge and provide recommendation.

CHAPTER 5. CONCLUSION, FINDINGS, RESEARCH CONTRIBUTION AND FURTHER RESEARCH

5.1 Salient findings of the study

In this study, we suggested a generic energy model for BESS that can be used in renewable energy plant applications based on all battery features and an extensive literature review of available battery models. We have given model parameters for the battery NAS as a case study. A nonlinear battery model was identified and proposed in this study for integration with a wind farm to smooth output while the battery works on a safe margin. For dynamic control of wind farm BESS, the study developed a system based on MPC which could mitigate wind turbine variability and intermittence problems. The MPC controller operated well under very strict realistic restrictions from collected data, which guaranteed the system's stability. The stochastic optimization of the proposed dynamic control approach of uncertain parameters as discrete or continuous functions of probability density is also investigated. The simulation results showed good performance of MPC in wind BESS tracking, including capacity, limited SOC and power load/unload limits. It is not only wind power that is the control scheme proposed. It can be used for other intermittent sources of energy, such as large-scale solar photovoltaic farms.

5.2 Achievement of the aims and objectives of the study

The study examined the dynamic control of integrated wind farm battery energy storage systems, mitigate fluctuations of wind farm variable output, and maintain power stability for grid connection. The objective for the study was to review informative and descriptive literature review, modelling of an integrated wind farm battery energy storage model, identify a suitable dynamic control system model and choose battery type for a South African Grid connected Wind Farm BESS, and conduct a simulation as to investigate the effects and impacts of integrated wind farm battery energy storage for grid connection.

- i. Review informative and descriptive literature.

While exploring literature, it became apparent that BESS was able to provide frequency support, reduce energy variability, and sustain an unreliable supply of non-variate local grids, and help maintain overall system efficiency and stability. The additional active power support from BESS helps increase the reliability and robustness of the shipping system.

- ii. Identify an effective dynamic control system model and type of battery for a South African grid connected to the Wind Farm BESS.

The MPC algorithm measures an open loop sequence of manipulated variables such that the plant's potential behaviour.

NAS is compatibility with the wind farm, the battery was chosen for the study in comparison to other battery technologies due to its high efficiency (89 per cent), high power capacity and long life with a discharge depth of 100 per cent (DOD) of up to 2,500 cycles. MPC dynamic system model was identified, and NAS battery type was chosen for the South African Grid connected Wind Farm BESS.

- iii. Modelling of an integrated wind farm battery storage for grid connection.

We derived our model parameters for this battery based on the manufacturer's NAS battery catalogue data collection, including charging and discharging patterns and other factors including temperature impact. This dynamic control of the integrated wind farm battery for grid connection is a non-linear model. The model increases the accuracy of the control design by considering the real property of the battery in the modelling of the device.

- iv. Conduct a simulation as to investigate the effects and impacts of integrated wind farm battery energy storage for grid connection.

The Simulation was based on data from the South African Wind Farm, the verification generally indicates a clear consensus between the simulations and the steps, although the simulations at higher wind speed tend to underestimate the intensity variations. But it was easy to edit parameters to obtain a new form of battery based on real facts, either from the experimental outcome or from the results, based on the model proposed in DIgSILENT.

Simulation of grid connected with wind farm battery energy storage for battery load and fault analysis, load change and outage were simulated. The results show that the dynamic control of integrated wind farms battery energy storage systems mitigates variations in wind farms and maintains grid power stability.

5.3 Research Contribution

The contributions to the study are four:

- i. The effects of system sustainability while the battery charges, discharges, and stores power.

- ii. A South African, model predictive control (MPC) for dynamic system is identified and NAS battery type is chosen for the study in comparison to other battery technologies.
- iii. The modelling and simulation of integrated wind farm energy storage systems dynamic control model for grid connection.
- iv. The wind farm fluctuations of supplied wind output power are reduced by our control system.

5.4 Further Research

This research only used BESS, but further work could involve different types of energy storage, such as Super Capacitors, Hydrogen Storage, etc. Another potential future work will be to perform a protection coordination. In addition, the use of a different renewable energy source such as Solar and a hybrid system (Solar and Wind) with an integrated BESS may be suitable for further study.

Moreover, investors in renewable energy plants who are worried about BESS expenditures are the only technical advantages considered. We propose further research to consider the cost of the battery in terms of the design of the control system and the cost function for each charging and discharge cycle, although this cost value is non-trivial and can alter the overall control strategy.

In general, further research on the robustness, uncertainty, and noise effects in future works is essential to enhance the overall performance of the dynamic control wind farm BESS. The quality of our modelling through robust optimizations is another direction of future research

REFERENCES

- Abhinav, R., & Pindoriya, N. M. (2016). Grid integration of wind turbine and battery energy storage system: Review and key challenges. *2016 IEEE 6th International Conference on Power Systems, ICPS 2016*.
<https://doi.org/10.1109/ICPES.2016.7583998>
- Acciona Windpower. (2011). *Unpublished Service and User Manual AW 300*.
- Acciona Windpower. (2019). *Unpublished Consolidated Generation data*.
- Admire Moyo. (2017). *Eskom sets sights on renewable energy storage | ITWeb*.
<https://www.itweb.co.za/content/JKjlyr7wRmvk6amV>
- Ali, D. M. M. (2016). Hydrogen Energy Storage. *Intech, i(tourism)*, 13.
<https://doi.org/http://dx.doi.org/10.5772/57353>
- Ali Lorden, Drew Anderson, Luke Donahue, C. M. (2010). *Wind Power Point Presentation*.
https://www.slideshare.net/kkublbeck/wind-power-point-presentation?next_slideshow=1
- Angelo, B. (2008). *Handbook of Power Quality - Angelo Bagginini - Google Books*.
<https://books.google.co.za/books?id=h1YDVXADtiQC&pg=PA61&lpg=PA61&dq=to+Angelo+Bagginini,+%22The+frequency+control+and+maintenance+within+allowed+limits+requires+the+existence+at+the+system+operator+level+important+power+reserves+that+can+be+called+automatica>
- Arulampalam, A., Barnes, M., Jenkins, N., & Ekanayake, J. B. (2006). Power quality and stability improvement of a wind farm using STATCOM supported with hybrid battery energy storage. *IEE Proceedings: Generation, Transmission and Distribution*, 153(6). <https://doi.org/10.1049/ip-gtd:20045269>
- Balda, J. C., Olejniczak, K. J., & Low, S. C. (1994). The Electromagnetic Transients Program (EMTP) as an effective tool to evaluate active power filters for harmonic compensation. *Electric Power Systems Research*, 30(3).
[https://doi.org/10.1016/0378-7796\(94\)00866-3](https://doi.org/10.1016/0378-7796(94)00866-3)
- Banzo, M., & Ramos, A. (2011). Stochastic optimization model for electric power system planning of offshore wind farms. *IEEE Transactions on Power Systems*, 26(3), 1338–1348. <https://doi.org/10.1109/TPWRS.2010.2075944>

- BP. (2017). *BP Statistical Review of World Energy 2017*. <https://www.bp.com/content/dam/bp/en/corporate/pdf/energy-economics/statistical-review-2017/bp-statistical-review-of-world-energy-2017-full-report.pdf>
- Branco, H., Castro, R., & Setas Lopes, A. (2018). Battery energy storage systems as a way to integrate renewable energy in small isolated power systems. *Energy for Sustainable Development*, 43. <https://doi.org/10.1016/j.esd.2018.01.003>
- Burton, T., Sharpe, D., Jenkind, N., & Bossanyi, E. (2001). Wind Energy Handbook. In *John Wiley & Sons, Ltd*. <https://doi.org/10.1007/s13398-014-0173-7.2>
- Conroy, J., & Watson, R. (2009). Aggregate modelling of wind farms containing full-converter wind turbine generators with permanent magnet synchronous machines: Transient stability studies. *IET Renewable Power Generation*, 3(1). <https://doi.org/10.1049/iet-rpg:20070091>
- Dang, D. Q., Wu, S., Wang, Y., & Cai, W. (2010). Model predictive control for maximum power capture of variable speed wind turbines. *2010 9th International Power and Energy Conference, IPEC 2010*, 274–279. <https://doi.org/10.1109/IPEC2010.5697119>
- Department of Energy. (2011). *Integrated Resource Plan For 2010-2030*. http://www.energy.gov.za/IRP/irp_files/IRP2010_2030_Final_Report_20110325.pdf
- DlgSILENT. (2021). *PowerFactory - DlgSILENT*. <https://www.digsilent.de/en/load-flow-analysis.html>
- DlgSILENT GmbH. (2010). DlgSILENT PowerFactory Application Example Battery Energy Storing Systems. *Battery Energy Storing Systems (BESS)*, 1–28. <https://www.digsilent.de/en/faq-reader-powerfactory/do-you-have-an-application-example-for-a-battery-energy-storage-system-bess.html>
- Duffey, C. K., & Stratford, R. P. (1989). Update of Harmonic Standard IEEE-519: IEEE Recommended Practices and Requirements for Harmonic Control in Electric Power Systems. *IEEE Transactions on Industry Applications*, 25(6). <https://doi.org/10.1109/28.44238>
- Duong, T., Zhou, H., & Khambadkone, A. M. (2010). A simple design of DC power

- system with multiple source-side converters to operate stably under constant power load. *2nd International Symposium on Power Electronics for Distributed Generation Systems, PEDG 2010*. <https://doi.org/10.1109/PEDG.2010.5545865>
- Edenhofer, O., Pichs-Madruga, R., Sokona, Y., Seyboth, K., Eickemeier, P., Matschoss, P., Hansen, G., Kadner, S., Schlömer, S., Zwickel, T., & Stechow, C. Von. (2011). IPCC, 2011: Summary for Policymakers. In: IPCC Special Report on Renewable Energy Sources and Climate Change Mitigation. In *Cambridge University Press*. <https://doi.org/10.5860/CHOICE.49-6309>
- Energy.Gov. (2013). *The Inside of a Wind Turbine | Department of Energy*. <https://www.energy.gov/eere/wind/inside-wind-turbine-0>
- ESA. (2018). *Hydrogen Energy Storage | Energy Storage Association*. <http://energystorage.org/energy-storage/technologies/hydrogen-energy-storage>
- Eskom. (2013). *Application For A Generator Connection To The Eskom Network*. http://www.eskom.co.za/Whatweredoing/Documents/IPP_GridApplicationForm_Rev8_5_Nov2013.pdf
- Eskom. (2019). *Grid connection code for Renewable Power Plants (RPPs) connected to the electricity system or the distribution system in South Africa*.
- European Wind Energy Association. (2021). *Contact*. <https://www.wind-energy-the-facts.org/contact.html>
- Farhad, S., Sumedha, R., & Arindam, G. (2015). *Static Compensators (STATCOMs) in Power Systems - Google Books*. [https://books.google.co.za/books?id=itSIBQAAQBAJ&printsec=frontcover&dq=2.4.5.3+Static+synchronous+compensator+\(STATCOM\)&hl=en&sa=X&ved=0ahUKewi6uqmHn-jnAhWpSRUIHUiwDTQQ6AEIOzAC#v=onepage&q&f=false](https://books.google.co.za/books?id=itSIBQAAQBAJ&printsec=frontcover&dq=2.4.5.3+Static+synchronous+compensator+(STATCOM)&hl=en&sa=X&ved=0ahUKewi6uqmHn-jnAhWpSRUIHUiwDTQQ6AEIOzAC#v=onepage&q&f=false)
- Fathima, A. H., & Palanisamy, K. (2014). Battery energy storage applications in wind integrated systems — A review. *2014 International Conference on Smart Electric Grid (ISEG)*, 1–8. <https://doi.org/10.1109/ISEG.2014.7005604>
- Ghasemi, A., Banejad, M., & Rahimiyan, M. (2018). Integrated energy scheduling under uncertainty in a micro energy grid. *IET Generation, Transmission and Distribution*, 12(12), 2887–2896. <https://doi.org/10.1049/iet-gtd.2017.1631>
- Glushakow, B. (2007). Effective lightning protection for wind turbine generators. *IEEE*

Transactions on Energy Conversion, 22(1).
<https://doi.org/10.1109/TEC.2006.889622>

Gupta, A. K., Bhushan, H., & Samuel, P. (2013). Generator Topologies with Power Electronics Converters for a Wind Energy Conversion System : A Review. *National Conference on Recent Trends in Energy Systems*, April, 1–6.

Gururaja Murthy.D. (2014). *Aerodynamics of wind turbines*. 18.
https://www.slideshare.net/GururajaMurthyD/aerodynamics-of-windturbines?qid=988ddf6b-c6b3-4ef2-b986-9434bcc26335&v=&b=&from_search=1

Gustavo, M., & Gimenez, J. (2011). Technical and Regulatory Exigencies for Grid Connection of Wind Generation. In *Wind Farm - Technical Regulations, Potential Estimation and Siting Assessment*. <https://doi.org/10.5772/16474>

Hansen, A.D., Jauch, C., Sørensen, P., Iov, F., & Blaabjerg, F. (2003). Dynamic Wind Turbine Models in Power System Simulation tool DIgSILENT. *Report Risoe*, 1400(August), 1–80. <https://doi.org/10.1016/j.triboint.2009.02.004>

Hansen, Anca D., Sørensen, P., Blaabjerg, F., & Becho, J. (2002a). Dynamic modelling of wind farm grid interaction. *Wind Engineering*, 26(4). <https://doi.org/10.1260/030952402321039403>

Hansen, Anca D., Sørensen, P., Blaabjerg, F., & Becho, J. (2002b). Dynamic modelling of wind farm grid interaction. *Wind Engineering*, 26(4), 191–210. <https://doi.org/10.1260/030952402321039403>

Hosseini, S. M., Carli, R., & Dotoli, M. (2020). Robust Optimal Energy Management of a Residential Microgrid Under Uncertainties on Demand and Renewable Power Generation. *IEEE Transactions on Automation Science and Engineering*, 1–20. <https://doi.org/10.1109/tase.2020.2986269>

Hu, J., Shan, Y., Guerrero, J. M., Ioinovici, A., Chan, K. W., & Rodriguez, J. (2021). Model predictive control of microgrids – An overview. *Renewable and Sustainable Energy Reviews*, 136(October 2020), 110422. <https://doi.org/10.1016/j.rser.2020.110422>

International Energy Agency. (2016). *World Energy Outlook 2016, Part B: Special Focus on Renewable Energy*.

<https://www.iea.org/media/publications/weo/WEO2016SpecialFocusonRenewableEnergy.pdf>

Jadidi, S., Badihi, H., & Zhang, Y. (2020). Passive fault-tolerant control strategies for power converter in a hybrid microgrid. *Energies*, 13(21), 1–28. <https://doi.org/10.3390/en13215625>

Johan.kroes. (2012). *Gouda Wind Facility NERSA Public Hearings Cape Town*.

Khalid, M., & Savkin, A. V. (2012). A method for short-term wind power prediction with multiple observation points. *IEEE Transactions on Power Systems*, 27(2), 579–586. <https://doi.org/10.1109/TPWRS.2011.2160295>

Khalid, M., & Savkin, A. V. (2013). Closure to discussion on “A method for short-term wind power prediction with multiple observation points.” In *IEEE Transactions on Power Systems* (Vol. 28, Issue 2, pp. 1898–1899). <https://doi.org/10.1109/TPWRS.2013.2255351>

Kintner-Meyer, M. C. W., Nguyen, T. B., Jin, C., Balducci, P. J., Elizondo, M. A., Viswanathan, V. V., Zhang, Y., & Colella, W. G. (2012). Evaluating the competitiveness of energy storage for mitigating the stochastic, variable attributes of renewables on the grid. *ASME 2012 6th International Conference on Energy Sustainability, ES 2012, Collocated with the ASME 2012 10th International Conference on Fuel Cell Science, Engineering and Technology, PARTS A AND B*. <https://doi.org/10.1115/ES2012-91482>

Korobotov, D. V., Sirotkin, E. A., Troickiy, A. O., & Solomin, E. V. (2017). Wind turbine power plant control. *2016 Dynamics of Systems, Mechanisms and Machines, Dynamics 2016*. <https://doi.org/10.1109/Dynamics.2016.7819031>

Lackner, M. a. (2009). *Wind Turbine Control Systems: Current Status and Future Developments*.

<https://www.google.com/url?sa=t&rct=j&q=&esrc=s&source=web&cd=10&ved=0CGIQFjAJ&url=http://web.mit.edu/windenergy/windweek/Presentations/P9-Lackner.pdf&ei=jiDGUtjuKoK4rAeEu4DIDQ&usq=AFQjCNGQihGD5PFmRsKRGMuDMzu1sIV04g&sig2=ITtObfKREnSOelSQeTIELQ&bvm=b>

Leithead, W. E., & Stock, A. (2016). Wind turbine control. In *UK Wind Energy Technologies*. <https://doi.org/10.4324/9781315681382>

- Liu, C. H., Lee, C. S., Wang, M. H., Tseng, Y. Y., & Kuo, Y. L. (2012). FML-based knowledge management system for university governance and management assessment. *IEEE International Conference on Fuzzy Systems*. <https://doi.org/10.1109/FUZZ-IEEE.2012.6251168>
- Liu, W., & Liu, Y. (2020). Hierarchical model predictive control of wind farm with energy storage system for frequency regulation during black-start. *International Journal of Electrical Power and Energy Systems*, 119(January), 105893. <https://doi.org/10.1016/j.ijepes.2020.105893>
- Liu, Y., Liu, S. L., & Wen, J. Y. (2014). Investigation on control strategies to smooth out wind farm output fluctuations using energy storage system. *Applied Mechanics and Materials*, 521. <https://doi.org/10.4028/www.scientific.net/AMM.521.117>
- Logue, D. L., & Krein, P. T. (2001). Preventing instability in dc distribution systems by using power buffering. *PESC Record - IEEE Annual Power Electronics Specialists Conference*, 1. <https://doi.org/10.1109/pesc.2001.953991>
- Luta, D. N. (2014). *Modelling of hybrid Solar Wind intergrated generation systems in an Electrical distribution network*. September.
- Mahlia, T. M. I., Saktisahdan, T. J., Jannifar, A., Hasan, M. H., & Matseelar, H. S. C. (2014). A review of available methods and development on energy storage; Technology update. *Renewable and Sustainable Energy Reviews*, 33, 532–545. <https://doi.org/10.1016/j.rser.2014.01.068>
- Martin O. L., H. (2008). *Aerodynamics of Wind Turbines*.
- Murad, N. S. F. M., Kamarudin, M. N., Rozali, S. M., & Shaharudin, N. (2017). Review on wind turbine technology and control. *Journal of Advanced Manufacturing Technology*, 11(2).
- Nate Richards. (2013). *What is onshore drilling versus offshore drilling?* <http://www.entranceconsulting.com/2013/10/23/onshore-versus-offshore-drilling/>
- NERSA. (2014). *Grid Connection code for Renewables Power Plants (RPPs) connected to the electricity Transimisiom Syteems (TS) or the Distribution System (DS) in South Africa*.
- NGK Insulators. (2020). *About NAS Batteries | Products | NGK INSULATORS, LTD*. <https://www.ngk-insulators.com/en/product/nas/about/index.html>

- Ochani, M. K., Zhang, H., Rafiq, H., & Nawaz, A. (2019). Coordinated Frequency Control Strategy of BESS integrating high proportion of Wind power plant with a Steam turbine. *2018 International Conference on Power System Technology, POWERCON 2018 - Proceedings*.
<https://doi.org/10.1109/POWERCON.2018.8601781>
- Ohki, Y. (2016). *World's Largest-Class Battery Energy Storage System*. 32(2).
<https://ieeexplore.ieee.org/stamp/stamp.jsp?arnumber=7414237>
- Onwunta, O. E. K. (2014). *Modelling and Simulation of the Impacts of Distributed Generation into the Smart Grid*. November, 318.
- P. C. Sen. (1997). *Principles of electric machines and power electronics*. John Wiley & Sons.
https://archive.org/stream/PrinciplesOfElectricalMachinesAndPowerElectronicsPCSen_201510/Principles_of_Electrical_Machines_and_Power_Electronics_P_C_Sen_djvu.txt
- Patel, M. R. (2005). Wind and Solar Power Systems. In *Wind and Solar Power Systems*. <https://doi.org/10.1201/9781420039924>
- Polinder, H. (2011). Overview of and trends in wind turbine generator systems. *IEEE Power and Energy Society General Meeting*.
<https://doi.org/10.1109/PES.2011.6039342>
- Ragheb, ©m. (2014). *OPTIMAL ROTOR TIP SPEED RATIO*.
- Rao, N. S. M., Panchal, N., & Shah, A. (2013). Wind farm-power evacuation & grid integration. *2013 IEEE Innovative Smart Grid Technologies - Asia, ISGT Asia 2013*. <https://doi.org/10.1109/ISGT-Asia.2013.6698750>
- Redlinger, R. Y., Andersen, P. D., & Morthorst, P. E. (2016). Wind energy in the 21st century: Economics, policy, technology and the changing electricity industry. In *Wind Energy in the 21st Century: Economics, Policy, Technology and the Changing Electricity Industry*. <https://doi.org/10.1057/9780230524279>
- Schaffarczyk, A. (2014). Understanding Wind Power Technology. In *Understanding Wind Power Technology*. <https://doi.org/10.1002/9781118701492>
- SFGATE. (2011). *Traditional Energy Sources vs. Green Power Sources | Home Guides | SF Gate*. <http://homeguides.sfgate.com/traditional-energy-sources-vs->

green-power-sources-79212.html

- Sheng, D., Dai, H., Chen, M., & Chi, Y. (2005). Discussion of wind farm integration in China. *Proceedings of the IEEE Power Engineering Society Transmission and Distribution Conference, 2005*. <https://doi.org/10.1109/tdc.2005.1547210>
- Shepherd, W., & Zhang, L. (2011). Electricity generation using wind power. In *Electricity Generation Using Wind Power*. <https://doi.org/10.1142/7703>
- Shi, R., Li, S., Zhang, P., & Lee, K. Y. (2020). Integration of renewable energy sources and electric vehicles in V2G network with adjustable robust optimization. *Renewable Energy*, 153, 1067–1080. <https://doi.org/10.1016/j.renene.2020.02.027>
- Shuchuang, T. (2015). *The Impact of Static VAR Compensator (svc) on Power System Stability* - - Google Books. https://books.google.co.za/books?id=1Fn9jwEACAAJ&dq=Static+Var+Compensator&hl=en&sa=X&ved=0ahUKEwiep7yloOjnAhVwTRUIHU_5DVIQ6AEIKTAA
- Sørensen, P. (2001). Simulation of Interaction between Wind Farm and Power System. In *Riso National Laboratory, Roskilde, Dec: Vol. Risø R-128* (Issue December).
- Sperstad, I. B., & Korpås, M. (2019). Energy storage scheduling in distribution systems considering wind and photovoltaic generation uncertainties. *Energies*, 12(7). <https://doi.org/10.3390/en12071231>
- Stiebler, M. (2008). Wind Energy Systems for Electric Power Generation. In *Wind Energy Systems for Electric Power Generation*. <https://doi.org/10.1007/978-3-540-68765-8>
- Taghi, M., & Fard, Z. (2017). *Modelling and Control of Wind Farms Integrated with Battery Energy Storage Systems*.
- Tande, J. O. G. (2003). Grid integration of wind farms. In *Wind Energy* (Vol. 6, Issue 3). <https://doi.org/10.1002/we.91>
- Thiringer, T. (2007). Experimental experiences of the summation of flicker contribution from individual wind turbines in a wind park. *Proceedings of the IASTED International Conference on Energy and Power Systems*.
- Tingfang, Y., & Xin, Y. (2010). Lightning protection of wind turbines. *ICIMA 2010 - 2010 2nd International Conference on Industrial Mechatronics and Automation*, 1.

<https://doi.org/10.1109/ICINDMA.2010.5538095>

Tong, W. (2010). Fundamentals of Wind Energy. In *Physics Bulletin* (Vol. 30, Issue 12). <https://doi.org/10.1088/0031-9112/30/12/057>

Tran, D., & Khambadkone, A. M. (2012). Dynamic control of energy storage system for stable operation of wind power plant. *2012 IEEE Energy Conversion Congress and Exposition, ECCE 2012*, 666–671. <https://doi.org/10.1109/ECCE.2012.6342757>

Tripathy, S., & Rourkela, N. (2014). *Different Generator Topologies used in Wind Turbine Applications*. https://www.researchgate.net/publication/262414623_A_Case_Study_of_Different_Generator_Topologies_used_in_Wind_Turbine_Applications

Union of concerned Scientist. (2014). *How Wind Energy Works*. <https://doi.org/10.1029/2002JD002076>

Varbanov, P. S., & Klemeš, J. J. (2010). Total sites integrating renewables with extended heat transfer and recovery. *Heat Transfer Engineering*, 31(9). <https://doi.org/10.1080/01457630903500858>

Wang, H., Tang, Y., Hou, J., & Zi, P. (2013). Grid-integration control strategy of large-scale battery energy storage system and its application to improve transient stability of interconnected power grid. *Dianwang Jishu/Power System Technology*, 37(2).

Wang, L., Chen, S. S., Lee, W. J., & Chen, Z. (2009). Dynamic stability enhancement and power flow control of a hybrid wind and marine-current farm using SMES. *IEEE Transactions on Energy Conversion*, 24(3). <https://doi.org/10.1109/TEC.2008.2008877>

Wang, L., Wang, K. H., Lee, W. J., & Chen, Z. (2010). Power-flow control and stability enhancement of four parallel-operated offshore wind farms using a line-commutated HVDC link. *IEEE Transactions on Power Delivery*, 25(2). <https://doi.org/10.1109/TPWRD.2009.2034915>

Wang, N. (2018). Advanced wind turbine control. In *Advanced Wind Turbine Technology*. https://doi.org/10.1007/978-3-319-78166-2_10

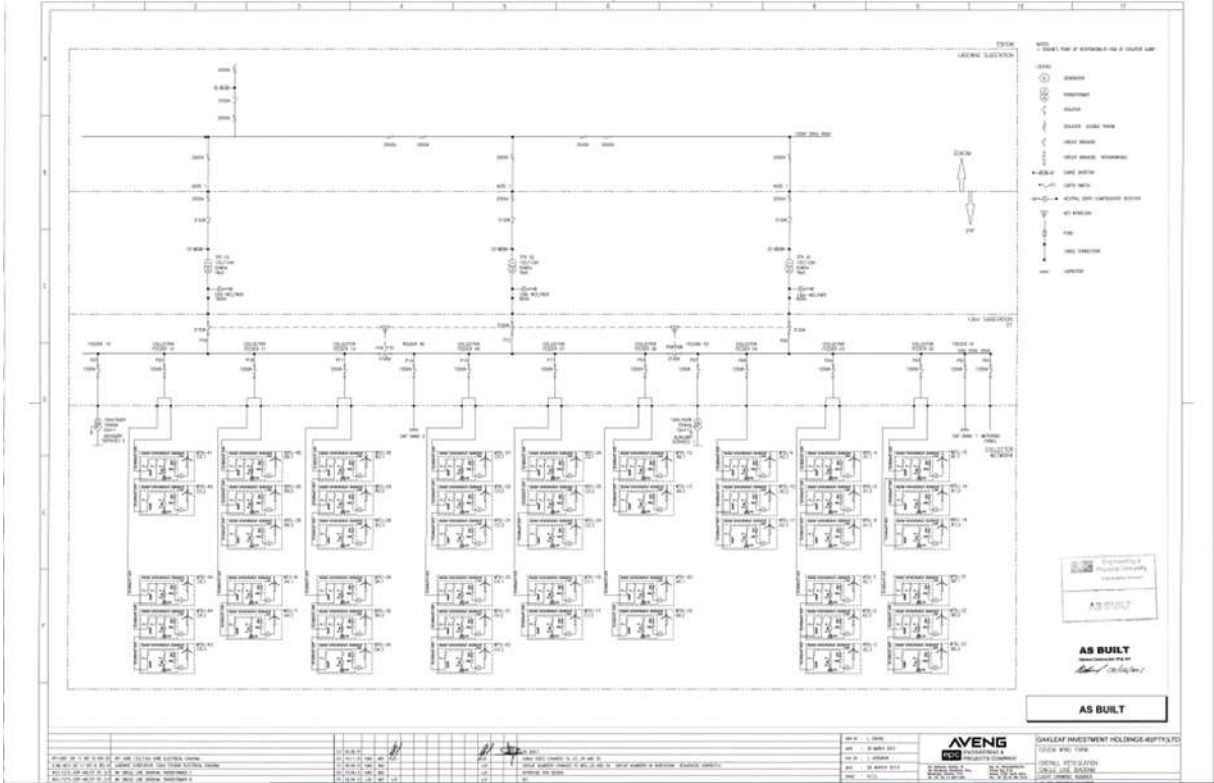
Wang, W., Ma, R., Xu, H., Wang, H., Cao, K., Chen, L., & Ren, Z. (2016). Method of

- energy storage system sizing for wind power generation Integration. *Asia-Pacific Power and Energy Engineering Conference, APPEEC, 2016-December*.
<https://doi.org/10.1109/APPEEC.2016.7779682>
- Wang, X. Y., Vilathgamuwa, D. M., & Choi, S. S. (2005). Decoupling load and power system dynamics to improve system stability. *Proceedings of the International Conference on Power Electronics and Drive Systems, 1*.
<https://doi.org/10.1109/peds.2005.1619697>
- Weber, H., & Kleimaier, M. (2009). Grid integration of wind generation. *2009 CIGRE / IEEE PES Joint Symposium: Integration of Wide-Scale Renewable Resources into the Power Delivery System*.
- Weber, T., Mushamalirwa, D., Deschatres, M., Hilberg, C., Maibach, P., Janssen, W., Leske, T., Kehrer, S., & Saint-Andre, D. (2010). Grid integration of offshore windfarm Cote d'Albatre to the French transmission grid. *43rd International Conference on Large High Voltage Electric Systems 2010, CIGRE 2010*.
- West, M., & Baldwin, T. (2013). Energy storage and supergrid integration. *45th North American Power Symposium, NAPS 2013*.
<https://doi.org/10.1109/NAPS.2013.6666892>
- World Energy Council. (2020). *Five Steps to Energy Storage. Innovation Insights Brief 2020*. 62. www.worldenergy.org
- Yang, D., Wen, J., Chan, K. W., & Cai, G. (2016). Dispatching of wind/battery energy storage hybrid systems using inner point method-based model predictive control. *Energies, 9*(8). <https://doi.org/10.3390/en9080629>
- Yun, P., Ren, Y., & Xue, Y. (2018). Energy-storage optimization strategy for reducing wind power fluctuation via markov prediction and PSO method. *Energies, 11*(12).
<https://doi.org/10.3390/en11123393>
- Zakeri, B., & Syri, S. (2015). Electrical energy storage systems: A comparative life cycle cost analysis. In *Renewable and Sustainable Energy Reviews*.
<https://doi.org/10.1016/j.rser.2014.10.011>
- Zareifard, M. T. (2017). *Modelling and Control of Wind Farms Integrated with Battery Energy Storage Systems* by. Mohammad Taghi Zareifard To cite this version : HAL Id : hal-01573257

August.

- Zhang, B. H., Guo, H. F., Li, Y. X., Chen, M., Li, Y. Q., & Zhou, J. S. (2014). Optimization of smoothing control in hybrid wind and battery energy storage system. *Advanced Materials Research*, 852. <https://doi.org/10.4028/www.scientific.net/AMR.852.703>
- Zhao, H., Wu, Q., Hu, S., Xu, H., & Rasmussen, C. N. (2015). Review of energy storage system for wind power integration support. *Applied Energy*. <https://doi.org/10.1016/j.apenergy.2014.04.103>
- Zheng, Y., Hill, D. J., Meng, K., Luo, F. J., & Dong, Z. Y. (2015). Optimal Short-term Power Dispatch Scheduling for a Wind Farm with Battery Energy Storage System. *IFAC-PapersOnLine*, 48(30). <https://doi.org/10.1016/j.ifacol.2015.12.432>
- Zou, Z., & Zhou, K. (2011). Voltage stability of wind power grid integration. *2011 International Conference on Electrical Machines and Systems, ICEMS 2011*. <https://doi.org/10.1109/ICEMS.2011.6073985>

APPENDIX 1: CIRCUIT DIAGRAM



APPENDIX 2: AVERAGE POWER CURVE

